Simulation of Hyperspectral Data from Multispectral Data Using Spectral Reconstruction Approach

Thesis submitted to the Andhra University, Visakhapatnam in partial fulfillment of the requirement for the award of *Master of Technology in Remote Sensing and GIS*

Submitted By
Varun Tiwari
M.Tech. (RS and GIS)

Supervised by

Mr. Vinay Kumar
Project Supervisor
Photogrammetry and Remote Sensing
Department,IIRS, Dehradun

Mr. Kamal Pandey
Project Supervisor
Remote Sensing & Geoinformatics
Group, IIRS, Dehradun

Indian Institute of Remote Sensing,
Indian Space Research Organization,
Department of Space, Govt. of India
Dehradun – 248001
Uttarakhand, India
August, 2015

DISCLAIMER

This work has been carried out in partial fulfillment of Masters of Technology program in Remote Sensing and Geographic Information System at Indian Institute of Remote Sensing, Dehradun, India. The author is solely responsible for the contents of the thesis.

Dedicated to my

Mummy and

Papa

CERTIFICATE

This is to certify that the project entitled **"*Simulation of Hyperspectral data from Multispectral data using Spectral Reconstruction Approach* "**is a bona fide record of work carried out by **Mr. Varun Tiwari** during 01 Aug 2014 to 14 Aug 2015. The report has been submitted in partial fulfillment of requirement for the award of Master of Technology in Remote Sensing and GIS with specialization in Satellite Image Analysis and Photogrammetry, conducted at Indian Institute of Remote Sensing (IIRS), Indian Space Research Organisation (ISRO), Dehradun from 19 Aug 2013 to 14 Aug 2015. The work has been carried out under the supervision of **Mr. Vinay Kumar,** Scientist 'SD', Photogrammetry and Remote Sensing Department and **Mr. Kamal Pandey**, Scientist 'SD', Remote Sensing & Geoinformatics Group, Indian Institute of Remote Sensing, ISRO, Dehradun, Uttarakhand, India.

No part of this report is to be published without the prior permission/intimation from/to the undersigned.

Mr. Vinay Kumar
Project Supervisor
Photogrammetry and Remote Sensing Department,IIRS, Dehradun

Mr. Kamal Pandey
Project Supervisor
Remote Sensing & Geoinformatics Group, IIRS, Dehradun

Ms. Shefali Agarwal
Photogrammetry and Remote Sensing Department,IIRS, Dehradun

Dr. S.P.S. Kushwaha
Dean (Academics) & Group Director, ERSSG
IIRS, Dehradun

DECLARATION

I, ***Varun Tiwari***, hereby declare that this dissertation entitled "***Simulation of Hyperspectral data from Multispectral data using Spectral Reconstruction Approach***" submitted to Andhra University, Visakhapatnam in partial fulfilment of the requirements for the award of ***M.Tech in Remote Sensing and GIS***, is my own work and that to the best of my knowledge and belief. It is a record of original research carried out be me under the guidance and supervision of **Mr. Vinay Kumar**, Scientist 'SD' and **Mr. Kamal Pandey**, Scientist 'SD', Remote Sensing & Geoinformatics Group, Indian Institute of Remote Sensing, ISRO, Dehradun. It contains no material previously published or written by another person nor material which to a substantial extent nor material which to a substantial extent has been accepted for the award of any other degree or diploma of the university or other institute of higher learning, except where due acknowledgement has been made in the text.

Place: Dehradun **Mr. Varun Tiwari**

Date: August, 2015

Acknowledgement

The presented thesis is part of the M.Tech project work carried out at the Indian Institute of Remote Sensing, ISRO, Dehradun. I would never have been able to finish my thesis without the contributions made by many of the people who deserve a special mention.

I'm thankful to my supervisor, Mr. Vinay Kumar, Scientist 'SD', Photogrammetry and Remote Sensing Department, IIRS for his valuable guidance, patience and support. I consider myself very fortunate for being able to work with a very considerate and encouraging scientist like him. He always considered me as a friend rather than a student and gave me freedom to explore my potentials and helped me in directing myself towards my goals.

I would like to express my gratitude towards my project co-supervisor Mr. Kamal Pandey, Scientist 'SD', Remote Sensing & Geoinformatics Group, IIRS for his valuable guidance throughout the project work. He always gave support for the in-depth discussions about various research problems and helped me in development of open source hyperspectral image simulation software.

I would like to express my thanks to Ms. Shefali Agrawal, Head PRSD, IIRS. The work would have not been possible without her valuable guidance and support. I am thankful to Mr. P. L. N. Raju, Group Head, PPEG, IIRS, Dr. S. P.S. Kushwaha, Dean (Academics) for their insightful observations and for providing the necessary facilities. I express my sincere gratitude towards Dr. A. Senthil Kumar, Director, IIRS for providing the necessary infrastructure, environment, assistance and a wide perspective to learn new things and accomplish M.Tech in Remote Sensing & GIS. It is because of them that a very energetic and conducive environment was available during the project work at IIRS.

I express my gratitude to the former Director of IIRS, Dr. Y. V. N. Krishnamurthy for his support and guidance. I would also like to thank Prof. Dr. D.R.M Samudraiah, SAC Ahmedabad for his valuable suggestions. Due gratitude is also expressed for Dr K. R. Murali and sensors development team, SAC Ahmedabad for providing Spectral Response Function (SRF) of Resourcesat-2 LISSIII & LISS IV sensors

I would like to thank entire IIRS faculty for their continuous support at various stages of project. I also thank Librarian, IIRS for providing all the necessary research material and books whenever required during the duration of course work. I also acknowledge the support of CMA for providing lab assistance whenever required.

I would like to thank specially Mr. Rigved Ranade, Mr. Shivesh Anand (BITS Pilani) and Ms. Vartika Verma (NIT Hamirpur) and Ms. Kritika Singh (BITS Pilani) for helping me in development of open source software image simulation software.

I owe many thanks to my classmate and all of my friends, especially Akshat, Manohar, Rohit, Ridhika, Richa, Jenia, Dr. Kuldeep, Amol, Sukant, Rajkumar, Vineet and Harjeet, Rajsweta, Mayank for their support and motivation. I would also like to thank all my M.Tech and M.Sc. batchmates for their support.

I am short of words to thank my parents Mr. Virendra Kumar Tiwari and Mrs. Pushpa Tiwari, who always stood by my side and supported me despite great difficulties. My parents are my strong pillars and I owe every bit of my work to their dedication, hard work, care & support. I am thankful to my sister, Supriya Tiwari for her continual and valuable guidance at each and

every step. I pay my respect to my grandparents Late Mr. R.B Tiwari, Late Mrs. Usha Rani Tiwari, who have played a very important role in my days of upbringing. Their encouragement has always motivated me to pursue my higher studies. My family is my source of inspiration and I owe everything to them.

Besides this, I thank all colleagues who have knowingly and unknowingly helped me in the successful completion of project.

Varun Tiwari

M.Tech 2013-2015

Success is never final, failure is not fatal: it is the courage to continue that counts…….

Winston Churchill

Abstract

Optical remote sensing sensors have been acquiring the data of earth's surface for the past few decades. These sensors are broadly classified in terms of spectral bands as panchromatic, multispectral and hyperspectral. Multispectral sensors acquires the data in fewer number of bands with broad bandwidth which is useful for classification of major Land Use Land Cover (LULC) classes. Because of the coarser bandwidth multispectral sensor cannot be used for detailed LULC studies. Innovation and up gradation of technology has given birth to hyperspectral sensors which emerged out to be a vibrant tool for detailed studies. These sensors acquired data which are contiguous and spectrally rich, thus enabling the identification of the features which are spectrally similar. But, acquisition of data from hyperspectral sensor is difficult and expensive as it requires sensitive detectors, large storage capacity and fast data processors. As overall cost are of critical importance for any earth observation system, so there is a need to simulate Hyperspectral Remote Sensing (HRS) data using available Multispectral Remote Sensing (MRS) data.

The present study focuses on simulation of HRS data utilizing MRS data using spectral reconstruction approach. Spectral reconstruction approach is a sensor independent technique which makes use of inheritance information of atmospherically corrected MRS data and normalized ground spectra for simulation of HRS data. In the present study, EO-1 ALI, Landsat 8 OLI, Resourcesat-2 LISS III and LISS IV datasets were used for simulation of HRS data and 70, 34, 38, 23 spectral bands with 10 nm bandwidth respectively were simulated. The simulated HRS data were validated using visual interpretation, statistical, spectral separability and classification approaches. Simulated HRS data from EO-1 ALI and Landsat-8 OLI has shown high correlation with EO-1 Hyperion data along with comparable and high SNR values. Simulated HRS results from LISS III and LISS IV have also produced high SNR values indicating satisfactory simulation. Spectral separability analysis was carried out for all the hyperspectral datasets (EO-1 Hyperion and simulated from MRS data) using Spectral Angle Mapper (SAM), Spectral Feature Fitting (SFF) and Binary Encoding (BE) with field spectra resulted high scores demonstrating high quality simulated product. SAM classification was also performed for validation and it was observed that simulated hyperspectral data shows comparable results with Hyperion. The simulated results were also able to separate out different LULC classes in a better way than their corresponding multispectral datasets.

The study also demonstrated the potential of simulation of the HRS data from high resolution Resourcesat-2 LISS IV MRS data (spatial resolution 5.8 m) which can be beneficial where problem of mixed pixel exists. The simulated high resolution HRS data can also be used for target detection related studies.

This research also emphasizes the use of open source programming language in the development of HRS data simulation tool box using Spy and Numpy libraries. A tool for the same has been developed using Python and associated libraries which is sensor independent and capable of simulating the HRS data using any MRS Datasets.

Keywords: Simulation, hyperspectral, multispectral, unmixing, normalization and python

Table of Contents

List of Figures

List of Tables

List of Abbreviations

ALI	Advance Land Imager
ART	Application Research Tool
BE	Binary encoding
DN	Digital Number
EO-1	Earth Observing-1
EMS	Electromagnetic Spectrum
ETM	Enhanced Thematic Mapper
ENVI	Environment for Visualizing Image
FCC	False Colour Composite
FLAASH	Fast Line-of-Sight Atmospheric Analysis of Spectral Hypercube
GUI	Graphic User's Accuracy Interface
HRS	Hyperspectral Remote Sensing
ISRO	Indian Space Research Organisation
LULC	Land Use Land Cover
LISS	Linear Imaging Self Scanning
LMM	Linear Mixture Model
MF	Matched Filter
MIR	Mid Infrared
MNF	Minimum Noise Fraction
MODTRAN	Moderate Resolution Atmospheric Radiance and Transmittance Model
MRS	Multispectral Remote Sensing
NIR	Near Infrared
OLI	Optical Land Imager
PDM	Pattern Decomposition Method
RS	Remote Sensing
SWIR	Short Wave Infrared
SNR	Signal to Noise Ratio
SAM	Spectral Angle Mapper
SFF	Spectral Feature Fitting
SPy	Spectral Python
SRF	Spectral Response Function
UPDM	Universal Pattern Decomposition Method

1 Introduction

1.1 Background

Multispectral Remote Sensing (MRS) innovations have been mainly utilized for acquiring and extracting information of Land Use Land Cover (LULC) features from earth's surface in the past few decades(Hossain et al., 2003). In a solitary perception, multispectral sensors acquire tens of spectral bands that ranges from the visible to Infra-Red (IR) i.e. 400 nm to 2500 nm. A new era started in remote sensing when Hyperspectral Remote Sensing (HRS) sensors emerged as an excellent tool for gathering contiguous spectral bands with narrow bandwidth that ranges from visible to Short Wave Infrared (SWIR) of the Electro Magnetic Spectrum (EMS). This enabled extensive investigations of earth surface peculiarities that are constrained with coarser bandwidth collected by multispectral data. HRS deliver spectral data comprising of many bands in a solitary gathering and it has a wide area of applications viz. mineralogy, reconnaissance, horticulture, target recognition etc. (Agarwal, 2004).

Apart from wide applications of hyperspectral data it has few limitations also(Sahoo et al., n.d.)(Sahoo,). Fast computers, sensitive detectors and large data storage capacities are required which makes the acquisition and processing cumbersome and exorbitant. Due to these limitations, very few number of space borne hyperspectral sensors are available till date. In the current scenario, only one space borne hyperspectral sensor i.e. EO-1 Hyperion with a spatial resolution of 30 m and narrow swath (7.5km) is available while a lot of multispectral sensors are providing data with similar spatial resolution around the globe over the past few decades("USGS EO-1 Website - http://eo1.usgs.gov," 2015). In Indian context also large number of multispectral sensors are acquiring data (LISS III, LISS IV, AWIFS) whereas only one hyperspectral sensor i.e. Hyperspectral imager(HySi) with coarser resolution on board Indian Mini Satellite (IMS-1) is available("Welcome to Bhuvan | ISRO's Geoportal | Gateway to Indian Earth Observation," 2015). Due to the availability of the vast multispectral datasets, it is indeed a requirement to simulate hyperspectral data utilizing multispectral data with a larger swath and high spatial resolution for detailed LULC studies. Simulated hyperspectral data will enable the identification and discrimination of subtle variations in the spectra of various features present over earth surface.

Very few attempts were made in the past few years(Kavzoglu, 2004)(Boggione et al., 2003)(Liu et al., 2009)(Yan et al., 2014a) for simulation hyperspectral data using multispectral data. The technique used for simulation was "***spectral reconstruction approach***". This approach is sensor independent and utilizes the concept of spectral unmixing.

Spectral unmixing is a technique for finding the proportion of LULC feature present inside a mixed pixel(Tseng, 2000). A pixel in any satellite image is considered to be to mixed pixel when it contains more than one LULC feature(Liguo et al., 2009a). The occurrence of pure pixel is rare in the satellite data with a spatial resolution of 30m and the probability of more heterogeneous features within a single pixel increases with decreasing spatial resolution.

Eventually a single pixel encapsulates different land cover classes. Various unmixing techniques have been evolved for feature identification and extracting their percentage contribution in the mixed pixels of satellite data(Heinz and Chang, 2001a) (Liguo et al., 2009a).

Spectral unmixing (Heinz and Chang, 2001b)(Settle and Drake, 1993a) highlights the relative abundance of materials that are containe

d in any satellite imagery based on spectral characteristics of the materials. The reflectance at each pixel (or end member) of the image is the sum of weighted fraction of endmembers within the pixel. Spectral unmixing results are exceptionally reliant on the input end members and varying the end members may alter the results. The spectral reconstruction technique, applied by Bo Liu, represented each pixel as a linear sum of standard end members (vegetation, water and soil) assuming that 95.5 percent of the image comprises of these endmembers.

Detailed LULC study is possible using simulated HRS data from MRS data which makes use of Spectral unmixing in spectral reconstruction approach when developing such hyperspectral sensors are difficult.

1.2 Problem Statement and Motivation

Data acquired from Hyperspectral sensors are contiguous and spectrally rich, thus enables identification of the features which are spectrally similar, whereas multispectral data fails to do so because of coarser spectral resolution. In spite of wider applications of HRS data very few number of space borne hyperspectral sensors are available. These sensors require sensitive detectors, high speed data processors and large data storage capability.

Due to this high end requirement there is a need to find a low cost solution for generating hyperspectral data. Simulation is one of the way to generate hyperspectral datasets from existing multispectral datasets for investigation of the earth peculiarity in detail. Numerous multispectral datasets are available with good spatial resolution and can be exploited for simulation of hyperspectral data for detailed LULC studies.

1.3 Research Objectives

Main Objective

- The main objective of the present study is to simulate hyperspectral data from multispectral data using spectral reconstruction technique.

Sub-Objectives

The sub objectives of this study are as follows:

- Simulation of hyperspectral data from EO-1 ALI Multispectral data.

- Validation of Simulated hyperspectral with EO-1 Hyperion data using visual interpretation, statistical analysis, signal separability analysis and classification approaches.
- Evaluation of the spectral reconstruction technique for simulating Hyper-spectral data from Landsat-8 OLI, Resourcesat- 2 LISS-III and LISS IV datasets.
- Development of open source tool for the simulation of HRS data from MRS data.

1.4 Research Questions

- How spectral reconstruction technique can be utilized for simulating hyper-spectral data from EO-1 ALI multispectral data?
- What are the various validation techniques for validating the simulated HRS data?
- How this technique can be evaluated for simulating Hyperspectral data using other multispectral datasets?
- How effectively simulated Hyperspectral data can be used for identification and discrimination of spectrally similar LULC features?
- How open source programming language assist in developing a HRS data simulation tool?

1.5 Structure of Thesis

This thesis has been subdivided in various chapters as given below:-

- Chapter1: Introduction. It covers the introduction to the multispectral and hyperspectral sensors / their advantage, disadvantage, availability of HRS and MRS Datasets in Indian context and its utilization in LULC mapping. The chapter also includes the problem statement and motivation, objectives and research questions.
- Chapter 2: Literature Review. This section covers the review of significant studies taken up in this regard in the past years and couple of imperative theoretical concepts which have been used in this area of exploration.
- Chapter 3: Study Area, Datasets and Tools. As the heading of this chapter indicates, it provide an insight of the study area, datasets and tools (software / hardware utilized used and developed in this research.
- Chapter 4: Methodology. This chapter contains detail about the research methodology adopted for meeting the objectives of this research.
- Chapter 5: Results and Discussion. This chapter covers the details about the results obtained from the study and discussion on the inference observed.
- Chapter 6: Conclusion and Recommendations. This chapter comprises the conclusion of the research in brief with few recommendations for advancement.

2 Literature Review

This section covers a review of significant studies taken up in the past few years and couple of imperative theoretical and practical concepts which have been used in this area of exploration.

2.1 Multispectral vs Hyperspectral Remote Sensing

Remote sensing (RS)(Agarwal, 2004)("Shaw: Spectral imaging for remote sensing - Google Scholar," 2015) (Shaw and Burke, 2003) refers to data capturing of earth surface objects without any physical contact. Various remote sensing satellites are available with unique and distinct characteristics which are cost effective and provides data with a global coverage of earth surface. These sensors are useful for various applications viz. meteorology, oceanography, geology, agriculture, pollution, glaciology and surveying etc. RS satellite sensors which are working in optical region acquires data in panchromatic, multispectral and hyperspectral mode. Panchromatic data is a single band data & generally available with high spatial resolution. On the other hand multispectral sensor operate in visible, Near Infrared (NIR), Mid-Infrared (MIR) and Thermal Infrared (TIR) regions of the electro-magnetic radiation (EMR) spectrum. It captures the data with a fewer number of bands (in 10s) and are useful for LULC mapping, but are unable to differentiate two spectrally similar features. With the evolution of technology, hyperspectral sensors came into picture which acquires data with 100s of contiguous spectral bands with narrow bandwidth (5-10nm) in the wavelength range of 400-2500nm. For detailed LULC (Land Use Land Cover) study hyperspectral sensors are now being widely used (Harsanyi and Chang, 1994). As these datasets have ample spectral information which enables precise identification of spectrally similar and unique materials which is not conceivable with traditional multispectral data.

2.2 Pre-processing of Multispectral and Hyperspectral Data

Satellite sensors either multispectral or hyperspectral captures the data as radiance but records the information as Digital Number (DN).The storage as DN values ensures noise free transmission from sensor on board satellite to ground receiving station. Therefore it is required to convert the DN data to radiance and then to surface reflectance using radiative transfer model for further investigation("Landsat_DN_to_Reflectance.pdf," 2015).

Conversion of multispectral data from DN to Radiance

There are two methods for converting multispectral data from DN to Radiance i.e by utilizing Gain and Bias of the sensor or by using L_{Min} and L_{Max} of a sensor given in the header information of the RS data.

Gain and Bias Method

The Gain and Bias Method uses the following equation for the converting DN image to radiance("Landsat_DN_to_Reflectance.pdf," 2015):

$$L = M * Q_{CAL} + A \qquad (2.1)$$

where,

L is the cell value as radiance

M is the multiplicative factor in ($W/m^2sr * \mu m$)/DN.

A is the additive factor in ($W/m^2sr * \mu m$).

Spectral Radiance Scaling Method

The equation use by spectral radiance scaling method is("Landsat_DN_to_Reflectance.pdf," 2015):

$$L_\lambda=(L_{Max\lambda}-L_{Min\lambda})/(Q_{CALMax}-Q_{CALMin}))*(Q_{CAL}-Q_{CALMin})+L_{Min} \quad (2.2)$$

where,

L_λ = radiance

Q_{CAL} = digital number

$L_{Min\lambda}$ = spectral radiance scales to Q_{CALMin}

$L_{Max\lambda}$ = spectral radiance scales to Q_{CALMax}

Q_{CALMin} = the minimum quantized calibrated pixel value

Q_{CALMax} = the maximum quantized calibrated pixel value.

Atmospheric correction of multispectral & hyperspectral data

Earth observation systems record signals, which always get obstructed by the atmosphere. The atmospheric contributions to the signals recorded from sensors become more critical in case where surface characteristics for land use classes need to be studied. To enable qualitative and quantitative studies of the earth surface, atmospheric perturbations need to be removed from the observed signal. The process of removing atmospheric contributions is commonly referred as atmospheric correction(Kawishwar, 2007).

Various atmospheric correction models have been developed in past for eliminating the effect of atmosphere on satellite images(Strobl et al., 2000)(Markelin, 2013). Some of them are Fast Line-of-Sight Atmospheric Analysis of Spectral Hypercube (FLAASH) developed on Moderate Resolution Atmospheric Radiance and Transmittance Model (MODTRAN), Atmosphere REMoval Program (ATREM), developed by ATCPRO on 5S Code (Simulation of the Satellite Signal in the Solar Spectrum) and ATmospheric Correction for Hyperspectral data (HATCH) based on 6S code (Second Simulation of the Satellite Signal in the Solar Spectrum)(Kawishwar, 2007).

Kruse, 2004(Kruse, 2004) has evaluated three atmospheric correction models ATREM, ACORN and FLAASH for getting surface reflectance data. ATREM (Atmospheric REMoval program) provides a basic level of atmospheric correction, however, is no longer being used. ACORN (Atmospheric CORrection Now) provides basic correction with enhancements for liquid water determination and some control over MODTRAN with additional multispectral

correction capabilities. However, Lu et al., 2002 had found FLAASH as best method for atmospheric correction of multispectral & hyperspectral data(Yuan and Niu, 2008). It is a more sophisticated algorithm based on MODTRAN that can compensate for atmospheric correction effects more accurately.

2.3 Data simulation

The simulation of remote sensing images is necessary for many chores, such as the definition of future earth observation systems, optimization of instrument parameters and for development and testing of complex data processing algorithms(Boggione et al., 2003)(Yan et al., 2014a). Therefore, it has a wide application in RS domain. SENSOR (Software Environment for the Simulation of Optical Remote sensing systems) is a tool for the simulation of hyperspectral remote sensing systems which is developed by German Aerospace Centre (DLR), Germany(Börner et al., 2001). The tool incorporate full model of the sensor hardware, the observed scene and the atmosphere which is in between sensor and the earth. The simulator is capable of

- Describing the geometrical relations between scene, sun, and the remote sensing system using a ray tracing algorithms
- Simulation environment by considering the radiometry
- Optical and an electronic sensor model for the generation of digital images.

G.A. Boggione (Börner et al., 2001) endeavoured to simulate high resolution panchromatic image from the coarser resolution multispectral images. In his work he revealed the potential of simulation approach for simulating ETM+ panchromatic bands by linearly combining ETM+ multispectral bands. This method takes into account the spectral overlapping between the simulated band and the MRS bands that can be linearly combined. Initially, the spectral MRS bands were transformed to a smaller grid size of 15 meters, then the same bands were linearly combined to improve the effective spatial resolution. The result of linear combination simulated a panchromatic image with better visual quality and good spatial resolution.

Hyperspectral Data simulation from Multispectral data

Many attempts using various algorithms were made in the past few years(Yan et al., 2014a)(Boggione et al., 2003) (Zhang et al., 2006a) (Schott et al., 2010)(Kavzoglu, 2004)(Yan et al., 2014a) to simulate the multispectral data using hyperspectral data whereas very few algorithms have been developed for simulating hyperspectral data from multispectral data. Zhang (Zhang et al., 2006)had proposed a spectral reconstruction Universal Pattern Decomposition Method (UPDM) for simulating multispectral data from Hyperspectral data.. However, similar spectral reconstruction approach was also applied by Bo Liu and Lei YAN (Liu et al., 2009) (Yan et al., 2014a)where they have simulated hyperspectral bands using EO-1 Advance Land Imager (ALI) multispectral data. The results of simulated HRS image were validated by comparing it with EO-1 hyperion data by applying visual interpretation, statistical & classification approaches.

Normalization of Ground Spectra

Normalization of the spectra collected from ground based spectroradiometer(Schläpfer et al., 1999) (Schläpfer et al., 1999)is done to compare the spectral signature of two different spectra from two different sensor having different spectral characteristics e.g. MRS and HRS sensors.

For normalization of ground spectra, spectral response function (SRF)("Spectral Response Functions," 2015)(Trishchenko et al., 2002) of the sensor is convolve with the ground spectra (simulation and correction of smile effect). Result of the normalization enables the use of same ground spectra for comparing the temporal data and different of different sensors.

For HRS data simulation normalized ground spectra was required and was one of the input for spectral unmixing and for generating the weighted fractional coefficients from multispectral data.

Spectral Unmixing

For simulation of hyperspectral data from multispectral data unmixing of multispectral data is required. Pixels in the RS data represents more than one LULC class are referred as mixed pixels and pixel representing only one feature is considered as pure pixel. Spectral unmixing is one of the technique used to identify the individual constituent materials present in the mixture, as well as the proportions in which they appear. Nirmal Keshava surveyed different types of unmixing technique and their characteristics to reveal the similarities and differences between algorithms(Keshava, 2003).

Spectral unmixing can be broadly classifies into two types i.e. linear and nonlinear(Parra et al., 1999). Linear unmixing model states that - "The reflected radiation conveys with the same proportions the characteristics of the associated materials if the total surface area is divided proportionally according to the fractional abundances of the constituent substances"(Tseng, 2000). Linear Mixture Model (LMM) is used in the area where features are organized proportionally within a pixel. It follows the linear equations for finding out the fractional coefficients in any RS image. Whereas, nonlinear unmixing model is used where the substances covering the area are not organized proportionally on the surface. As a result, occurrence radiation can encounter reflections with various substances, and the total range of reflected radiation might no more maintain the linear proportion. Therefore, for solving out such problem we assume that each pixel in an image can be expressed as a nonlinear combination of spectral pattern. Unlike LMM, nonlinear unmixing model utilize nonlinear equations for finding out the fractional coefficients in any RS image.

J. J. Settle a & N. A. Drake(Settle and Drake, 1993a) demonstrated the use of least square linear unmixing model for estimating the relative proportion of ground cover components in a mixed pixel. The result of LMM were compared with maximum likelihood and it was observed that LMM is faster and accurate classification technique for estimation of ground cover information. It also provides a knowledge of the error on each fractional proportion which is not obtained by using maximum likelihood classification technique.

Yi-Hsing TSENG (Tseng, 2000) used the two different linear spectral unmixing technique i.e. least squares (LS) unmixing and the Matched filter (MF) unmixing for the classification of hyperspectral images. It was observed that MF unmixing method proved itself to be an effective technique in classifying a hyperspectral image and provided a 90% classification accuracy whereas the LS unmixing technique did not show promising results. However, it was also explored that applying the LS unmixing to the Minimum Noise Fraction (MNF) transformed images the classification accuracy can be improved up to 20%.

Daniel C. Heinz(Heinz and Chang, 2001a)(Heinz and Chang, 2001) used the fully constrained least squares linear spectral mixture analysis method for material quantification in hyperspectral image. It is basically a least squares approach that simultaneously imposes two constraints, the ASC (abundance sum-to-one constraint) and the ANC (abundance non negativity constraint), on the linear mixture model.

Fabio Maselli(Maselli, 1998)proposed an advanced linear spectral unmixing technique which overcomes the drawback i.e. number of spectral components must be less or equal to the scene dimensionality (the so-called "condition of identifiability"). In this approach it is stated that if many spectral end-members are available, a subset with a prefixed number of end-members, that optimally decompose the candidate pixel, are first selected by a procedure based on the Gramm–Schmidt orthogonalization process. This procedure has been tested in different environmental situations and it was proved that the reduction in the residual error by this method is much higher (up to 70–80%) and the abundance images produced are more accurate estimates of the real components.

The least square linear spectral unmixing techniques can efficiently distinguish the spectral signature of different feature and hence are able to find the contribution of each class in a single pixel.

Linear unmixing model is mathematically represented (Settle and Drake, 1993a)as:

$$\boldsymbol{Pi} = \sum_{\boldsymbol{j=1}}^{\boldsymbol{n}} (\boldsymbol{Rij}.\boldsymbol{Fj}) + \boldsymbol{E} \qquad \textbf{(2.3)}$$

where, i= Number of bands (1 to m);

j= Number of End member(1 to n);

P_i= Reflectance value of ith pixel in remote sensing image

R_{ij}=Ground spectra of the jth component

Fj= fraction of coefficient to the jth component within the pixel.

Ei= Error for the jth spectral band.

The solution to the linear spectral unmixing problem requires the following conditions:

$$\sum_{\boldsymbol{j=1}}^{\boldsymbol{n}} \boldsymbol{Fj} = \mathbf{1} \text{ and } \boldsymbol{Fj} \geq \boldsymbol{0}, \quad \boldsymbol{for\ j=1,\ldots.n} \qquad \textbf{(2.4)}$$

PDM (Pattern Decomposition Method)

K. Muramatsu (Muramatsu et al., 2000)(Daigo et al., 2004) (Pattern decomposition method in the albedo space for Landsat TM and MRS data analysis) developed a sensor dependent Pattern Decomposition Method (PDM) for reducing the dimensionality of the RS data sets based on spectral unmixing approach. In this method, the spectral response patterns for each pixel in an image are decomposed into three components using three standard spectral patterns of vegetation, water and soil normalized to unity. K. MURAMATSU applied this technique to thee satellite images obtained from Landsat Thematic Mapper, where 94% of the six dimensional data are effectively transformed into three-dimensional components.

However, similar technique was applied by M. Daigo(Daigo et al., 2004) for hyper-multi-spectral data analysis a concept of supplementary spectral patterns was introduced for the study of specific ground objects including three standard features (vegetation, water and soil). PDM technique was applied to the ground samples i.e. set of continuous spectral reflectance data in the wavelength range from 350 nm to 2500 nm and were decomposed into four standard pattern components (three standard pattern component viz. vegetation, water & soil and one supplementary component).

Further a new revised Vegetation Index (VI) was proposed as a simple function of the pattern decomposition coefficients including standard pattern and supplementary vegetation pattern for examining the wilted leaf of vegetation.

UPDM (Universal Pattern Decomposition Method)

LIFU ZHANG(Zhang et al., 2006) developed UPDM (Universal Pattern Decomposition Method) to obtain sensor- independent pattern coefficients for reflectance data. In this method, the spectral response patterns of vegetation, water and soil were normalized with the Spectral Response Function (SRF) of Landsat/ETM +, Terra/MODIS and ADEOS-II/GLI("USGS EO-1 Website - http://eo1.usgs.gov," 2015).
The normalized ground spectra for each pixel in an image was decomposed into 1260 bands with 1 nm spacing using linear unmixing technique.

The sensor- independent UPDM technique is used for simulation of various datasets. Once the data is simulated, there is requirement to validate the simulated result using various methods like spectral separability analysis and classification.

2.4 Spectral Separability Analysis

Spectral separability analysis is used to identify materials based on their spectral characteristics. It uses technique such as such as Binary Encoding (BE), Spectral Angle Mapper (SAM) and Spectral Feature Fitting (SFF) to quantify the match of an unknown spectrum to the materials in a ground spectra/spectral library. A collection of spectra measured in the field or laboratory for materials (minerals, vegetation types, etc.) that are often used as a baseline, or "true" spectra, for identification of materials from remote sensing imagery("Hyperspectral Analysis: SAM and SFF Tutorial (Using ENVI) | Exelis VIS Docs Center," 2015).

Binary encoding (BE)

The binary encoding technique encodes the data and endmember spectra into zeros and ones, based on whether a band falls below or above the spectrum mean, respectively. An exclusive OR function compares each encoded reference spectrum with the encoded data spectra.

The output of the spectral separability analysis is weighted score for each of the materials in the input spectral library. The highest score indicates the closest match and indicates higher confidence in the spectral similarity. It is possible that similar materials may have relatively high scores, but unrelated materials should have low scores("Hyperspectral Analysis: SAM and SFF Tutorial (Using ENVI) | Exelis VIS Docs Center," 2015).

Spectral Angle Mapper (SAM)

The technique determines the spectral similarity between two spectra by calculating the angle between the spectra and treating them as vectors in a space with dimensionality equal to the number of bands shown in Figure 1. This techniques is relatively insensitive to illumination and albedo effects.

SAM compares the angle between the endmembers spectrum vector and each pixel vector in n-D space. Smaller angles represent closer matches to the reference spectrum. Pixels further away than the specified maximum angle threshold in radians are not classified("Hyperspectral Analysis: SAM and SFF Tutorial (Using ENVI) | Exelis VIS Docs Center," 2015).

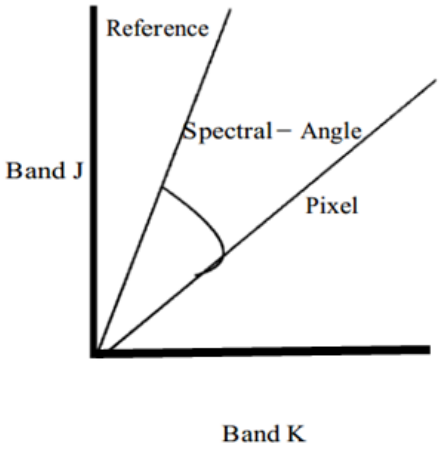

Figure 1: Spectral angle Mapper

SAM ("Hyperspectral Analysis: SAM and SFF Tutorial (Using ENVI) | Exelis VIS Docs Center," 2015) determined the similarity by applying following equation:

$$a = \cos^{-1}\left(\frac{\sum_{i=1}^{nb} t_i r_i}{\sqrt{\sum_{i=1}^{nb} t_i^2}\sqrt{\sum_{i=1}^{nb} r_i^2}}\right) \quad \textbf{(Eqn 2.5)}$$

Here,

nb : the number of bands in the image,

t: pixel spectrum,

r: reference spectrum and alpha: spectral angle

Spectral Feature Fitting (SFF)

Spectral Feature Fitting (SFF) is an absorption-feature-based method for matching image spectra to reference endmembers. Spectral feature fitting requires that reference endmembers be selected from either the image or a spectral library, that both the reference and unknown spectra have the continuum removed, and that each reference endmember spectrum be scaled to match the unknown spectrum. A "scale" image is produced for each endmember selected for analysis by first subtracting the continuum-removed spectra from one, thus inverting them and making the continuum zero. A single multiplicative scaling factor is then determined that makes the reference spectrum match the unknown spectrum. Assuming reasonable spectral ranges have been selected, a large scaling factor is equivalent to deep spectral feature, while a small scaling factor indicates a weak spectral feature. A least-square-fit is then calculated band-by-band between each reference endmember and the unknown spectrum. The total root-mean-square (RMS) error is used to form an RMS image for each endmember("Hyperspectral Analysis: SAM and SFF Tutorial (Using ENVI) | Exelis VIS Docs Center," 2015).

Classification

Various classification techniques have been discovered for the classification of the remote sensing images. One of the technique widely used for multispectral and hyperspectral image classification is Spectral Angle Mapper(SAM) (Roberts et al., 1998). This technique has been used for spectral separabiltiy analysis as well. SAM is an automated method for directly comparing image spectra to a known spectra (usually determined in a lab or in the field with a spectrometer) or an endmember. This method treats both spectra (the image spectra and reference spectra) as vectors and calculates the spectral angle between them. This method is insensitive to illumination since the SAM algorithm uses only the vector direction and not the vector length.

H. Lumme (Lumme, 2004)done the comparative analysis of SAM, Maximum Likelihood and Spectral Correlation Mapper (SCM) method for classifying soil and vegetation using field spectra. Where it was found that the overall accuracy of the Maximum Likelihood classification was 91 percent, but the results deteriorated under varying illumination.

Whereas, SAM and SCM were faster and they led to better classification results in poor illumination also.

2.5 Python Programming language

Free and open source tools offer excellent implementation and tool development for data processing and visualisation. Python is a general-purpose interpreted, interactive, object-oriented, and high-level programming language invented by Guido van Rossum during 1985-1990. It is an open source programming language which provides environment for implementing application specific algorithms. It is released under the Python Software Foundation License and is available for download free of charge under Linux, Mac OSX and Windows XP/Vista/7/8("Welcome to Python.org," 2015).

It is a high level programming language allowing access to advanced data structures, 2-D and 3-D graphical functions. It is widely used for mathematical computation, simulation, 2-D & 3-D visualization, optimization, statistical analysis, signal and application development. Python supports multiple paradigms, including object-oriented, imperative and functional programming or procedural styles.("Welcome to Spectral Python (SPy) — Spectral Python 0.16.0 documentation," 2015)("Welcome to Python.org," 2015). It has a large and comprehensive standard library available for variety of applications and software development.

Spectral Python (Spy)

Spectral Python (Spy)("Welcome to Spectral Python (SPy) — Spectral Python 0.16.0 documentation," 2015) is a python module for hyperspectral data handling. It is freely available and released under the General Public License, GNU Spy incorporates functions for reading, visualizing, analyzing, manipulating and classification for HRS data.

Spy is not a self-sufficient library, it need certain dependencies and supporting libraries. These dependencies includes Python 2.6+ or 3.3 +, NumPy, Pillow or Python Imaging Library (PIL), wxPython, matplotlib, Ipython and PyOpenGL.

3 Study Area and Materials Used

3.1 Study Area

The study area selected is the city of Rishikesh and its surrounding area (Longitude 30° 07’ and Latitude 78° 19') in Uttarakhand state of India (Figure 2). The area lies in the foothills of the Himalayas at mean altitude of 390 meters above mean sea level and has an undulating terrain covering a part of Rajaji national park, Ganga river and range of Shivaliks. Forest, urban, water body, grassland and cropland are the prominent LULC classes present in the study area.

To the northwest of the study area Chandrabhaga seasonal river lies which drains into the Ganges in the north east during the monsoon. The Ganga which flows from north east finally meets Pashulok Barrage situated in south of Rishikesh. Because of the presence of Ganga river the southern part of the study area is dominated with urban, grassland & cropland. The major urban classes includes commercial and residential area.

The western part of the study area is dominated by a forest area viz. ‘Barkot Forest Range’ and it also contains scrubs and cropland. The major classes of forest are Tectonagrandis (Teak) & Shorea robusta (Sal) and of cropland are wheat/rice & sugarcane.

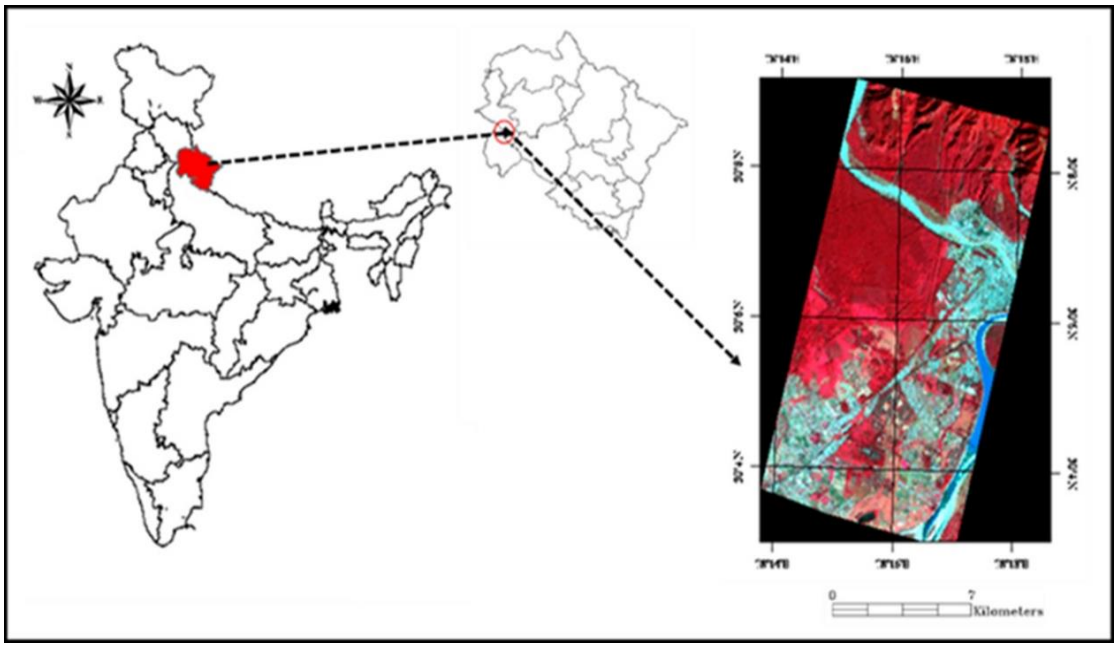

Figure 2 Study Area

3.2 Materials used

To achieve the objective in present study the following satellite data products, ancillary data, software and field surveyed data have been used.

Data sets used

The study has utilized following satellite datasets

Table 1: Data sets used

S.No	Satellite /Sensor	Acquisition Date	Resolution (m)
1	EO-1 Hyperion	27 November 2009	30
2	EO-1 ALI	27 November 2009	30
3	Landsat-8 OLI	7th December 2013	30
4	Resourcesat-2 LISS III	26th November 2013	23.5
5	Resourcesat-2 LISS IV	31st March 2014	5.8

- **EO-1 Hyperion data**

Hyperion is an EO-1 (Earth Observation-1) sensor which was developed under NASA's new millennium program in November, 2000. The Hyperspectral Imager (Hyperion) instrument provides high quality calibrated data that can support evaluation of hyperspectral technology for Earth observing missions. Hyperion is a push broom imaging instrument. Each image taken in this configuration captures the spectrum of a line 30m along-track by 7.5Km wide perpendicular to the satellite motion. There are 242 unique spectral channels collected with a complete spectrum covering from 357 - 2576 nm. The Level 1 Radiometric product has a total of 242 bands but only 198 bands are calibrated. Because of an overlap between the VNIR and SWIR focal planes, there are only 196 unique channels. Calibrated channels are 8-57 for the VNIR, and 77-224 for the SWIR. The reason for not calibrating all 242 channels is mainly due to the detector's low responsively. The bands which are not calibrated are set to zero in those channels. The digital values of the Level-1 product are 16-bit radiances and are stored as a 16-bit signed integer.("USGS EO-1 Website - http://eo1.usgs.gov," 2015)

Table 2: Specification of EO-1 Hyperion

Sensor altitude	705 Kms	**No. of rows**	256
Spatial resolution	30 metres	**No. of columns**	3128
Radiometric Resolution	16 bits	**VNIR**	0.45-1.35 µm
Swath	7.5 Kms	**SWIR**	1.40-2.48 µm
IFOV (mrad)	0.043		

- **EO-1 ALI satellite data**

The Advanced Land Imager (ALI) Multispectral (MS) instrument is the primary instrument in the first EO-1 (Earth Observation-1) satellite. The ALI employs novel wide-angle optics and a highly integrated multispectral and panchromatic spectrometer. Operating in a push

broom fashion with swath width of 37 km at an orbit of 705 km. It has nine MS bands plus a Panchromatic (Pan) band, three more than ETM+, but does not have the thermal band. The spatial resolution of the MS bands is the same as that of ETM+ (30 m) but it is better in the Pan band (10 m versus 15 m). ("USGS EO-1 Website - http://eo1.usgs.gov," 2015)

Table 3: Specification of EO-1 ALI

Band	Wavelength(μm)	Ground Sample Distance(m)
PAN	0.48 - 0.69	10
MS - 1'	0.433 - 0.453	30
MS - 1	0.45 - 0.515	30
MS - 2	0.525 - 0.605	30
MS - 3	0.63 - 0.69	30
MS - 4	0.775 - 0.805	30
MS - 4'	0.845 - 0.89	30
MS - 5'	1.2 - 1.3	30
MS - 5	1.55 - 1.75	30
MS - 7	2.08 - 2.35	30

- **Landsat - 8 (OLI) satellite data**

Landsat 8 carries two instruments: The Operational Land Imager (OLI) sensor includes refined heritage bands, along with three new bands: a deep blue band for coastal/aerosol studies, a SWIR band for cirrus detection, and a Quality Assessment band. The Thermal Infrared Sensor (TIRS) sensor provides two thermal bands. These sensors (with swath of 185 km) provide improved signal-to-noise (SNR) radiometric performance quantized over a 12-bit dynamic range. Improved signal to noise performance enable better characterization of land cover state and condition. Products are delivered as 16-bit images (scaled to 55,000 grey levels).The specification of the dataset is given in table 4("Landsat 8," 2015):

Table 4: Specification of Landsat 8 OLI

Bands	Description	Spectral Range (μm)	Instrument	Resolution
OLI band 1	coastal blue	0.43–0.45	OLI	30 m
OLI band 2	blue	0.45–0.51	OLI	30 m

OLI band 3	green	0.53–0.59	OLI	30 m
OLI band 4	red	0.64–0.67	OLI	30 m
OLI band 5	near infrared	0.85–0.88	OLI	30 m
OLI band 6	SWIR-1	1.57–1.65	OLI	30 m
OLI band 7	SWIR-2	2.11–2.29	OLI	30 m
OLI band 8	panchromatic	0.50–0.68	OLI	15 m
OLI band 9	cirrus	1.36–1.38	OLI	30 m

- **Resourcesat -2 LISS III and LISS IV**

The Linear Imaging Self Scanner instrument is the primary instrument on the Resourcesat-2 satellite launched by Indian Space Research Organization (ISRO) in the year 2011. The satellite operates in a circular, sun-synchronous, near polar orbit with an inclination of 98.69 deg, at an altitude of 817 Km. The satellite takes 101.35 minutes to complete one revolution around the earth and completes about 14 orbits per day. The entire earth is covered by 341 orbits during a 24 day cycle.("Welcome to Bhuvan | ISRO's Geoportal | Gateway to Indian Earth Observation," 2015)("Resourcesat-2_Handbook.pdf," 2015). The three instruments on-board Resourcesat- 2 are LISS III, LISS IV & AWiFS. The specifications of LISS III & LISS IV are given in table 5.

Table 5: Specification of LISS III and LISS IV of Resoursat-2

Specification	LISS III	LISS IV
No. of Bands	4	1 (Mono), 3 MX
Spectral Range (μ)	B2 0.52 – 0.59 B3 0.62 – 0.68 B4 0.77 – 0.86 B5 1.55 – 1.70	B2 0.52 – 0.59 B3 0.62 – 0.68 B4 0.77 – 0.86 B3-default band for mono
Resolution (m)	23.5	5.8
Swath (Km)	140	70
Quantisation	10	10

Instruments used

- Spectro radiometer (SVC HR 1024)
- Handheld GPS

Software used

- ENVI 5.0 – For data pre-processing
- Python- For implementing complex algorithms for HRS data simulation
- Excel- For calculations and analysis.

Other data sets used

SRF (spectral response function) of the following data sets are used for atmospheric correction and simulation:

- EO-1 ALI
- EO-1 Hyperion
- Landsat-8 OLI
- RS- 2 LISS III & LISS IV

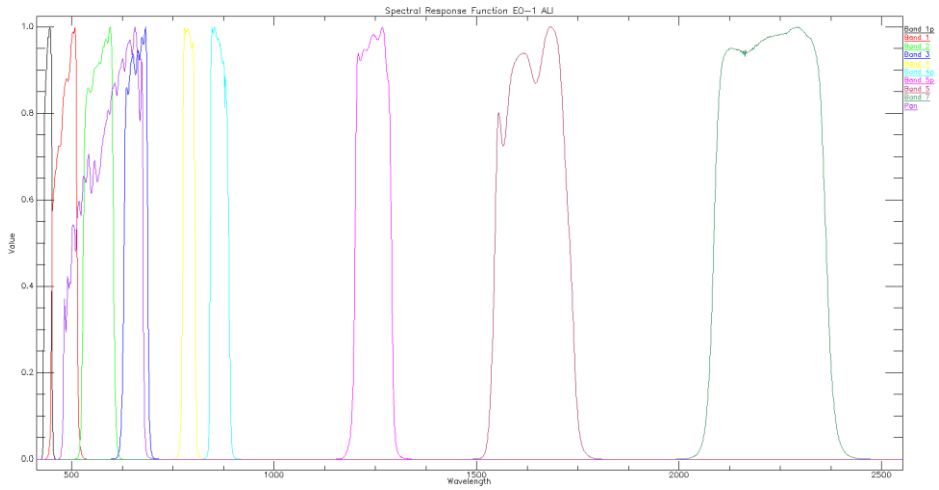

Figure 3: SRF of EO-1 ALI

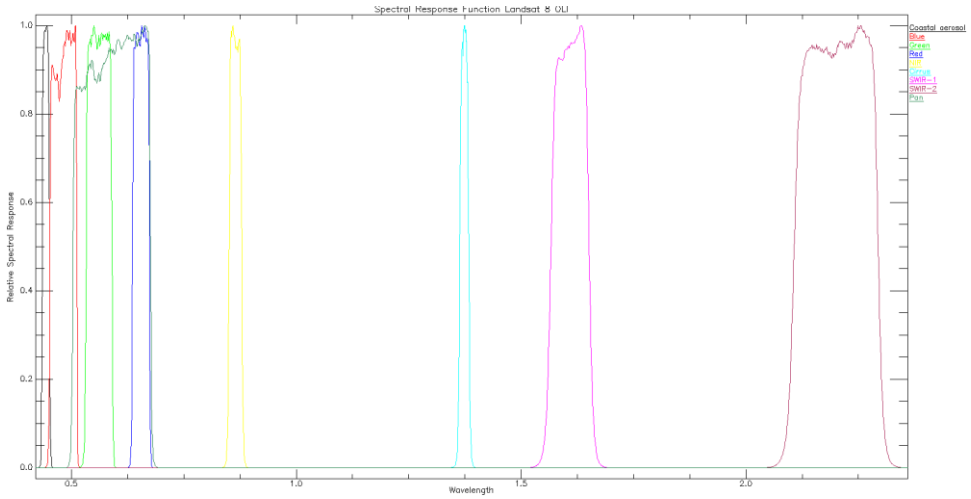

Figure 4: SRF of Landsat 8 OLI

4 Methodology

The chapter presents the methodological approach followed for the simulation of HRS data from MRS data using spectral reconstruction technique. The research has been divided four phases:-

- Data pre-processing
- Field data collection
- Simulation of hyperspectral data
- Development of open source software for HRS data Simulation.

A detailed description of the methods adopted for the present study is enlightened in the block diagram (Figure 5)

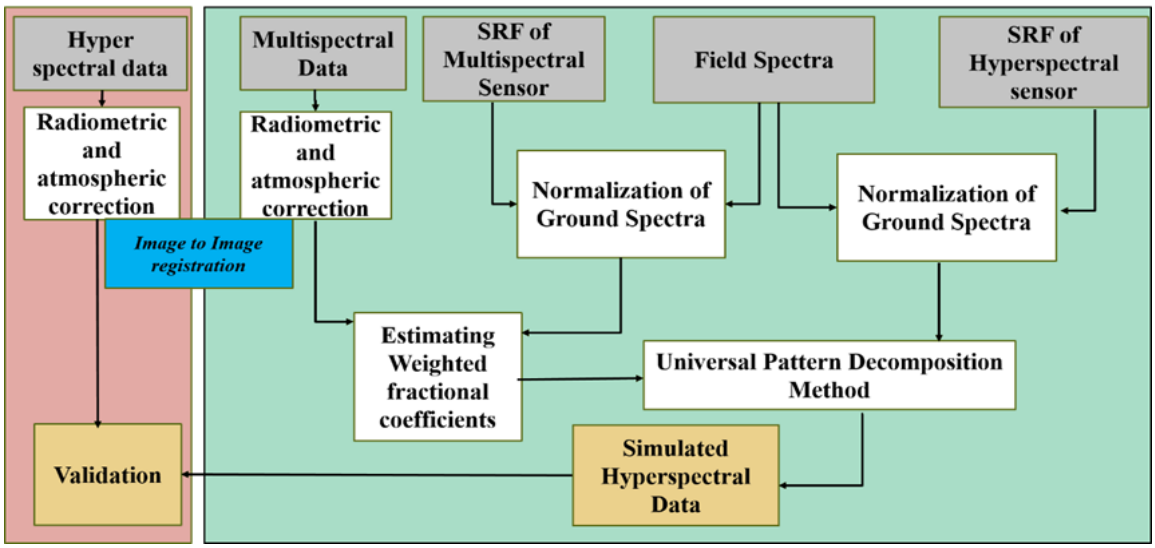

Figure 5: Project Methodology

4.1 Data Pre-processing

Data pre-processing of MRS and HRS data includes radiometric and atmospheric correction. Detailed description of the pre -processing steps are explained in the section below.

Multispectral Data Pre-processing
Multispectral data pre-processing includes following steps demonstrated in Figure 6:

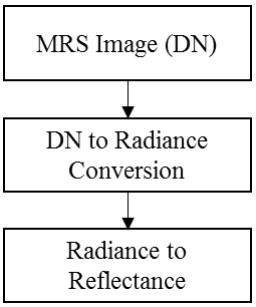

Figure 6: Methodology for MRS data Pre-processing

- **DN to radiance Conversion**

The sensor receives radiance energy but stores the information in digital form for the noise free transmission from sensor to ground station. Hence it is required to convert the data back to the radiance. Gain bias and spectral radiance scaling method are the two methods which uses the header information to transform the DN data into radiance. The equations used for converting the DN data to radiance are:

- Gain bias Method (Equation 2.1)
- Spectral Radiance Scaling Method (Equation 2.2)

In the present study, Gain and bias method ("Landsat_DN_to_Reflectance.pdf," 2015)is used to convert DN of EO-1 ALI data to radiance whereas for converting Landsat 8 OLI & Resourcesat-2 LISS –III and LISS IV DN data spectral radiance scaling method is used.

The calibration coefficients for each sensor can be obtained from the metadata file. The calibration coefficient's for EO-1 ALI, Landsat-8 OLI and Resourcesat-2 LISS III & LISS IV is given in the table 6- table 9.

Table 6:Calibration coefficients for EO-1 ALI

Band	Multiplicative calibration coefficient, M (W/m^{2}sr * µm)/DN.	Additive calibration coefficient , A (W/m^{2}sr * µm)
PAN	0.024	-2.2
MS - 1'	0.045	-3.4
MS - 1	0.043	-4.4
MS - 2	0.028	-1.9
MS - 3	0.018	-1.3
MS - 4	0.011	-0.85
MS - 4'	0.0091	-0.65
MS - 5'	0.0083	-1.3
MS - 5	0.0028	-0.6
MS - 7	0.00091	-0.21

Table 7: Calibration coefficients for Landsat 8 OLI

Band	Q_{CalMax}	Q_{CalMin}	$L_{Min\lambda}$	$L_{Max\lambda}$
1 Costal aerosol	65535	1	783.06348	64.66564
2 Blue	65535	1	801.86658	66.21840
3 Green	65535	1	738.91321	61.01969
4 Red	65535	1	623.09320	51.45524
5 NIR	65535	1	381.30197	31.48804
7SWIR 1	65535	1	31.96155	-2.63940
8 SWIR 2	65535	1	705.17004	58.23317

Table 8: Calibration coefficients for Resourcesat-2 LISS III

Band (μm)	Q_{CalMax}	Q_{CalMin}	$L_{Max\lambda}$	$L_{Min\lambda}$
B2 0.52 – 0.59	1024	0	52.00	0
B3 0.62 – 0.68	1024	0	47.00	0
B4 0.77 – 0.86	1024	0	31.50	0
B5 1.55 – 1.70	1024	0	7.50	0

Table 9: Calibration coefficients for RS 2 LISS IV

Band (μm)	Q_{CalMax}	Q_{CalMin}	$L_{Max\lambda}$	$L_{Min\lambda}$
B2 0.52 – 0.59	1024	0	52.00	0
B3 0.62 – 0.68	1024	0	47.00	0
B4 0.77 – 0.86	1024	0	31.50	0

The acquired dataset from different sensors have a different swath. Therefore, common area covered is taken by sub-setting the datasets (EO-1 ALI, Landsat 8 OLI, Resourcesat-2 LISS III and LISS IV).

- **Atmospheric correction**

To remove the adverse effects of atmosphere FLAASH atmospheric correction method is used for transforming the radiance data to surface reflectance. FLAASH is a sophisticated algorithm based on MODTRAN and incorporated in ENVI software developed by EXELIS. Input parameter FLAASH takes into account are scaling factor, average elevation of the study area, scene centre coordinates, sensor type, flight date and time, and information about aerosol distribution, visibility, and water vapour conditions(Strobl et al., 2000)(Kruse, 2004).

The input parameters used by the FLAASH atmospheric correction module are in table 10.

Table 10:Input parameter used for the atmospheric correction of Multispectral datasets

FLAASH Parameters	EO-1 ALI	Landsat 8 OLI	LISS III	LISS IV
Scene Centre Latitude	30º05´37.32´´E	30º05´37.32´´E	30º05´37.32´´E	30º05´37.32´´E
Scene Centre Longitude	78º16´13.44´´E	78º16´13.44´´E	78º16´13.44´´E	78º16´13.44´´E
Scaling Factor	40(VNIR) & 80(SWIR)	10	1	1
Pixel Size	30 M	30 M	23.5 M	5.8 M
Sensor Type	Unknown MSI	Unknown MSI	Unknown MSI	Unknown MSI
Flight Date	27th November 2009	7th December 2013	26th November 2013	31th March 2014
Average Flight Time	5:9:55	5:20:00	5:42:14	5:37:00
Sensor Altitude	705km	705km	817km	817km
Ground Elevation	0.360km	0.360km	0.360km	0.360km
Atmospheric Model	MLS	MLS	MLS	MLS
Initial Visibility	40km	40km	40km	40km
Water Retrieval	No	No	No	No
Aerosol Model	Rural	Urban	Urban	Urban
Aerosol Retrieval	None	None	None	None
Initial visibility	40km	40km	40km	40km

Hyperspectral Data Pre processing

The figure 7 gives over all methodology for HRS data pre-processing:

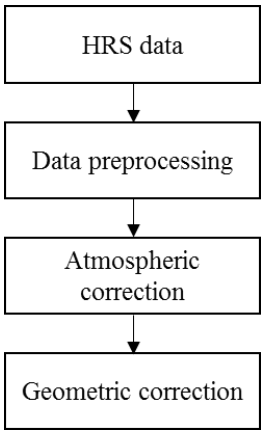

Figure 7: Methodology for HRS data Pre-processing

In this study EO-1 Hyperion data is required for validation of the results obtained. The EO-1 Hyperion dataset suffers from abnormal pixels and striping which needs to be preprocessed to rectify these anomalies prior to the atmospheric correction. The pre-processing steps required for correcting EO-1 Hyperion data are as follows:

- **Identification and removal of bad bands**

The Hyperion level 1 radiometrically corrected (L1R) product comprise of the 242 bands out of which 198 are non-zero. This is because of the substantial water assimilation and spectral cover between the two spectrometers set in the VNIR and SWIR regions. Some of the bands contain noise, negative values or no information (Table 10). This needs to be rectified before proceeding further. For the data used in the study a total of 132 bands are left after removal of bands with no information, negative values and noise. The details of the bands found noisy is depicted in table 11.

Table 11:Band containing no information

Bad bands	9,57,79,98,100,134,183,182,220,56,219,216,200,199,198,191,192,190,189,188,184,183,56

- **Identification and removal of bad columns**

There are numerous reasons for the irregular pixels, some of them are due to sensor related errors. The Hyperion framework secures information in the push broom mode, in which there is a separate detector to accumulate data for every column in the image it produces. One of the reason for data stripping is that the locators are not aligned appropriately. Some of the bands of the dataset used in the study are affected with bad column table 12. The bad column were recognized and replaced by taking the average DN value of the adjacent column in order to avoid imposing severe change in the spectra.

Table 12:Identified Bands with bad columns

No of Bands	Bad column number
12,13,14,15,16,17,18	114,113
27	47
53	25
55	13,17,20,32,37,39
54	25,13
83	224,245,252,256
94,95,97,99	91,130,191
100	129,130,131
116	137
119	239
152,153	136
162,163	147
200,201	6,7,8

It is observed that some bad pixel having negative values are randomly distributed in the data set which are difficult to identify manually. For removing those bad pixels in the dataset a 3x3 and 5x5 filter Figure 8 is designed which is convolved with the image in the nested loop condition.

1	1	1
1	0	1
1	1	1

1	1	1	1	1
1	1	1	1	1
1	1	0	1	1
1	1	1	1	1
1	1	1	1	1

Figure 8: Kernel used for bad pixel removal

- **Atmospheric correction of EO-1 Hyperion data**

After the correction of sensor related error which existed in the L1R (Level 1 radiometrically corrected) Hyperion data, atmospheric correction is carried out to get the surface reflectance. FLAASH model is used for atmospheric correction of EO-1 Hyperion data. The input parameters used by FLAASH(San and Suzen, 2010)(Kruse, 2004)(Yuan and Niu, 2008) for correction of EO-1 Hyperion data are in table 13:

Table 13: Input parameter used for the atmospheric correction of EO-1 Hyperion data

Parameter	Value
Scene Centre Latitude	23^0 40’ 33.60”
Scene Centre Longitude	78º15´48.59´´E
Scaling factor	400 VNIR and 800 SWIR
Sensor Type	Hyperion
Flight Date	Nov 27th 2009
Average Flight Time	5:2:00
Sensor Altitude	705km
Ground Elevation	0.390km
Atmospheric Model	MLS
Water Retrieval	Yes (1135m)
Aerosol Model	Urban
Aerosol Retrieval	None
Initial visibility	40km
Spectral Policing	Yes (9 bands)
Wavelength Recalibration	No

Geometric Correction

All the multispectral dataset were co-registered with respect to LISS IV data. The atmospherically corrected EO-1 Hyperion data was then co-registered using EO-1 ALI data by identifying sufficient and uniformly distributed GCPs.

4.2 Field Data Collection

GPS locations and Spectral data collection

Ground spectra of different features were collected within the study area using spectro-radiometer along with respective GPS coordinate (using hand held GPS) and photographs. The data acquired by spectro-radiometer is in the wavelength range of 350-2500nm. These ground spectra includes major forest classes such as Sal (Shorea robusta), Teak (Tectona grandis), Acasia, Mango (Mangifers indica), Lantana, Grass land, Curry leaves, cropland, urban features (cemented roof, road, bricks), water body and sand etc. depicted in Figure 9

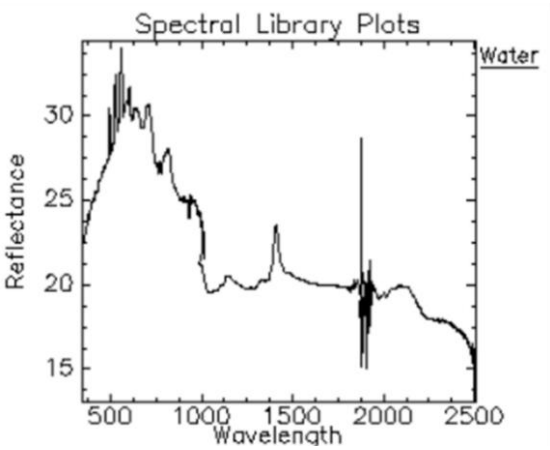

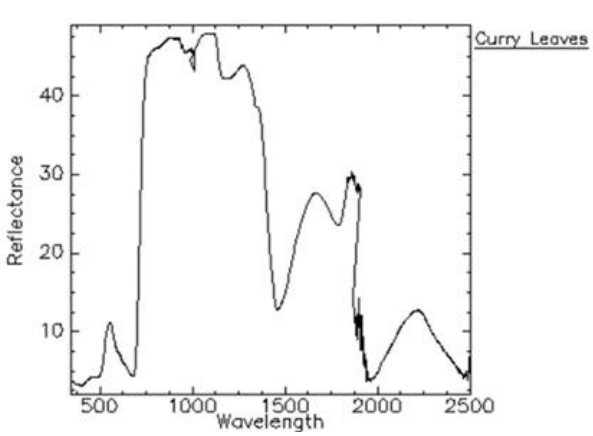

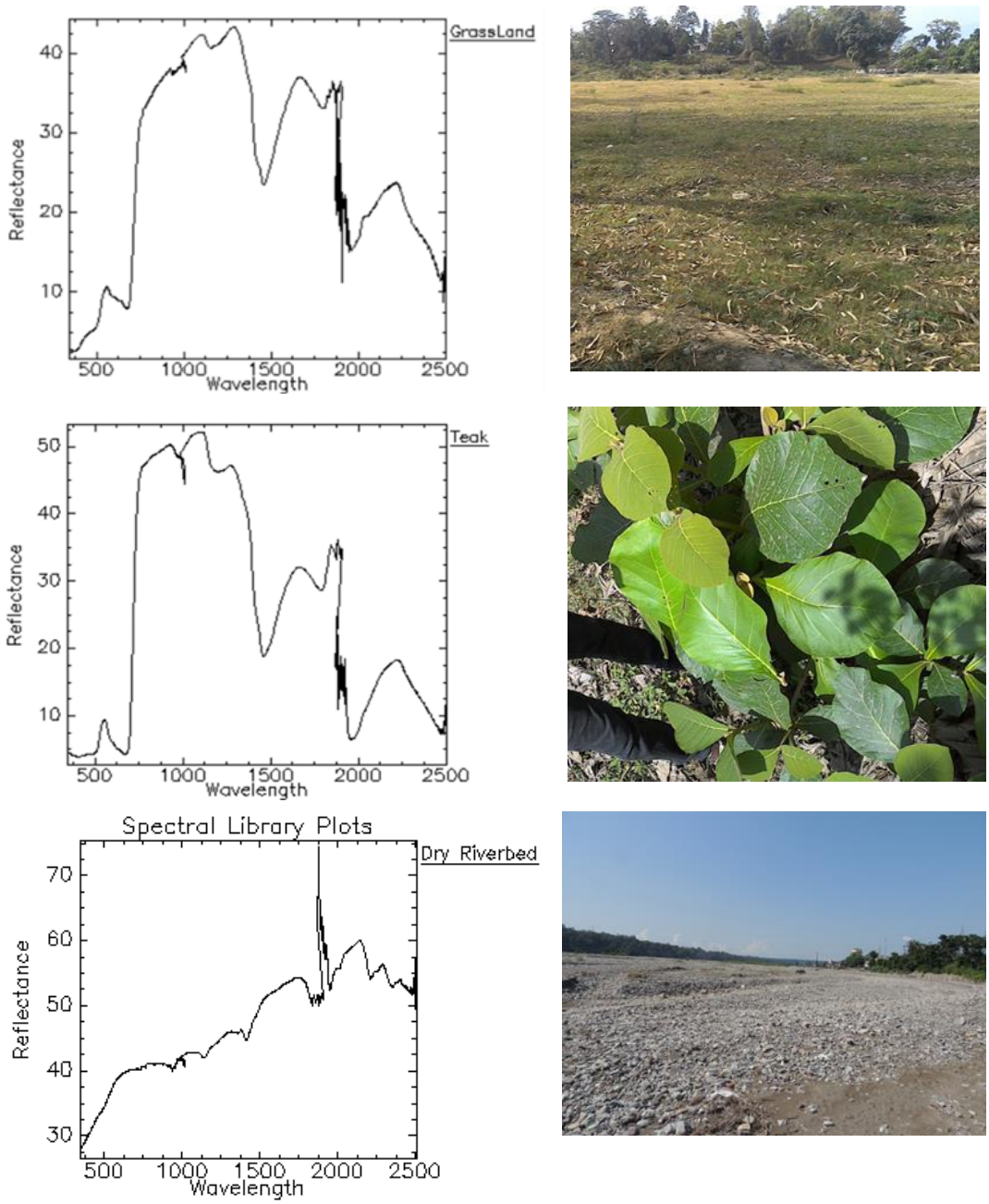

Figure 9: Ground spectra collected using HR1024 spectro radiometer

A spectral library was created using the ground spectra of various LULC features Figure 10.

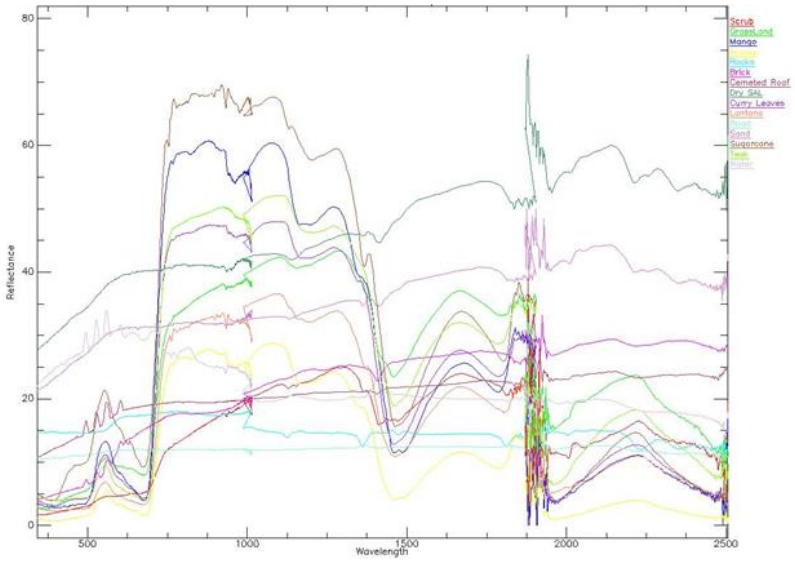

Figure 10: Spectral library

4.3 HRS Data Simulation

HRS data simulation has been carried out in following three steps.

- Normalization of ground spectra
- Estimation of weighted fractional coefficient image from MRS data.
- Simulation of HRS data.

Normalization of ground spectra

Ground spectra is generally collected in the contiguous wavelength range of 400 nm to 2500 nm. But different sensor MRS & HRS acquire data in different wavelength and have different spectral bandwidth. In order to compare the spectral signature of two different sensor normalization is to be carried out.

Normalization is the process in which ground spectra with fine spectral resolution is convolve with the Spectral Response Function (SRF) of the sensor. In this study, ground spectra of vegetation, water, dry riverbed and cropland collected from field is convolved with the SRF of each sensor (EO-1 ALI, LS-8 OLI, Resourcesat-2 LISS III & LISS IV). The normalized spectra of these features serves as one of the input required for HRS data simulation

Estimation of weighted fractional coefficient's from MRS data

In this study, linear unmixing method is used for estimating the abundance of ground spectra present in each pixel of the image. Linear unmixing method takes normalized ground spectra and atmospherically corrected data for estimating the weighted fractional coefficients images.

In LMM, each pixel of the MRS data is assumed to be a linear mixture of normalized ground spectra in the image.

$$P_i = \sum_{j=1}^{n}(R_{ij}.F_j) \qquad \textbf{from eqn. (2.3)}$$

where, i= Number of bands (1 to m);

j= Number of end member(1 to n);

P_i= Reflectance value of ith pixel in remote sensing image

R_{ij}=Field spectra of the jth component (Vegetation, Water, Dry riverbed etc)

F_j= fraction of coefficient to the jth component within the pixel.

In the matrix form the linear unmixing equation (equation 2.3) can be represented as

$$P = RF \qquad (4.1)$$

$$P = \begin{bmatrix} P_1 \\ P_2 \\ : \\ P_m \end{bmatrix} \quad R = \begin{bmatrix} R_{11} & R_{12} & \dots & R_{1n} \\ R_{21} & R_{22} & \dots & R_{11} \\ : & : & : & : \\ R_{m1} & R_{m2} & \dots & R_{mn} \end{bmatrix} \quad F = \begin{bmatrix} F_1 \\ F_2 \\ : \\ F_n \end{bmatrix}$$

For multispectral sensor equation (4.1) can be represented as

$$P_M = R_M F_M \qquad (4.2)$$

Where, suffix M denotes multispectral sensor.

Using least square method F_M can be computed as

$$F_M = (R_M{}^T R_M)^{-1} R^T{}_M P_M \qquad (4.3)$$

In the present study, linear unmixing is applied to MRS (EO-1 ALI, Landsat-8 OLI, Resourcesat-2 LISS III & LISS IV) data for estimating the fractional coefficients of each ground spectra present in the image. In case of EO-1 ALI, Landsat-8 OLI, Resourcesat-2 LISS III & LISS IV data, normalized spectra of vegetation, water, dry riverbed & cropland is used. But for Resourcesat-2 LISS IV data only 3 normalized spectra i.e. vegetation, water & dry riverbed is used. This is because LISS IV have only three bands and according to the principle of matrix dimensionality if the number of unknown variable is more than number of equations then the system becomes inconsistent and gives no solution.

Simulation of HRS data

The inputs required for HRS simulation is fractional coefficient image of MRS data. The normalized ground spectra of feature such to SRF of EO-1 Hyperion sensor. The bands are

reconstructed by applying spectral reconstruction technique by using these two inputs. The equations used for reconstruction is depicted below:

$$P_H = R_H F_H \quad (4.4)$$

As we know that

$$F_M = (P_M^T P_M)^{-1} P^T{}_M R_M \quad (4.5)$$

Here by replacing F_M with F_H we get

$$P_H = R_H (P_M^T P_M)^{-1} P^T{}_M R_M F_H \quad (4.6)$$

Here subscript H denotes Hyperspectral sensor.

4.4 Development of open source software for HRS data simulation

Python programming language is used for the development of the open source software for HRS data simulation. It is a high level language which gives environment for implementing application specific algorithms. Python has a large and wide-ranging of standard library available for variety of applications and software development. In the present study, Spectral python (Spy)("Welcome to Spectral Python (SPy) — Spectral Python 0.16.0 documentation," 2015) and PyQt library("Installing PyQt4 — PyQt 4.11.4 Reference Guide," 2015) is used for the development of HRS data simulation software.

Figure 11 demonstrate the overall flow of the tool development life cycle for the simulation of HRS data. The lifecycle is broadly divided into two modules. The first module deals with estimating the fractional coefficient image/unmixing coefficient image of the each ground spectra used. While the second module i.e. HRS data simulation module deals with HRS data simulation.

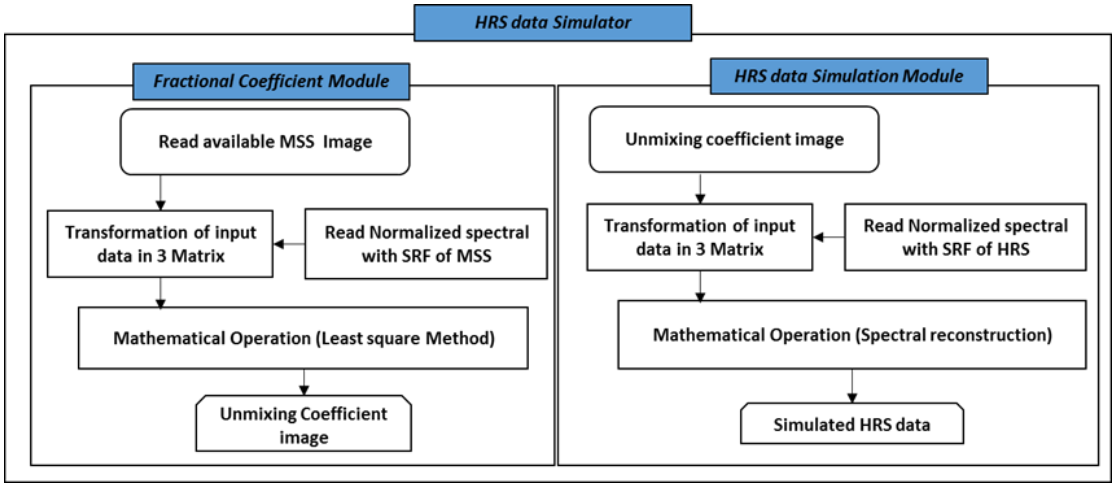

Figure 11: Methodology for software development

Module for Unmixing

Spectral Unmixing module is basically used for finding out the abundance of the ground spectra present in MRS data. The input required for this module are MRS data and normalized ground spectra with SRF of input MRS sensors data. Data reading of the multispectral image and normalized spectra of MRS are accomplished using Spy & Numpy libraries. MRS image is transformed to 3D matrix using Spy Library. After that least square method is carried out to find out the weighted fraction coefficients for MRS image of each ground spectra taken. GUI of linear unmixing module is depicted in Figure 12.

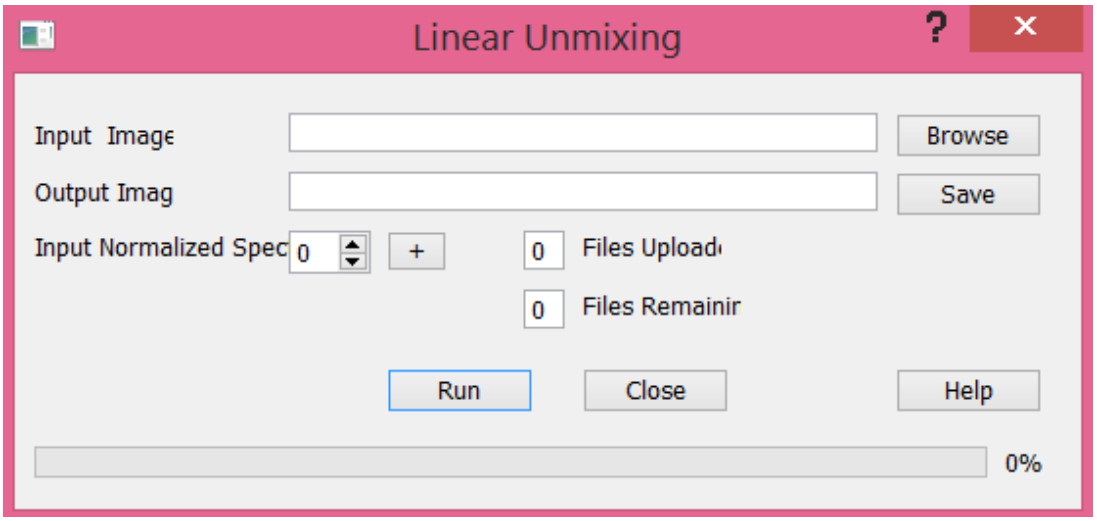

Figure 12: GUI of Unmixing Module

Module for HRS data simulation

This module deals with simulation of HRS data. The input required by this module are fractional coefficient image of MRS data and normalized ground spectra which is normalized to SRF of HRS sensors which are read using these Spy and Numpy libraries. Fractional coefficient image is transformed to 3D matrix using Spy Library. After that spectral reconstruction method is applied to reconstruct the HRS bands. The GUI of HRS data simulation module is depicted in Figure 13.

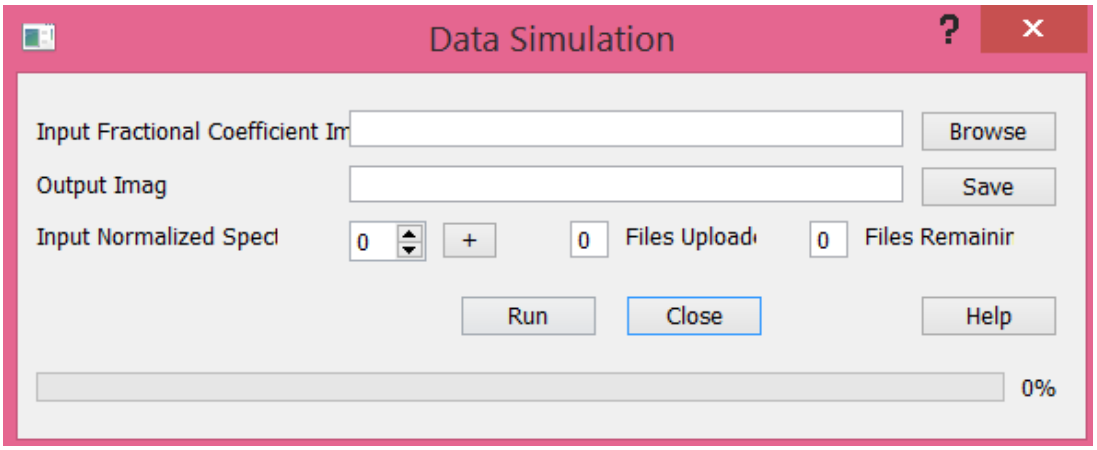

Figure 13: GUI of HRS data Simulation Module

4.5 Validation

Once the hyperspectral data is simulated from multispectral data, the validation is carried out using different approaches like visual interpretation, statistical analysis (correlation, spectral separability analysis etc.) and classification. The details of these techniques is depicted in table 14

Table 14: Validation of the simulated HRS data

S. No	Validation Method	Approach
1.	Visual Interpretation	Comparative analysis of different LULC features and their spectra
2.	Statistical Analysis	• SNR calculation • Spectral band to band correlation • Spectral separability analysis
3.	Classification	• Spectral Angle Mapper (SAM)

Note: Validation of HRS data from EO-1 ALI & Landsat 8 OLI is done using all the three approaches depicted in table 14. In case of HRS data simulated from Resourcesat 2 LISS III & LISS IV, spatial resolution is different whereas for finding band to band correlation, spatial resolution should be same. Therefore, validation of Resourcesat 2 LISS III & LISS IV cannot be done using correlation method.

5 Results and Discussion

This chapter includes detailed discussion of the results obtained as per the steps in methodology for simulating hyperspectral data. It also consists information about validating the results using visual interpretation, statistical analysis and classification. The software developed for simulation of HRS data using MRS data as a part of this project is also discussed in this chapter.

5.1 Atmospheric correction

FLAASH Atmospheric correction model is used for the correction of EO-1 ALI, Landsat 8 OLI, Resourcesat-2 LISS III & LISS IV and EO-1 Hyperion data. Results of the spectral profiles before and after atmospheric correction of the datasets were compared by considering the atmospheric absorption and diagnostic absorption feature. (Figure 14 to Figure 18). The spectra of vegetation, water and dry river bed was observed and they have shown significant improvement in the spectral profile after atmospheric correction. The results obtained for the three features after atmospheric correction are explained below in terms of their spectral profile.

Vegetation: The spectral diagnostic absorption is highlighted in the red band due to the chlorophyll content present in the leaves. In NIR wavelengths the internal structure of healthy leaves which acts as diffuse reflector has been observed as more reflection in NIR.

Dry Riverbed: The radiation incident upon sandy features like dry riverbed, urban etc. is reflects high in optical EMR region. Therefore dry riverbed is showing strong reflectance nature in all the bands of the datasets after correction.

Water: Majority of the radiation incident upon water is absorbed or transmitted in NIR region which is clearly observed in the resultant spectra.

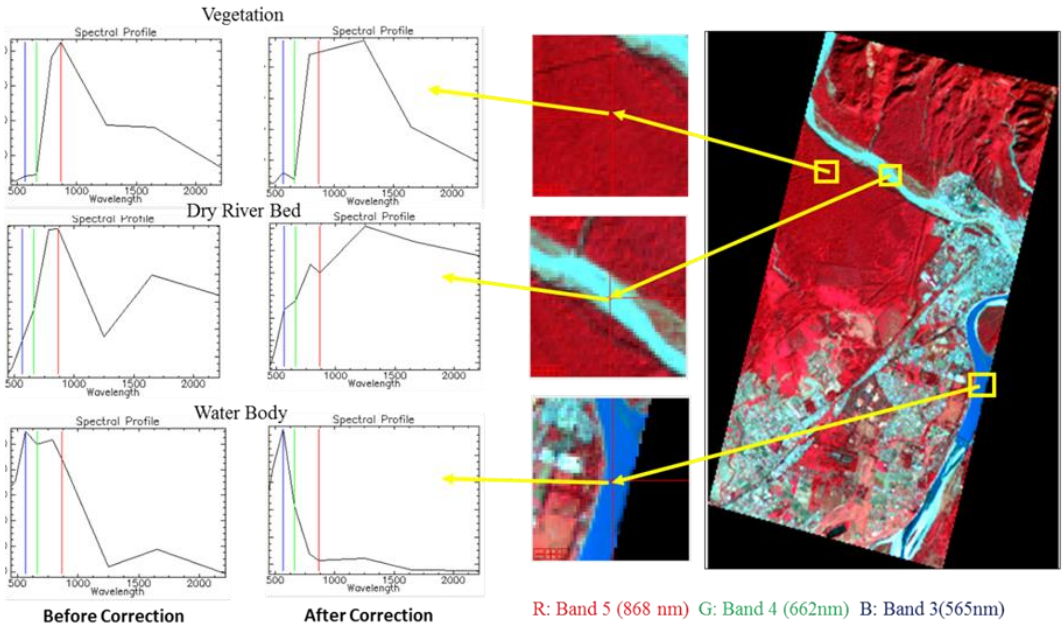

Figure 14: ALI before and after correction

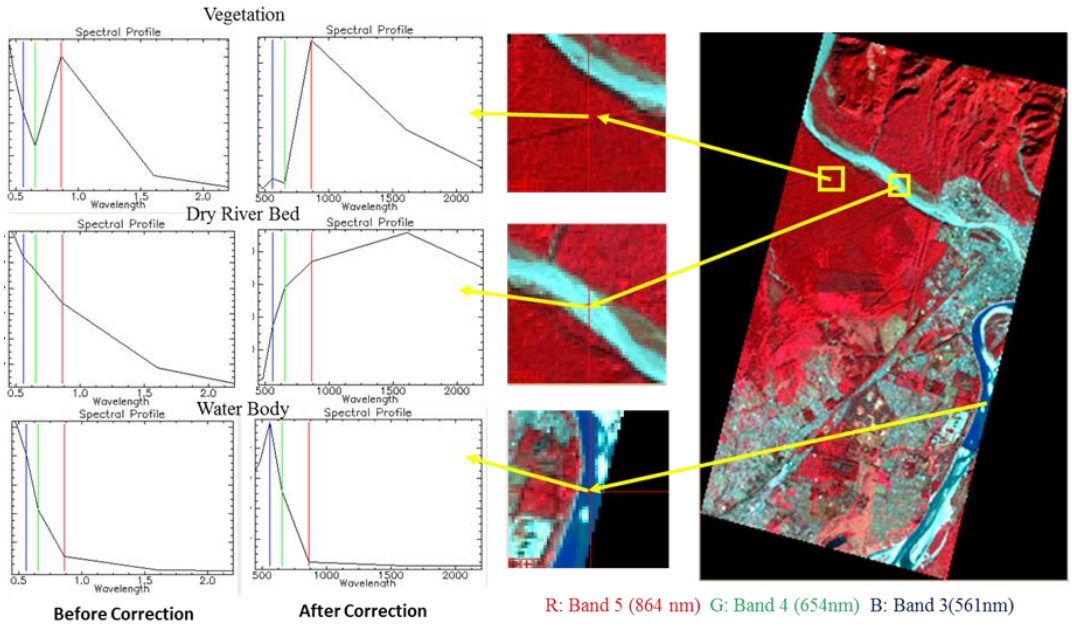

Figure 15: OLI before and after correction

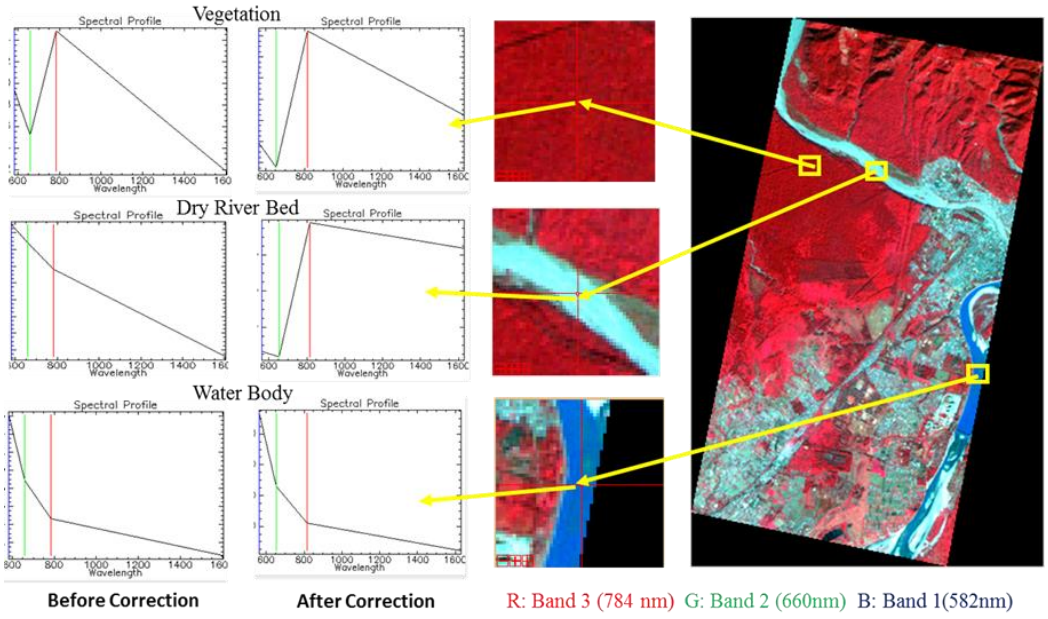

Figure 16: LISS III before and after correction

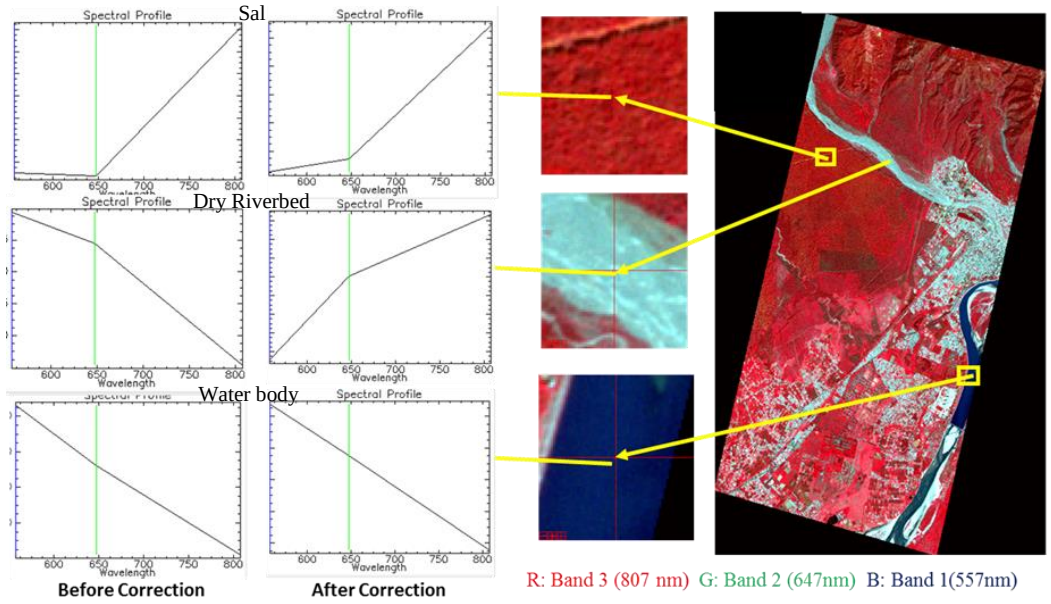

Figure 17: LISS IV before and after correction

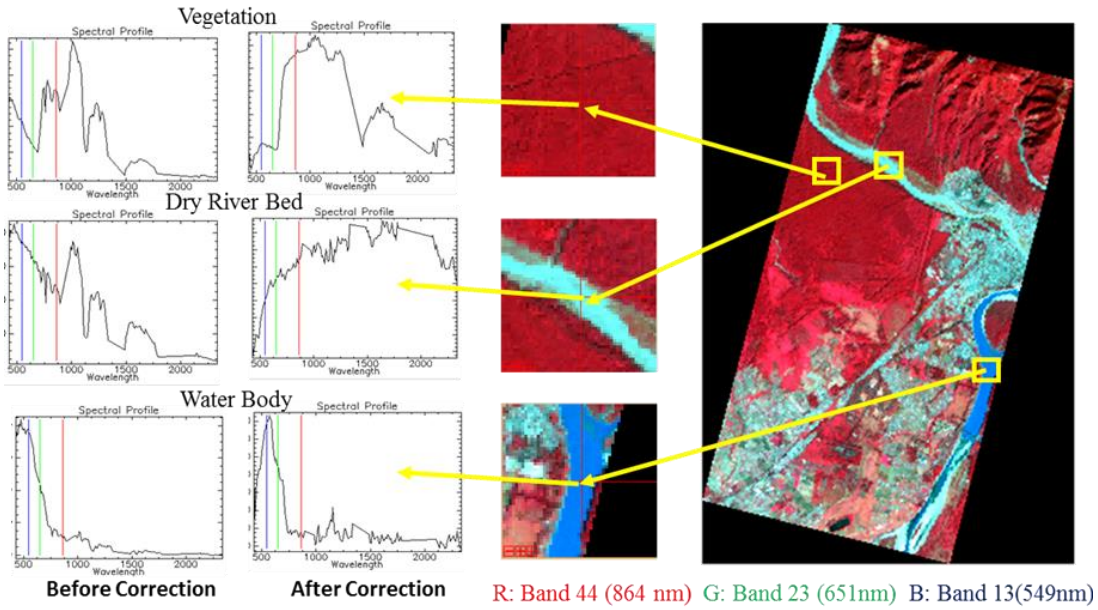

Figure 18: Hyperion before and after correction

5.2 Estimated weighted fractional coefficients

Weighted fractional coefficient images generated for each multispectral datasets (EO-1 ALI, Landsat 8 OLI, Resourcesat-2 LISS III & LISS IV) after linear unmixing are shown in Figure 19 to Figure 22. Each pixel in the fractional coefficient image is showing its abundance of each end member (vegetation, water, urban & agriculture). The abundance value ranges from zero to one. The pixels appearing brightest in the image corresponds to 1 i.e. showing maximum abundance whereas the pixel appearing darkest correspond to ground spectra which is submissive or doesn't contribute any abundance in the pixel.

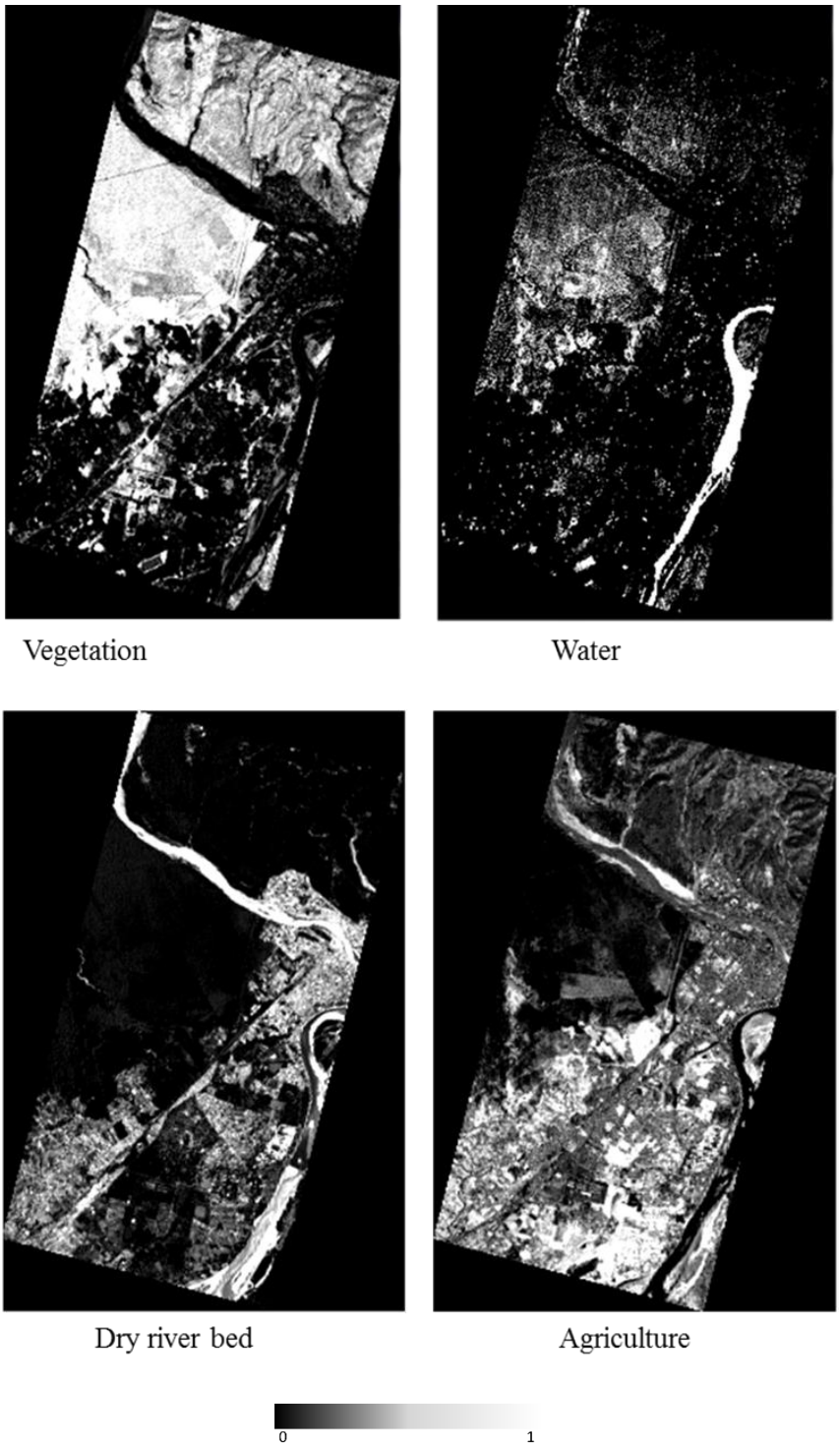

Figure 19: Weighted Fractional Coefficient of EO-1 ALI MRS data

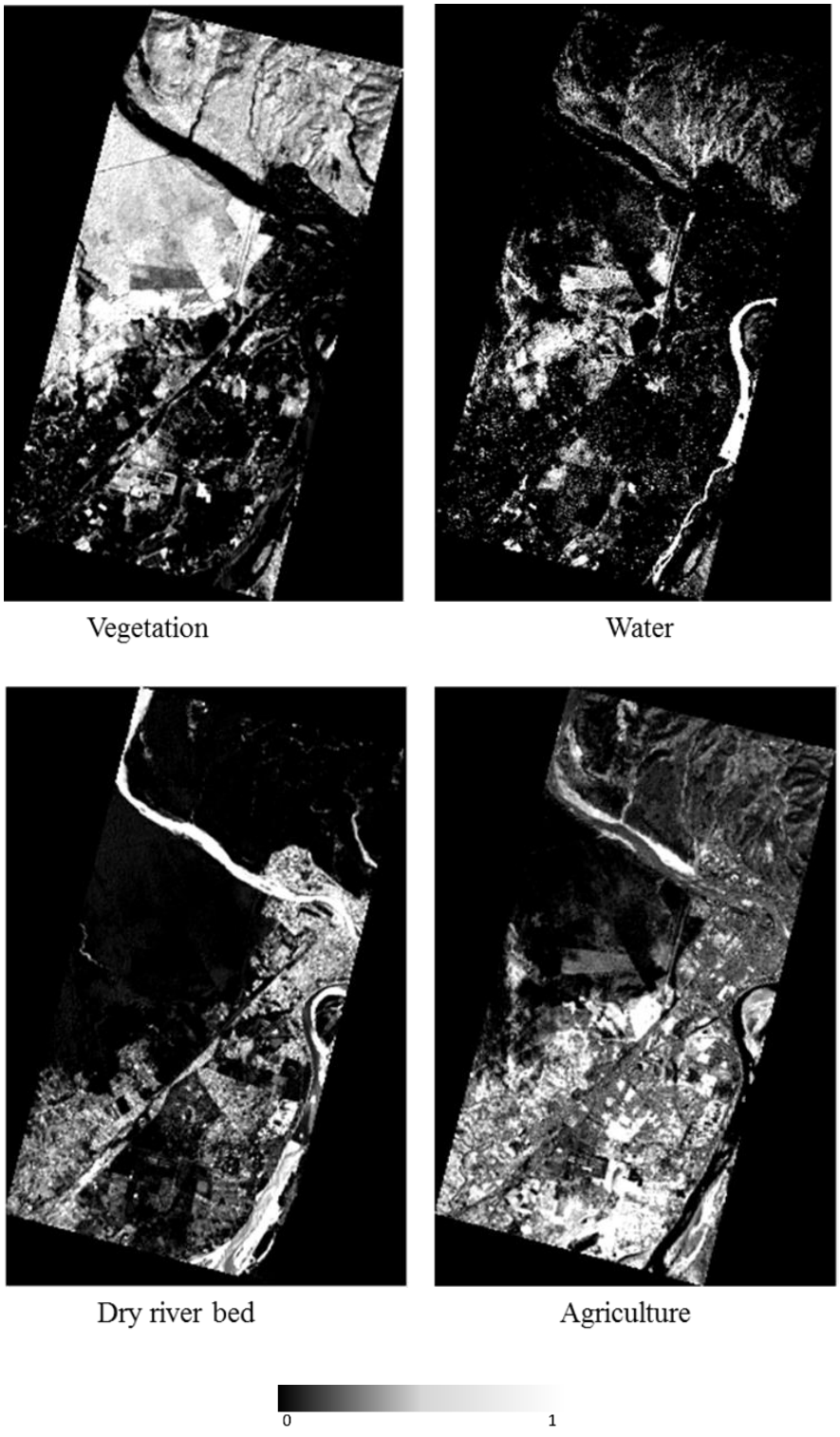

Figure 20 : Fractional coefficients of Landsat 8 OLI

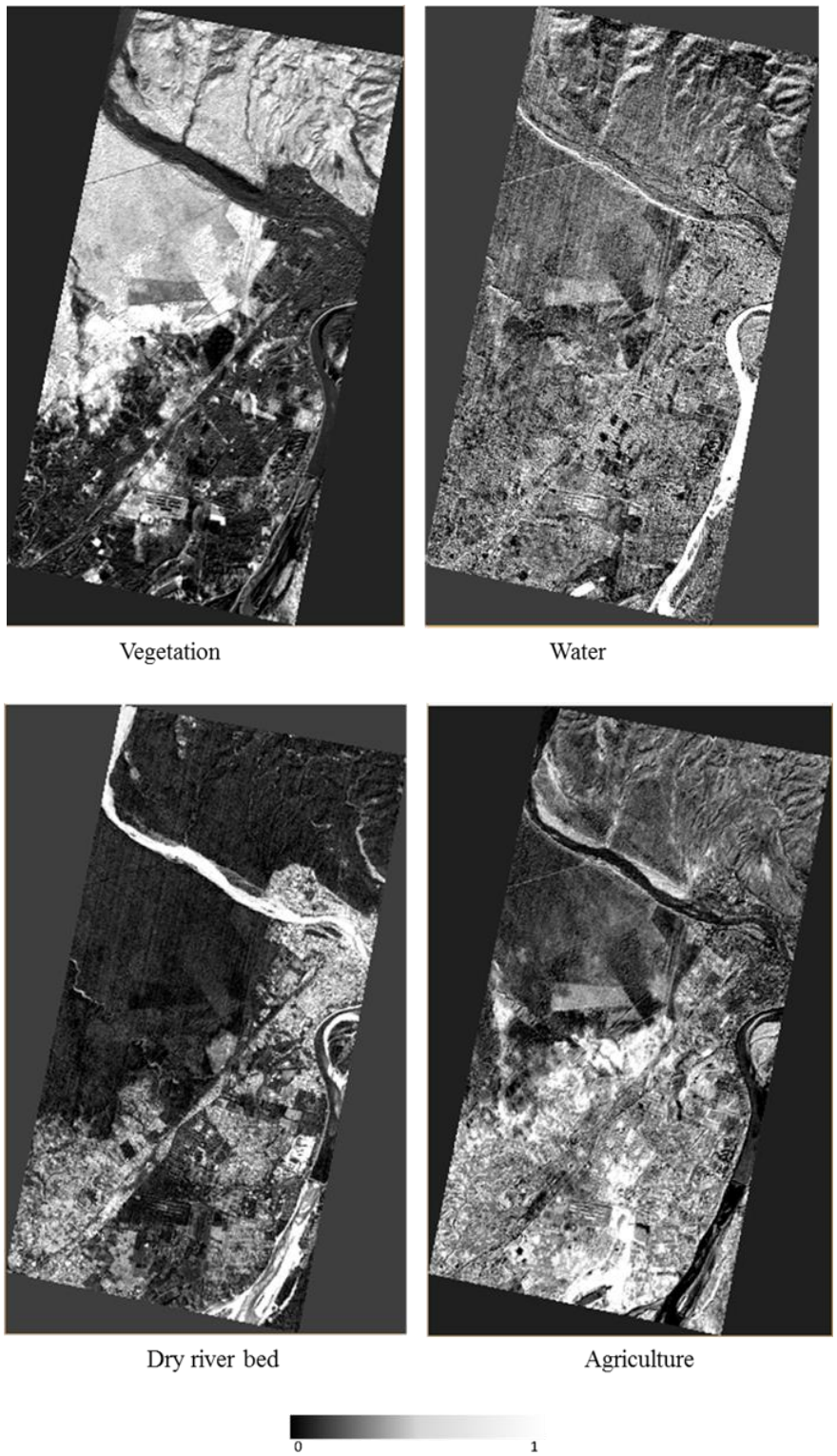

Figure 21: Fractional Coefficient image of LISS III

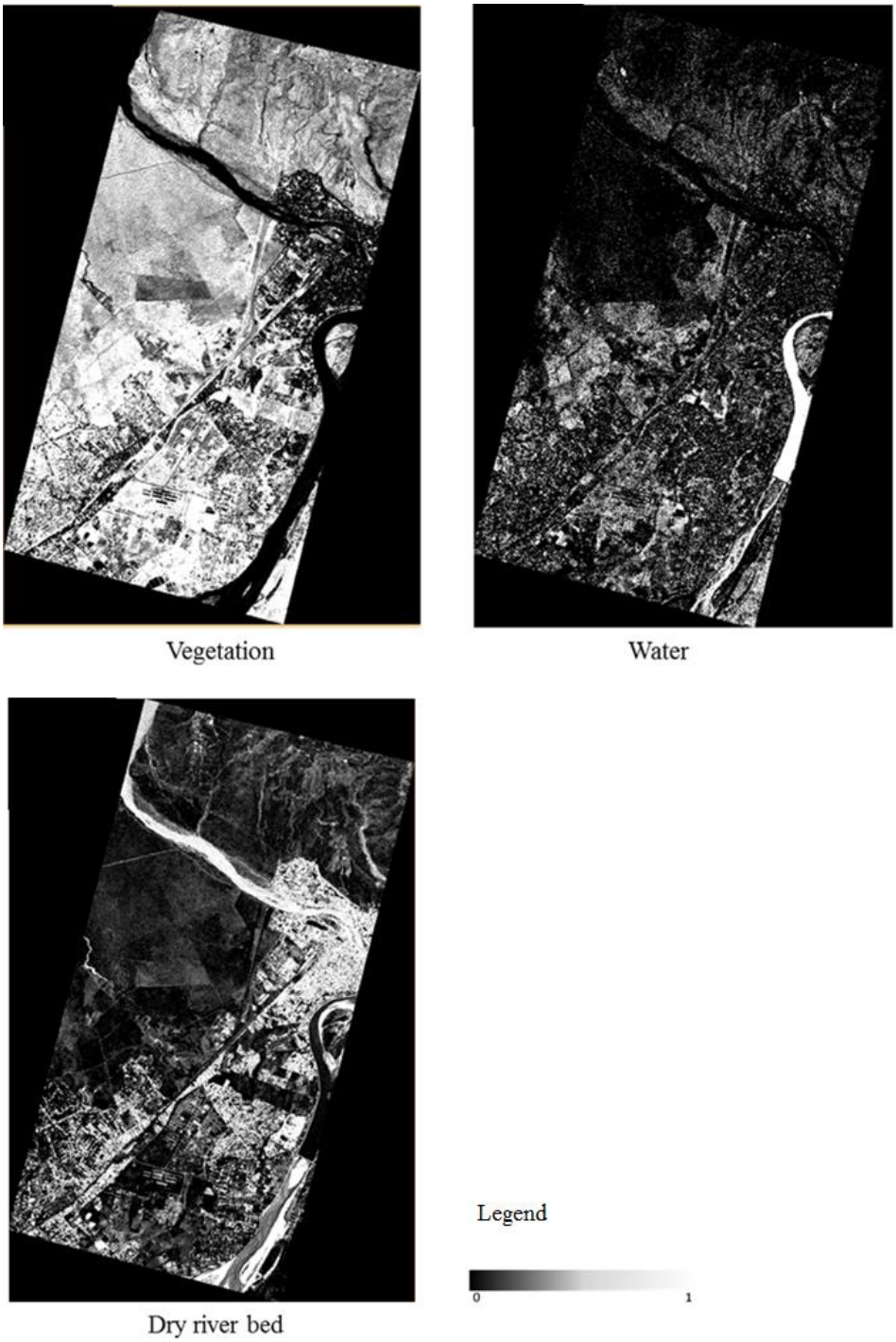

Figure 22: Fractional coefficient of LISS IV

5.3 Simulated hyperspectral data

Spectral reconstruction approach is used for the simulation of hyperspectral data from multispectral data. The simulated hyperspectral data from each multispectral (EO-1 ALI, Landsat 8 OLI, Resourcesat-2 LISS III & LISS IV) datasets are discussed below.

Simulated HRS data from EO-1 ALI MRS data

In total 70 spectral bands are simulated from EO-1 ALI data in the common wavelength range as of EO-1 Hyperion data. The simulated HRS data is compared with EO-1 Hyperion data and it is observed that most of the bands appears same while preserving tone, texture and shape. It is also found that the spectra of randomly selected features are retaining the diagnostic absorption characteristics. Figure 23 shows the standard False Colour Composite (FCC) and spectra of various features of the EO-1 Hyperion data and the simulated HRS from EO-1 ALI data.

Simulated HRS data from Landsat-8 OLI MRS data

In case of HRS data simulation from Landsat 8 OLI data a total of 34 bands have been simulated. Visually simulated bands are appearing similar while preserving its image characteristics like texture, shape except tone. Spectral signature of randomly selected features from both the images (Hyperion & simulated) are showing similar characteristics. Figure 24 shows the standard FCC and spectra of various features of EO-1 Hyperion data and the simulated HRS data from OLI data.

Simulated HRS data from Resourcsat-2 LISS III MRS data

Over all 38 spectral bands has been simulated from Resourcsat-2 LISS III MRS data with spatial resolution of 23.5m. Tone, texture, shape in the simulated HRS image are well-preserved. Figure 25 shows the standard FCC and spectra of three features of LISS III MRS data and simulated HRS from Resourcesat-2 LISS III data.

Simulated HRS data from Resourcsat-2 LISS IV MRS data

Twenty three spectral bands with spatial resolution of 5.8 meters are simulated from LISS IV MRS data. Tone, texture, shape of the feature in the simulated HRS data are preserved. It is observed that spectra generated from the simulated HRS data is satisfactory for various studies. Figure 26 shows the standard FCC and spectra of some features of the simulated HRS data from Resourcesat-2 LISS IV.

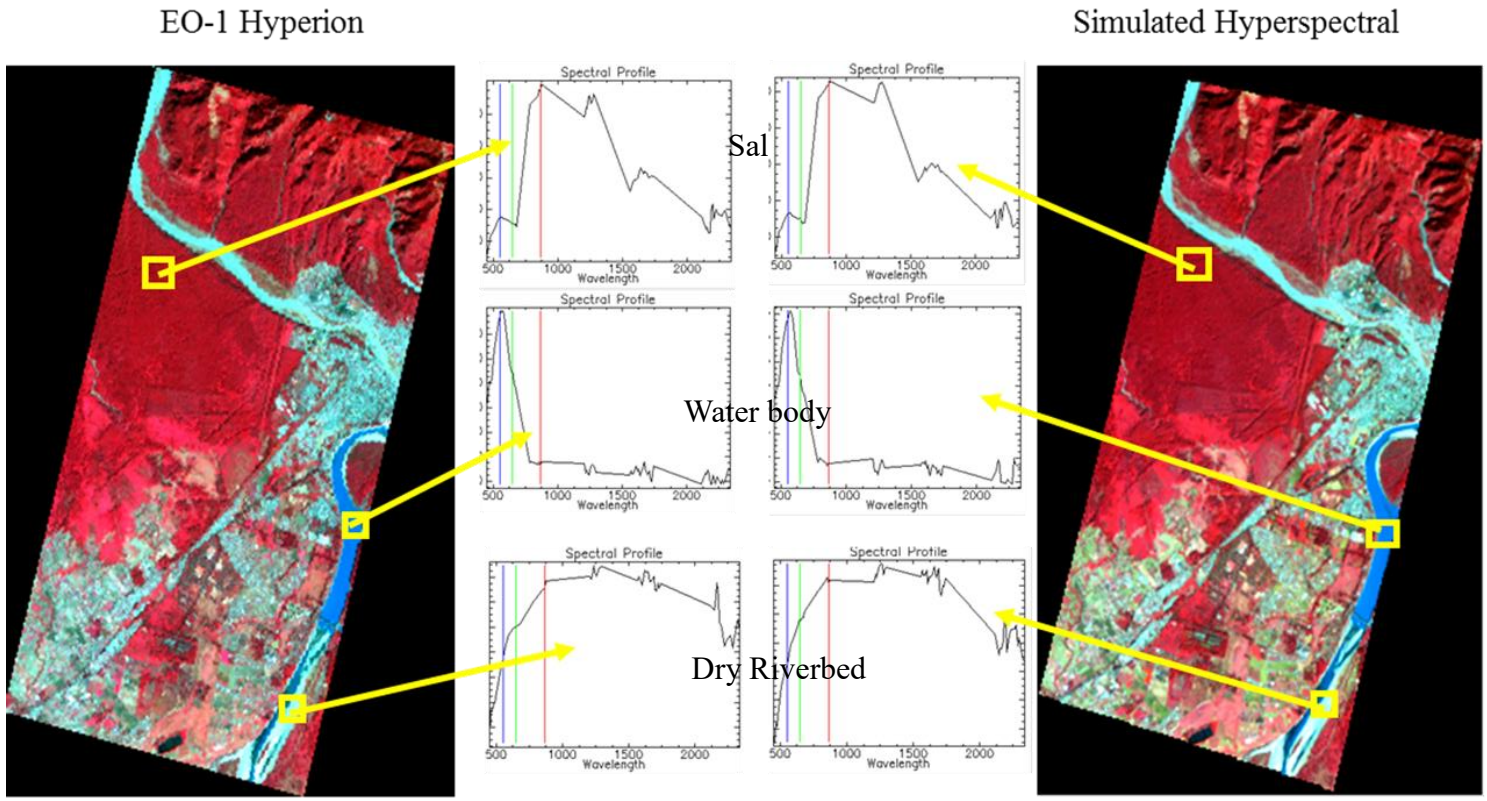

Figure 23: Simulated HRS data from ALI MRS data

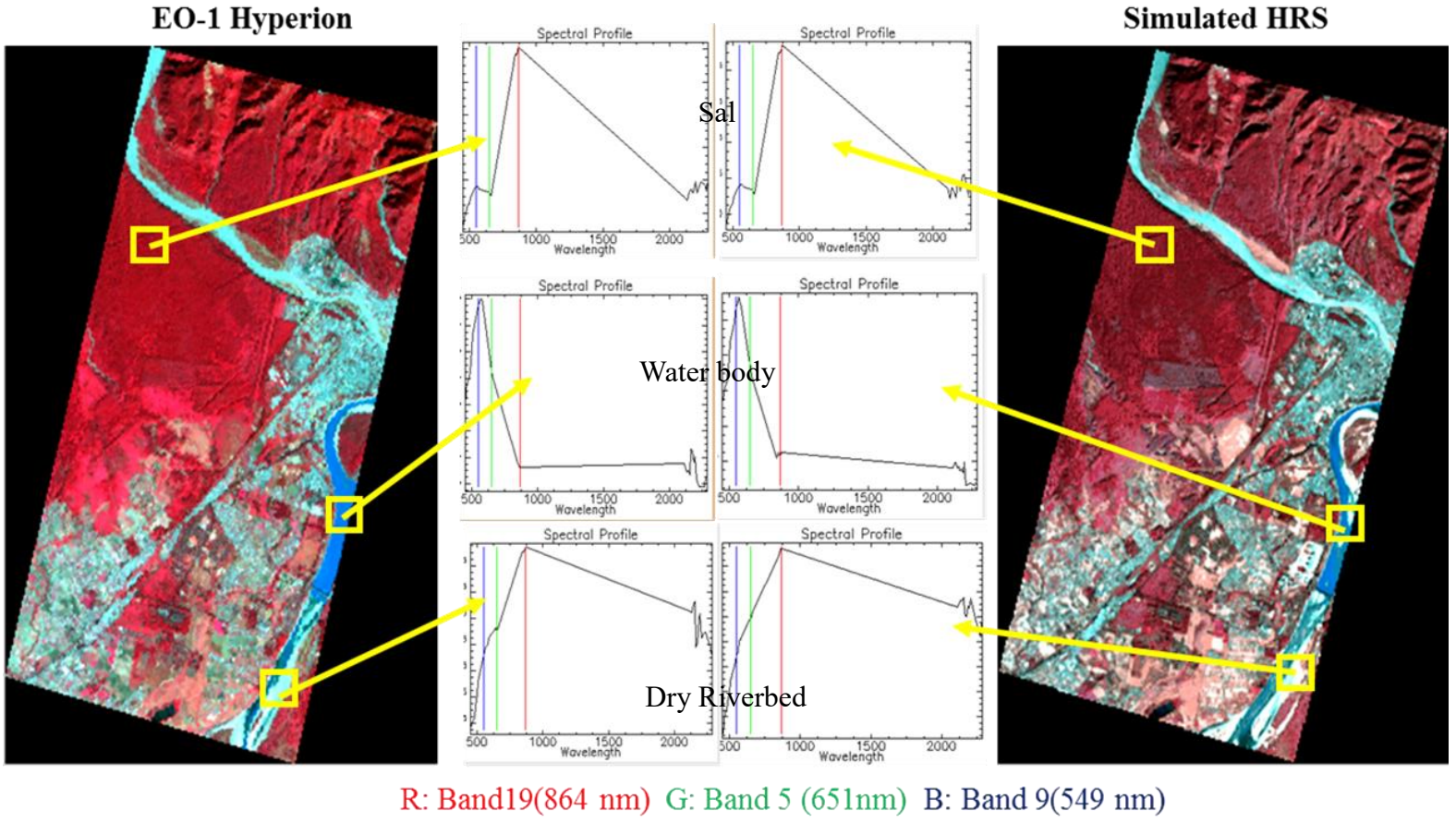

Figure 24: Simulated HRS data Landsat 8 OLI MRS Data

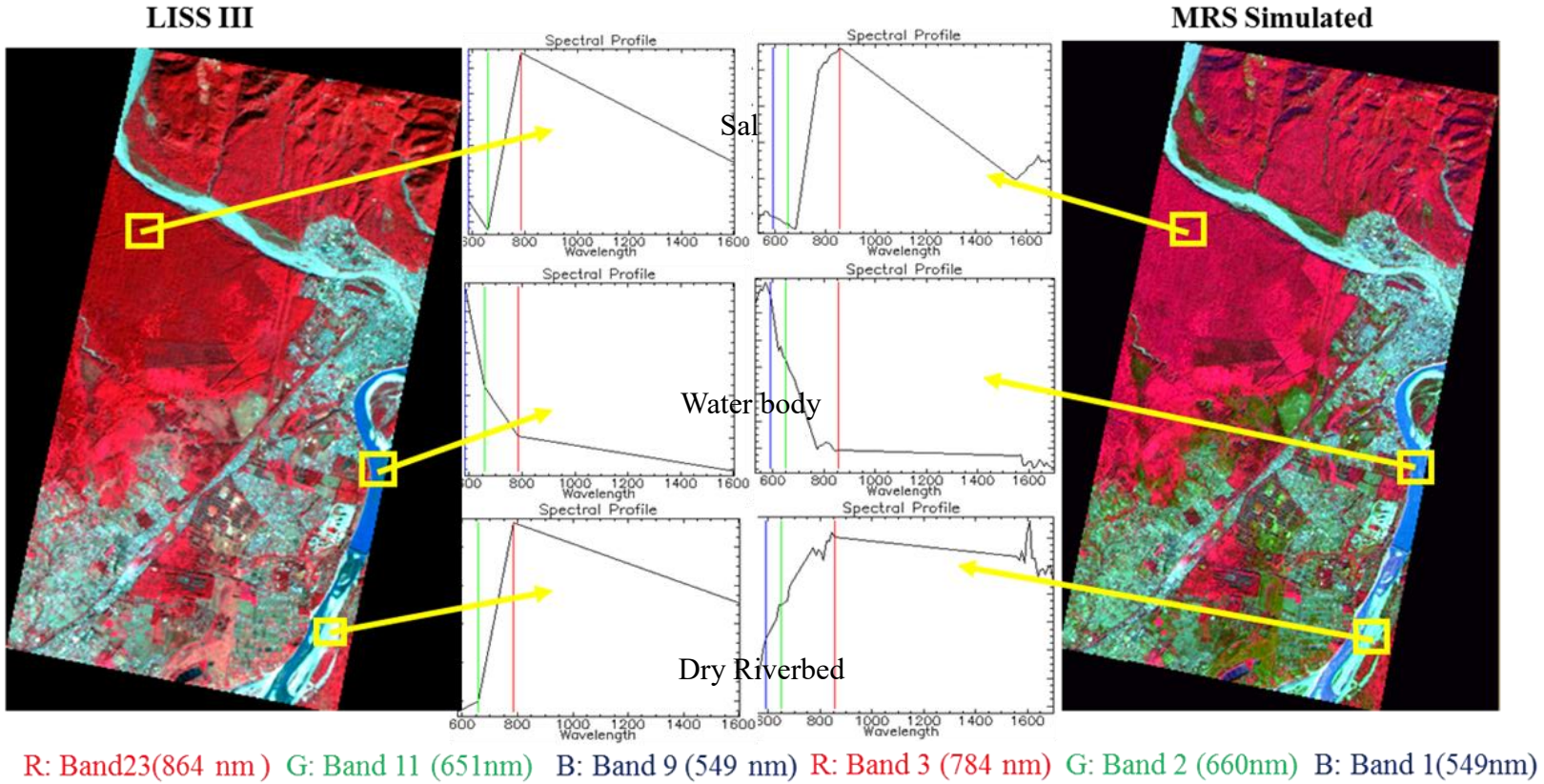

Figure 25: Simulated HRS from Resourcesat-2 LISS III MRS Data

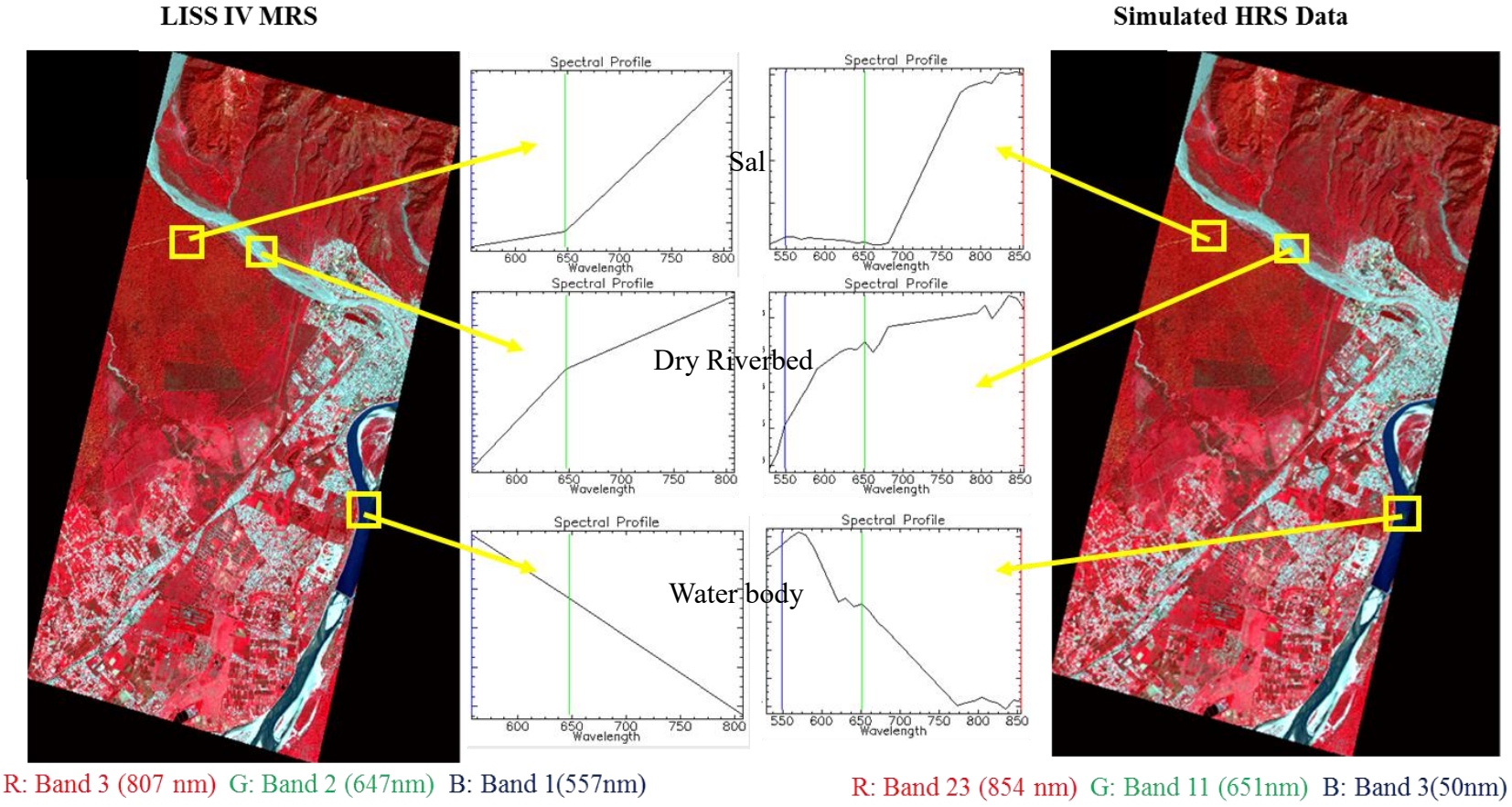

Figure 26: Simulated HRS from Resourcesat-2 LISS IV MRS Data

Statistical approach

- **Correlation**

Correlation between EO-1 Hyperion and simulated HRS data from EO-1 ALI & Landsat-8 OLI data is calculated for validation of results.

It is observed that most of the simulated spectral bands demonstrated very high correlation indicating good simulation of the hyperspectral bands. The values of correlation coefficients for each simulated band (from EO-1 ALI & Landsat-8 OLI) with EO-1 Hyperion band is given in table (15-16).

Table 15: Correlation between Simulated HRS & EO-1 Hyperion Data

Bands	Correlation	Bands	Correlation	Bands	Correlation
1	0.84	**26**	0.92	**51**	0.92
2	0.84	**27**	0.92	**52**	0.92
3	0.87	**28**	0.92	**53**	0.92
4	0.89	**29**	0.92	**54**	0.92
5	0.89	**30**	0.92	**55**	0.90
6	0.90	**31**	0.92	**56**	0.90
7	0.90	**32**	0.93	**57**	0.90
8	0.91	**33**	0.92	**58**	0.89
9	0.90	**34**	0.92	**59**	0.89
10	0.91	**35**	0.92	**60**	0.91
11	0.91	**36**	0.92	**61**	0.91
12	0.91	**37**	0.92	**62**	0.90
13	0.91	**38**	0.92	**63**	0.91
14	0.91	**39**	0.92	**64**	0.91
15	0.91	**40**	0.92	**65**	0.91
16	0.91	**41**	0.92	**66**	0.91
17	0.91	**42**	0.92	**67**	0.90
18	0.91	**43**	0.92	**68**	0.89
19	0.91	**44**	0.92	**69**	0.90
20	0.91	**45**	0.92	**70**	0.89
21	0.91	**46**	0.92		
22	0.91	**47**	0.92		
23	0.91	**48**	0.92		
24	0.91	**49**	0.92		
25	0.91	**50**	0.92		

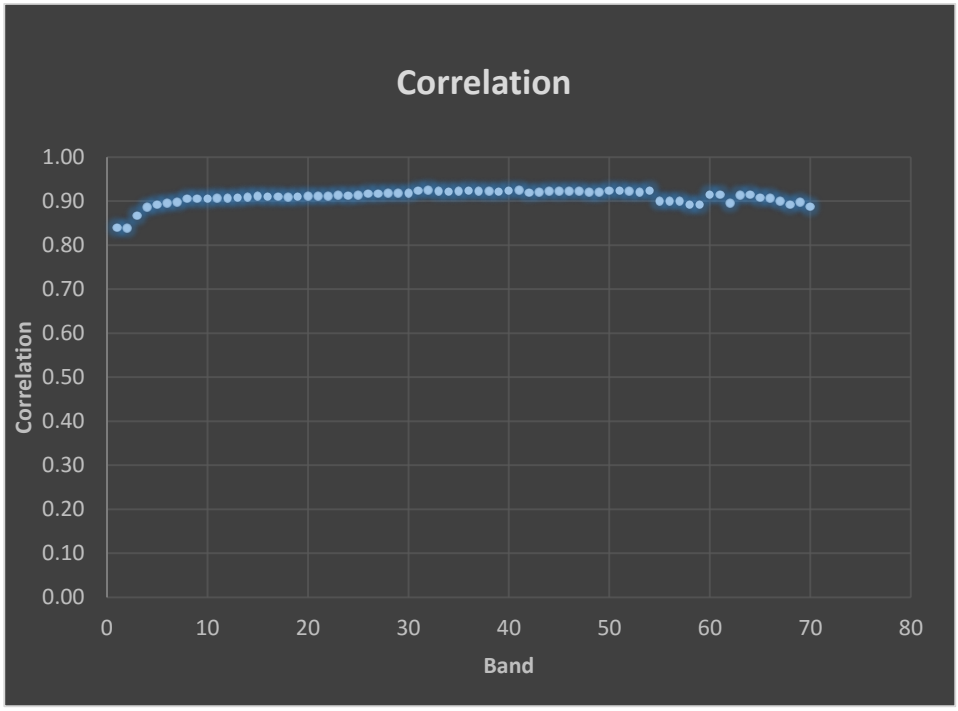

Figure 27: Band to Band Correlation between EO-1 Hyperion and Simulated HRS from ALI

Table 16: Simulated HRS from Landsat 8 OLI & EO-1 Hyperion Data

Bands	Correlation	Bands	Correlation	Bands	Correlation	Bands	Correlation
1	0.81	11	0.90	21	0.86	31	0.88
2	0.82	12	0.89	22	0.86	32	0.87
3	0.84	13	0.89	23	0.87	33	0.87
4	0.86	14	0.89	24	0.87	34	0.86
5	0.87	15	0.89	25	0.86		
6	0.88	16	0.88	26	0.86		
7	0.88	17	0.92	27	0.88		
8	0.89	18	0.92	28	0.88		
9	0.90	19	0.92	29	0.88		
10	0.90	20	0.92	30	0.89		

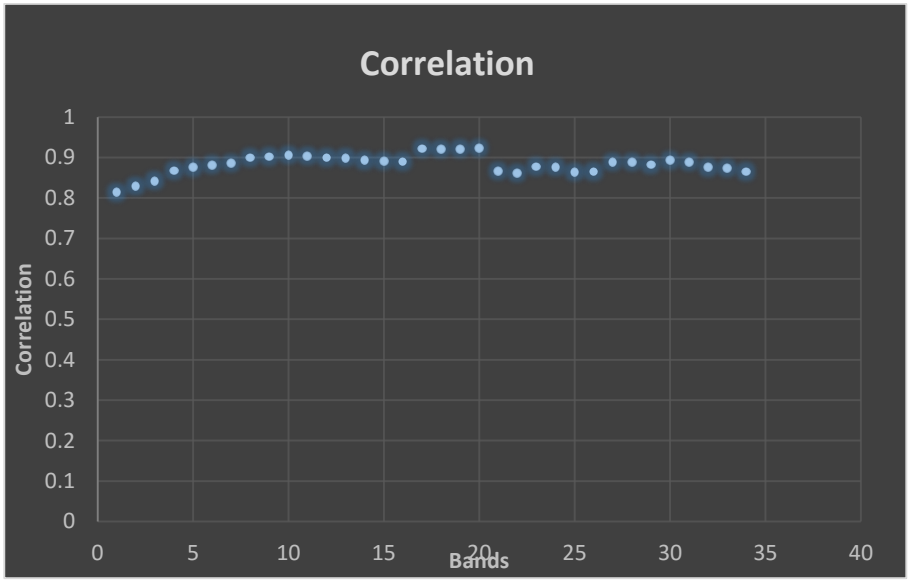

Figure 28: band to band correlation between EO-1 Hyperion and simulated HRS from Landsat 8 OLI

Figure 29 shows the band no. 8 (538nm) of EO-1 Hyperion and simulated HRS (from EO-1 ALI) data. Both the bands are appearing similar due to high correlation value i.e.0.91.

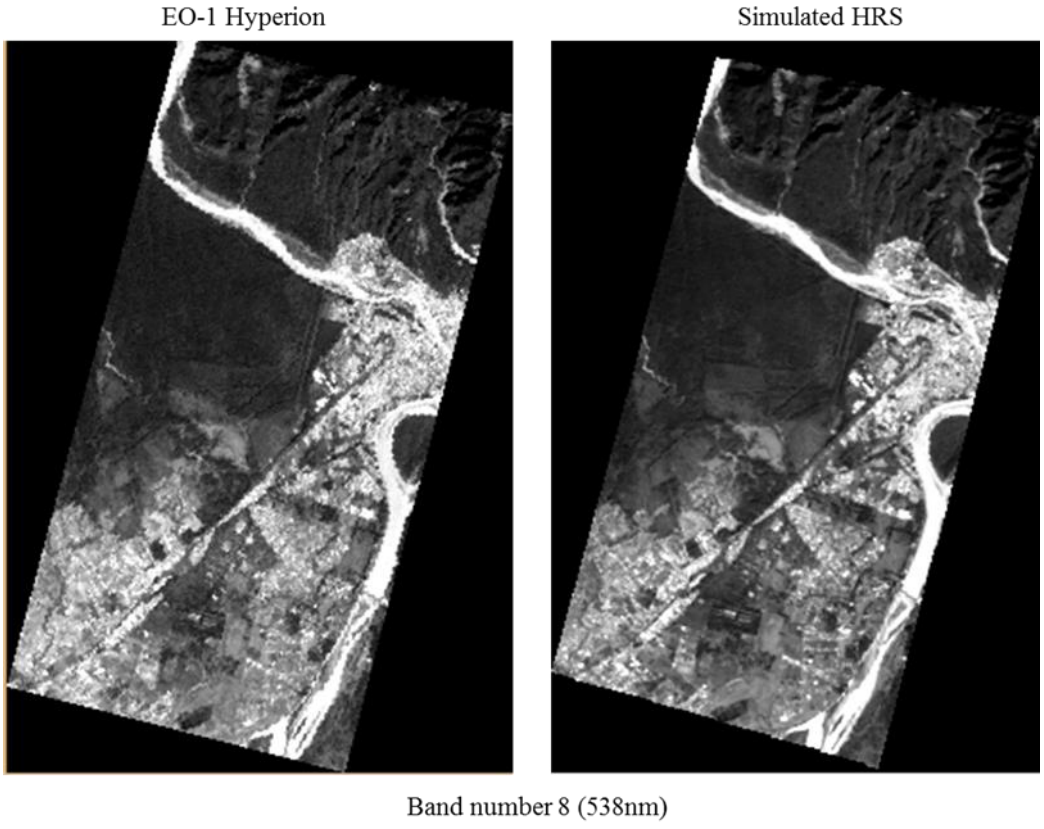

Figure 29: Band number 8 of EO-1 Hyperion & simulated HRS from (ALI)

- **Signal to Noise Ratio**

Signal to noise ratio is used to characterize quality of signal detected of a measuring system (e.g. camera or any electronic sensor). It is expressed as the ratio of the mean signal over standard deviation of a target of interest. The standard approaches for calculation SNR is by using a 50% albedo target or define targets that are of interest. The mean and standard deviation of the brighter and darker pixel is calculated by taking ROI from the area of interested. Then ratio of mean to standard deviation is done to obtained signal to noise ratio.

table 17- table 20 shows the SNR of EO-1 Hyperion and simulated HRS from EO-1 ALI data. A quick

Table 17: SNR of Simulated HRS from ALI and EO-1 Hyperion

Bands	SNR (Hyperion)	SNR (Simulated HRS from ALI)	Bands	SNR (Hyperion)	SNR (Simulated HRS from ALI)
1	1.77	1.68	**36**	1.62	1.74
2	1.80	1.66	**37**	1.61	1.74
3	1.69	1.63	**38**	1.59	1.73
4	1.60	1.59	**39**	1.60	1.72
5	1.64	1.60	**40**	1.58	1.72
6	1.59	1.57	**41**	1.57	1.70
7	1.58	1.55	**42**	1.61	1.72
8	1.57	1.52	**43**	1.57	1.71
9	1.55	1.53	**44**	1.61	1.72
10	1.53	1.52	**45**	1.58	1.72
11	1.55	1.53	**46**	1.60	1.71
12	1.57	1.54	**47**	1.63	1.70
13	1.54	1.55	**48**	1.57	1.71
14	1.54	1.64	**49**	1.61	1.72
15	1.53	1.65	**50**	1.62	1.71
16	1.53	1.65	**51**	1.62	1.70
17	1.52	1.69	**52**	1.63	1.72
18	1.54	1.69	**53**	1.57	1.73
19	1.54	1.70	**54**	1.61	1.72
20	1.52	1.57	**55**	1.62	1.82
21	1.53	1.56	**56**	1.81	1.78
22	1.53	1.56	**57**	1.80	1.77
23	1.50	1.56	**58**	1.82	1.79

24	1.51	1.55	**59**	1.79	1.81
25	1.50	1.54	**60**	1.78	1.81
26	1.62	1.57	**61**	1.82	1.80
27	1.49	1.60	**62**	1.81	1.82
28	1.51	1.59	**63**	1.80	1.79
29	1.54	1.58	**64**	1.82	1.78
30	1.52	1.59	**65**	1.80	1.82
31	1.49	1.57	**66**	1.82	1.82
32	1.47	1.56	**67**	1.79	1.79
33	1.52	1.54	**68**	1.78	1.80
34	1.56	1.56	**69**	1.80	1.80
35	1.52	1.57	**70**	1.82	1.80

Figure 30 shows the comparison between SNR of EO-1 Hyperion & Simulated HRS from EO-1 ALI data. Bands from 1 to 12 of simulated HRS data have low SNR values whereas bands from 38 to 70 have high SNR values which demonstrates acceptable simulation of HRS bands.

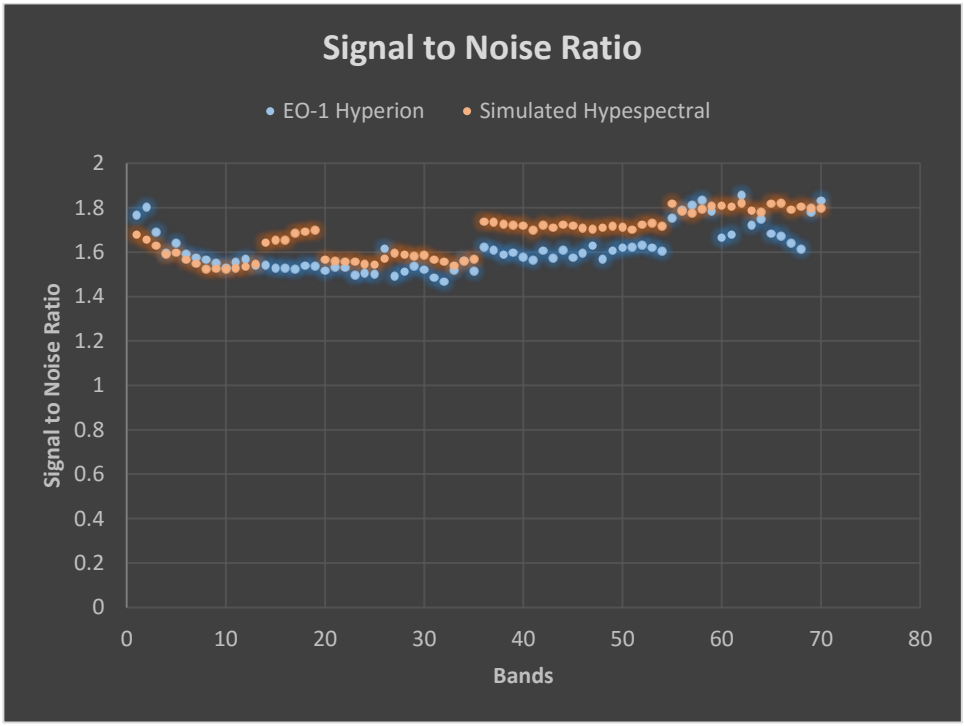

Figure 30: SNR between EO-1 Hyperion Vs Simulated HRS from EO-1 ALI

Table18 shows the SNR values of EO-1 Hyperion and simulated HRS from Landsat- 8 OLI data. Here, most of the bands in simulated HRS data are demonstrating high SNR values for all the simulated bands in comparison to EO-1 Hyperion shown in Figure 31. . Simulated HRS

results from Resourcesat-2 LISS III and LISS IV have also produced high SNR values (Table 19-20) indicating satisfactory simulation.

Table 18: SNR of simulated HRS from Landsat 8 OLI and EO-1 Hyperion

Bands	SNR (Hyperion)	SNR (Simulated HRS from OLI)	Bands	SNR (Hyperion)	SNR (Simulated HRS from OLI)
1	2.27	2.1	**18**	2.84	2.77
2	2.34	2.34	**19**	2.85	2.85
3	2.30	2.30	**20**	2.82	2.82
4	2.30	2.30	**21**	2.79	2.79
5	2.31	2.31	**22**	2.86	2.86
6	2.28	2.28	**23**	2.83	2.83
7	2.29	2.29	**24**	2.86	2.86
8	2.33	2.33	**25**	2.93	2.93
9	2.33	2.33	**26**	2.99	2.99
10	2.32	2.32	**27**	2.84	2.84
11	2.32	2.32	**28**	2.85	2.85
12	2.33	2.33	**29**	2.99	2.99
13	2.35	2.35	**30**	2.89	2.89
14	2.48	2.48	**31**	2.82	2.82
15	2.50	2.50	**32**	2.89	2.89
16	2.51	2.51	**33**	2.85	2.85
17	2.81	2.81	**34**	2.80	2.80

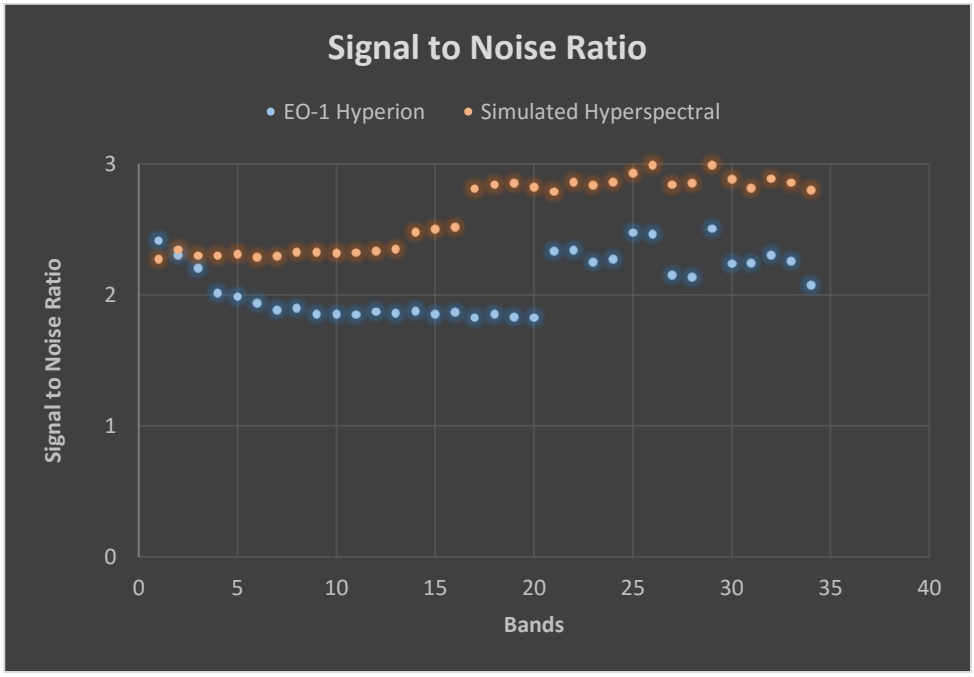

Figure 31: SNR between EO-1 Hyperion vs simulated HRS from OLI

Table 19: SNR of simulated SNR from RESOURCESAT- 2 LISS III

Bands	SNR	Bands	SNR
1	1.31	**20**	1.51
2	1.36	**21**	1.47
3	1.35	**22**	1.47
4	1.35	**23**	1.48
5	1.35	**24**	1.36
6	1.33	**25**	1.35
7	1.33	**26**	1.40
8	1.35	**27**	1.36
9	1.31	**28**	1.32
10	1.33	**29**	1.35
11	1.32	**30**	1.41
12	1.30	**31**	1.38
13	1.32	**32**	1.37
14	1.32	**33**	1.41
15	1.47	**34**	1.39
16	1.47	**35**	1.40
17	1.46	**36**	1.35
18	1.45	**37**	1.39

19	1.52	**38**	1.38

Table 20: SNR of simulated SNR from RESOURCESAT- 2 LISS IV

Band	SNR	Band	SNR
1	1.41	**13**	1.43
2	1.41	**14**	1.44
3	1.41	**15**	1.47
4	1.41	**16**	1.47
5	1.41	**17**	1.47
6	1.41	**18**	1.47
7	1.41	**19**	1.47
8	1.43	**20**	1.47
9	1.43	**21**	1.47
10	1.43	**22**	1.47
11	1.43	**23**	1.47
12	1.43		

Spectral separability analysis

In the present study, spectral separability analysis is carried out to find out similarity between image spectra of hyperspectral data (EO-1 Hyperion and simulated HRS data from MRS data) and field spectra of various LULC features. Equal weightage of 0.33 was given while performing spectral separability analysis using SAM, SFF and BE for spectral matching.

Ground spectra at two different locations for two different features (Sal and Curry Leaves) were collected and used for the spectral separability analysis Figure 32 (point no. 1 is dominated by SAL forest whereas point no. 2 is mixed vegetation dominated by curry leaves).

Table 21: Satellite data XY Location and latitude longitude of selected features

Data	LULC Features	XY	Lat, Long
EO-1 Hyperion	Sal	X: 620 Y:1079	30° 07’ 19.76’’,78° 16’ 0.91’’
	Curry Leaves (Curry Patta)	X: 646 Y:1023	30° 08’14.88’’ 78° 16’27.81’’
EO-1 ALI Simulated HRS	Sal	X: 620 Y:1079	30° 07’ 19.76’’,78° 16’ 0.91’’
	Curry Leaves (Curry Patta)	X: 646 Y:1023	30° 08’14.88’’ 78° 16’27.81’’
Landsat 8 OLI Simulated HRS	Sal	X: 646 Y:1023	30° 07’ 19.76’’,78° 16’ 0.91’’
	Curry Leaves (Curry Patta)	X: 646 Y:1023	30° 08’14.88’’ 78° 16’27.81’’
Simulated HRS (LISS III)	Sal	X: 6068 Y:2107	30° 07’ 19.76’’,78° 16’ 0.91’’
	Curry Leaves (Curry Patta)	X: 6096 Y:2036	30° 08’14.88’’ 78° 16’27.81’’
Simulated HRS (LISS IV)	Sal	X: 801 Y:711	30° 07’ 19.76’’,78° 16’ 0.91’’
	Curry Leaves (Curry Patta)	X: 918Y:400	30° 08’14.88’’ 78° 16’27.81’’

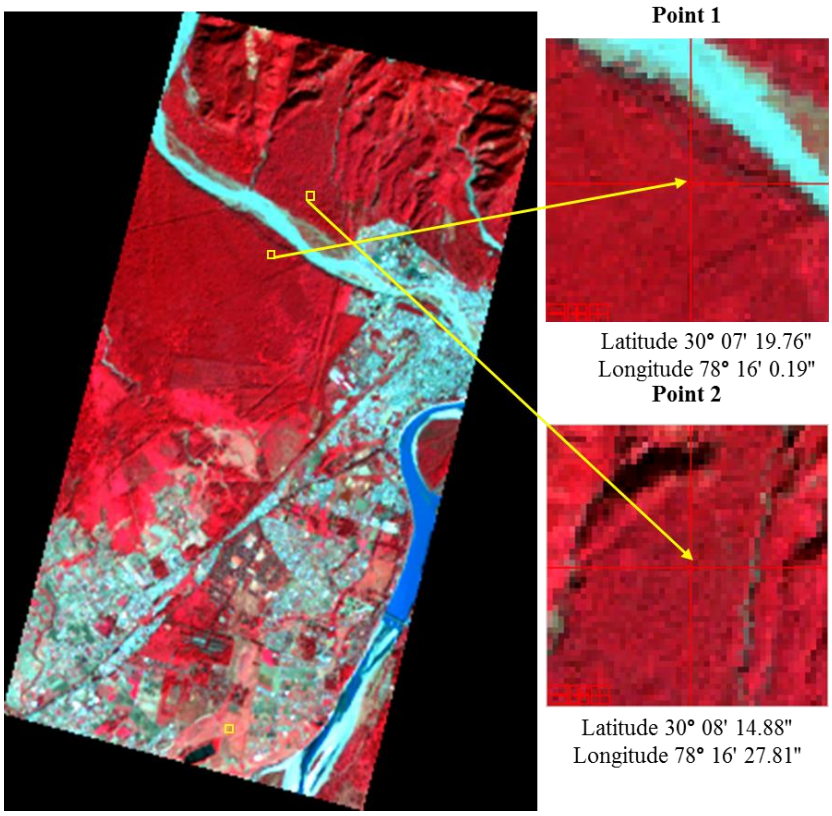

Figure 32: Ground Truth Locations

The results of the spectral separability analysis for all the hyperspectral datasets (EO-1 Hyperion and simulated) is illustrated in figure 33-37 .The results comprise of overall and individual score for SAM, SFF & BE techniques. The observations are as follows:

- The overall score for Sal and curry leaves is similar for Hyperion, simulated HRS data from ALI and OLI whereas the scores are at higher end for LISS-III and LISS IV.

- **EO-1 Hyperion data**

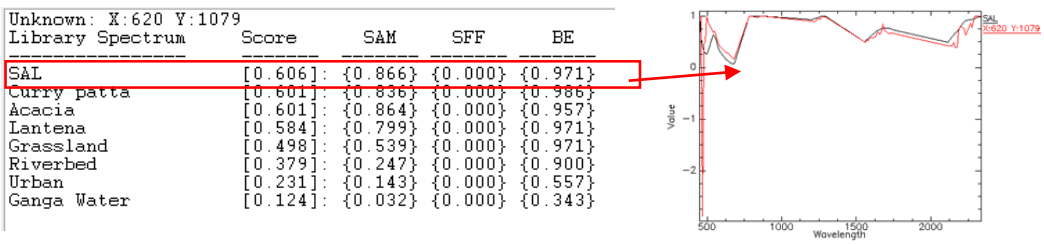

Unknown: X:620 Y:1079

Library Spectrum	Score	SAM	SFF	BE
SAL	[0.606]:	{0.866}	{0.000}	{0.971}
Curry patta	[0.601]:	{0.836}	{0.000}	{0.986}
Acacia	[0.601]:	{0.864}	{0.000}	{0.957}
Lantena	[0.584]:	{0.799}	{0.000}	{0.971}
Grassland	[0.498]:	{0.539}	{0.000}	{0.971}
Riverbed	[0.379]:	{0.247}	{0.000}	{0.900}
Urban	[0.231]:	{0.143}	{0.000}	{0.557}
Ganga Water	[0.124]:	{0.032}	{0.000}	{0.343}

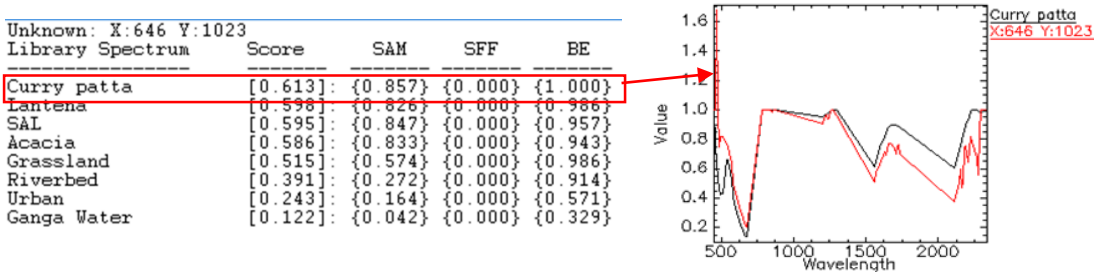

Figure 33: Separability score of EO-1 Hyperion

- **Simulated HRS (EO-1 ALI):**

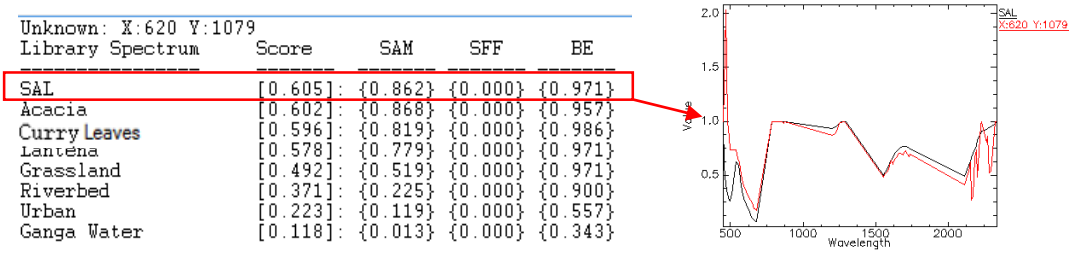

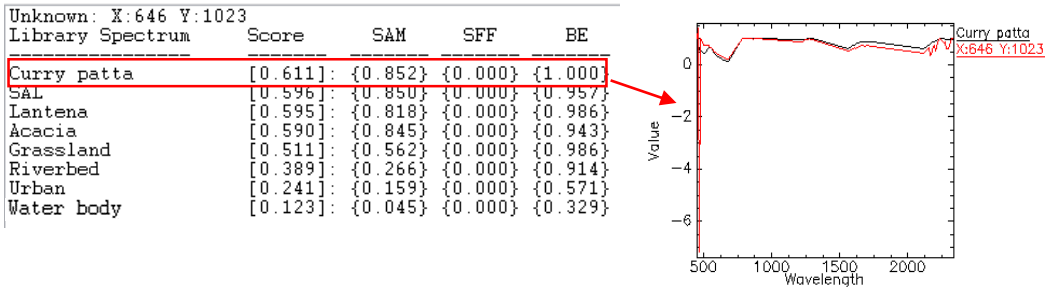

Figure 34: Separability score for simulated HRS from EO-1 ALI

- **Simulated HRS (Landsat 8 OLI Data):**

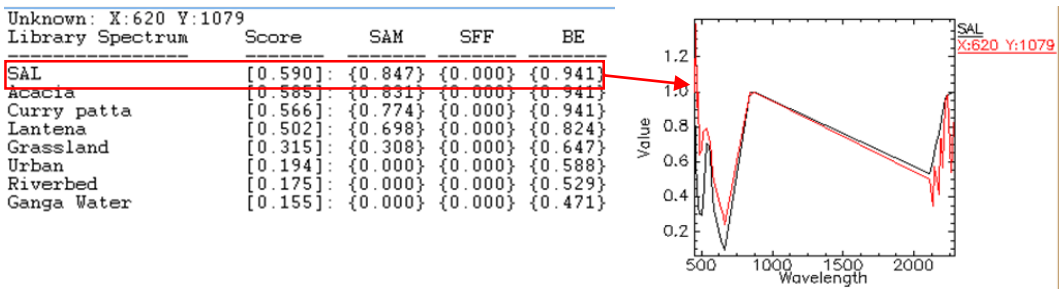

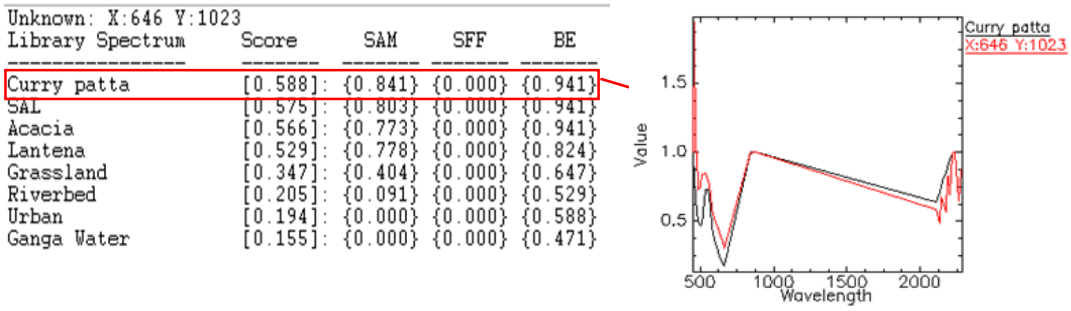

Figure 35: Separability score for simulated HRS from Landsat 8 OLI

- **Simulated HRS (Resourcesat -2 LISS III):**

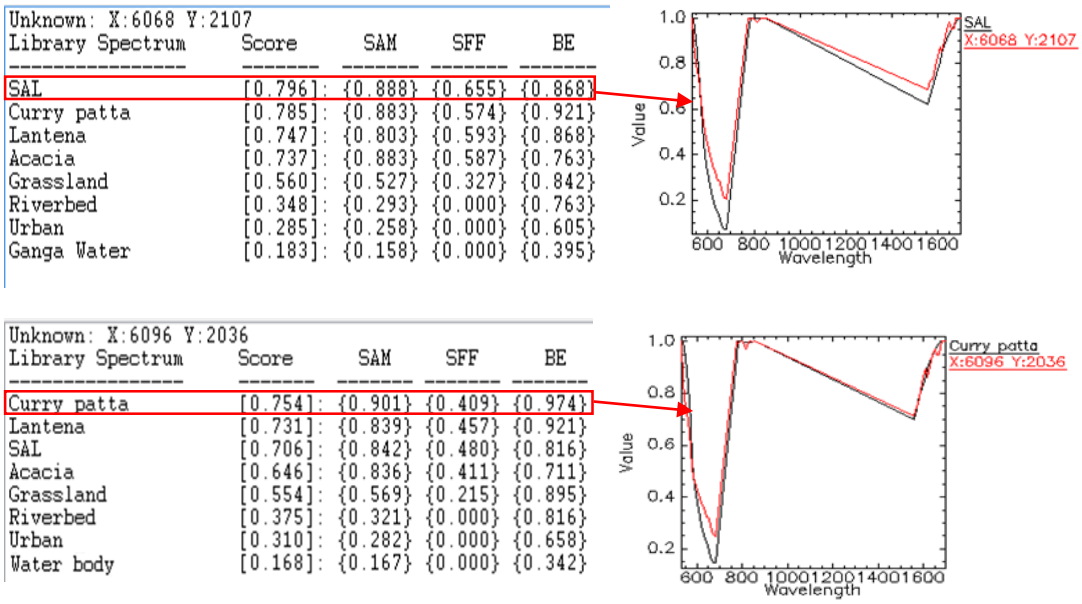

Figure 36: Separability score for simulated HRS from LISS III

- **Simulated HRS (Resourcesats-2 LISS IV):**

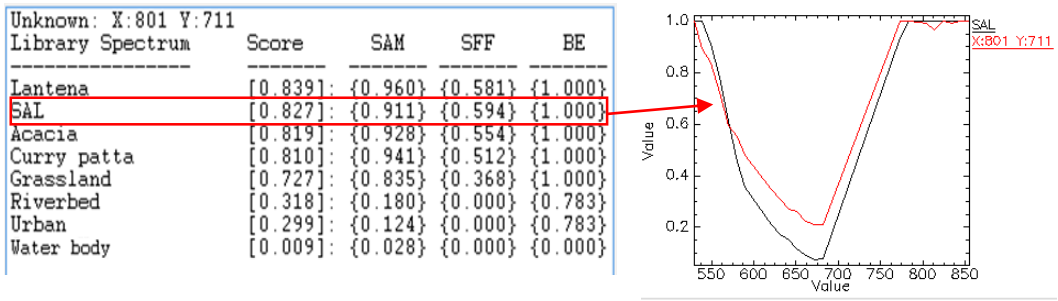

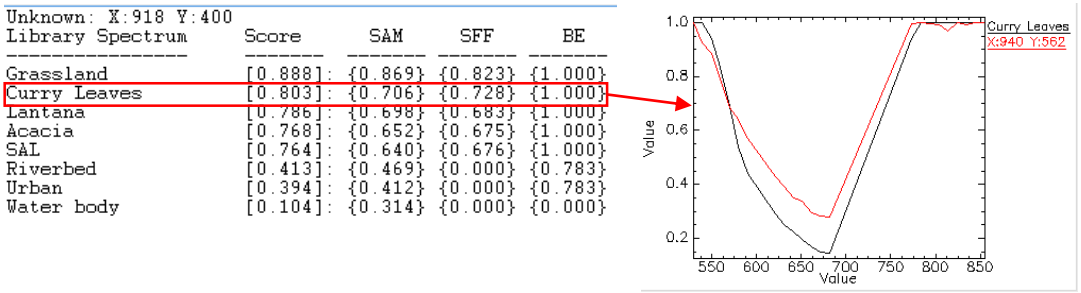

Figure 37: Separability score for simulated HRS from LISS IV

5.4 Classification and accuracy assessment

Spatial resolution	Classified Map	Overall Accuracy	Kappa Coefficient
30 m	EO-1 Hyperion	84.82	0.829
	Simulated HRS (from EO-1ALI) data	74.35	0.717
	EO-1 ALI MRS data	58.91	0.522
	Simulated HRS (from Landsat-8 OLI) data	69.82	0.6631
	Landsat-8 OLI MRS data	62.97	0.5854
23.5 m	Simulated HRS (from Resourcesat-2 LISS III) data	69.42	0.6412
	Resourcesat-2 LISS III MRS data	65.70	0.6034
5.8 m	Simulated HRS (from Resourcesat-2 LISS IV) data	79.48%	0.7259
	Resourcesat-2 LISS IV MRS data	63.98%	0.5336

Table 22: Accuracy assessment of all classified results

Spectral Angle Mapper technique has been used for classifying all the multispectral and their corresponding simulated hyperspectral datasets along with Hyperion data for cross validation.

The classification results are shown from Figure 38 to 46. The classified output of EO-1 hyperion data (Figure 38) is able to classify all major LULC classes (Vegetation, water body, urban, dry riverbed, cropland etc.) along with different vegetation species (Shorea robusta, Tectona grandis, Scrub etc.). The results were cross validated with ground samples and high level of accuracy is obtained for all the classes. The classified output obtained from simulated HRS (EO-1 ALI) data (Figure 40) is also able to classify the spectrally similar vegetation species and major LULC classes, the accuracy assessment results are also satisfactory and acceptable. The classified results of corresponding EO1 ALI MRS data (Figure 39) are inferior, moreover some of the classes like Shorea robusta, Tectona grandis and scrubs are misclassified at some places, This can be attributed to the coarser spectral resolution.

Similarly the classified outputs of simulated HRS data from others MRS data like Landsat 8 OLI (Figure 42), Resourcesat 2 LISS III (Figure 44) and Resourcesat 2 LISS IV (Figure 46) are also able to classify major LULC classes with improved accuracy from their corresponding MRS data. Classification results obtained from Multispectral data of Landsat 8 OLI (Figure 41), Resourcesat 2 LISS III (Figure 43) and Resourcesat 2 LISS IV (Figure 45) are not able to classify spectrally similar features e.g. (scrubs, mixed forest, cropland) due to their coarser bandwidth.

The classified outputs were further subjected to accuracy assessment and the results are shown in Table 22.

Following points are observed from the classification and accuracy assessment results:

- Overall accuracy and kappa coefficient of all the classified products obtained from simulated HRS data is improved as compared to their corresponding classified products derived from multispectral data.
- The extent of misclassification which was observed in the classified MRS products is reduced significantly in the classified products of simulated HRS data.
- Majority of LULC classes like urban, forest and cropland etc. have shown improved classification results in the classified products generated from simulated data.
- The classified output obtained from the simulated products are able to discriminate LULC classes of similar nature e.g. mixed urban vs. dense urban etc. which is limitation of products generated from multispectral dataset.

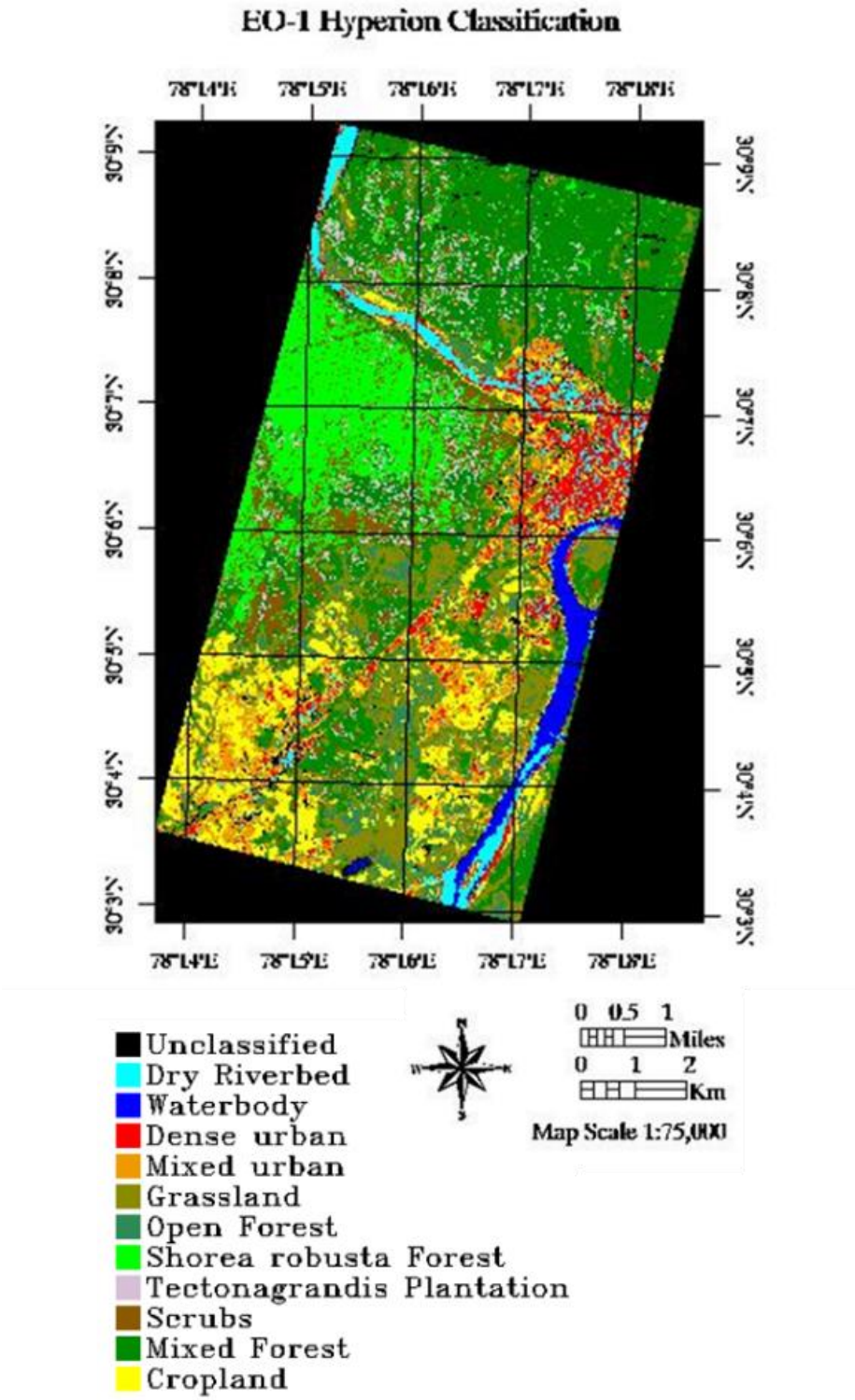

Figure 38: Classified EO-1 Hyperion data

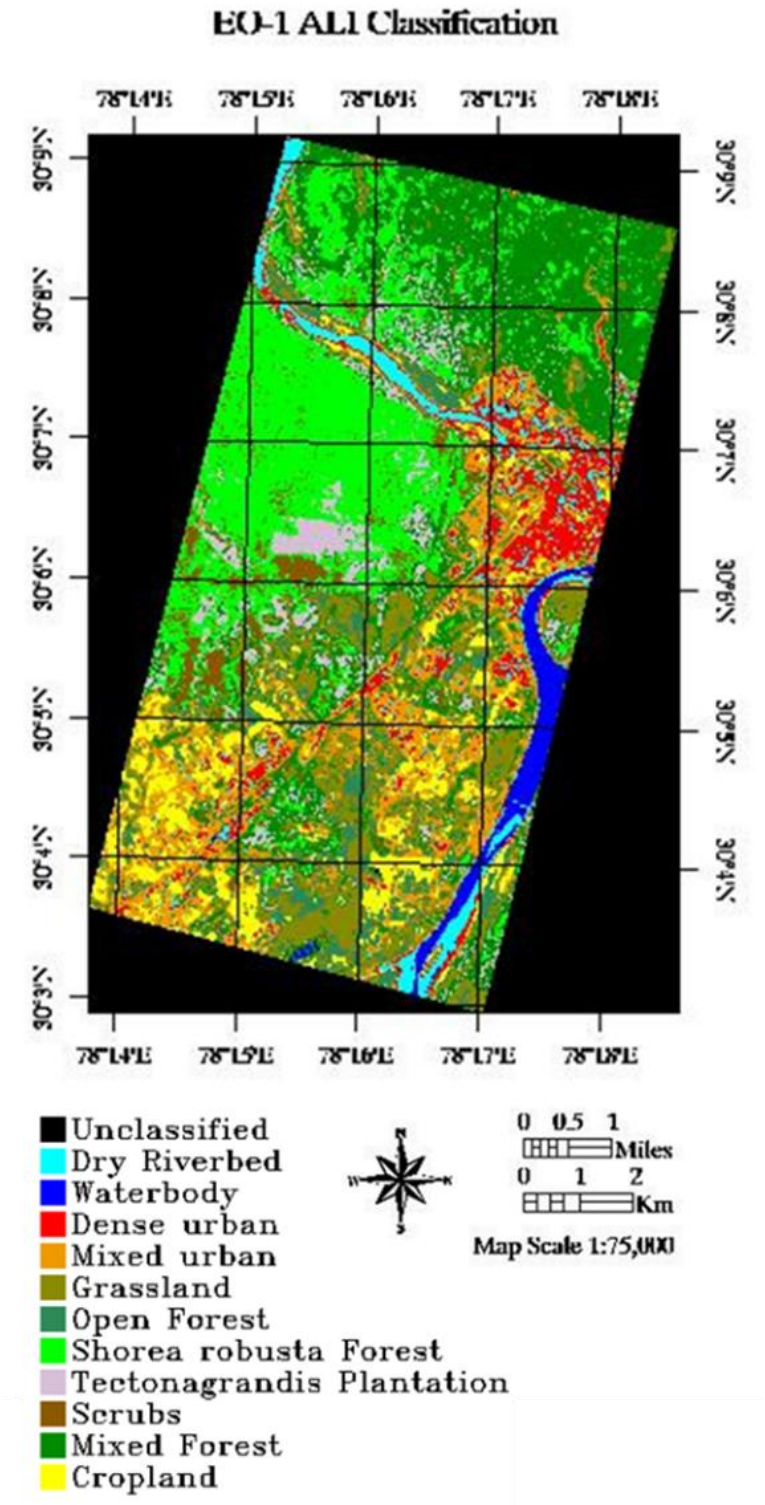

Figure 39: Classified EO-1 ALI data

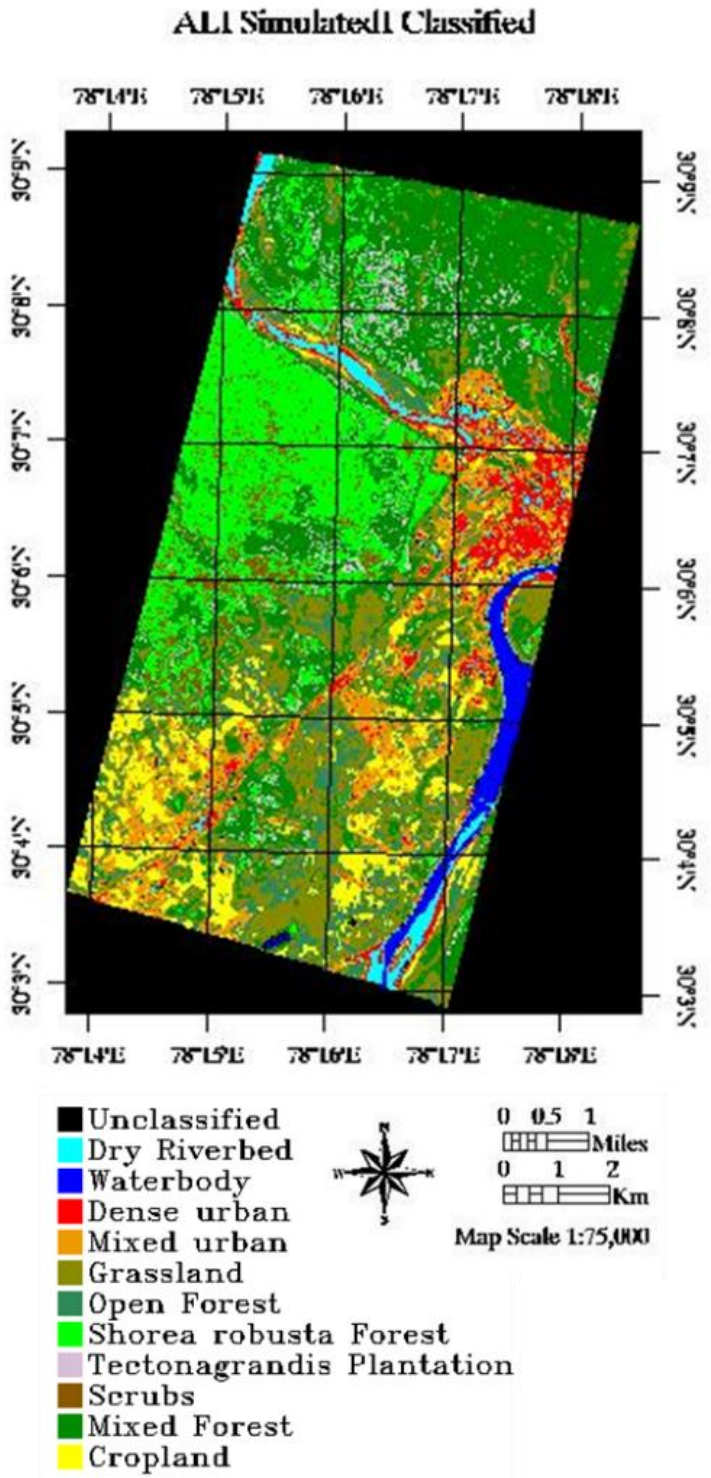

Figure 40: Classified simulated HRS data (from EO-1 ALI)

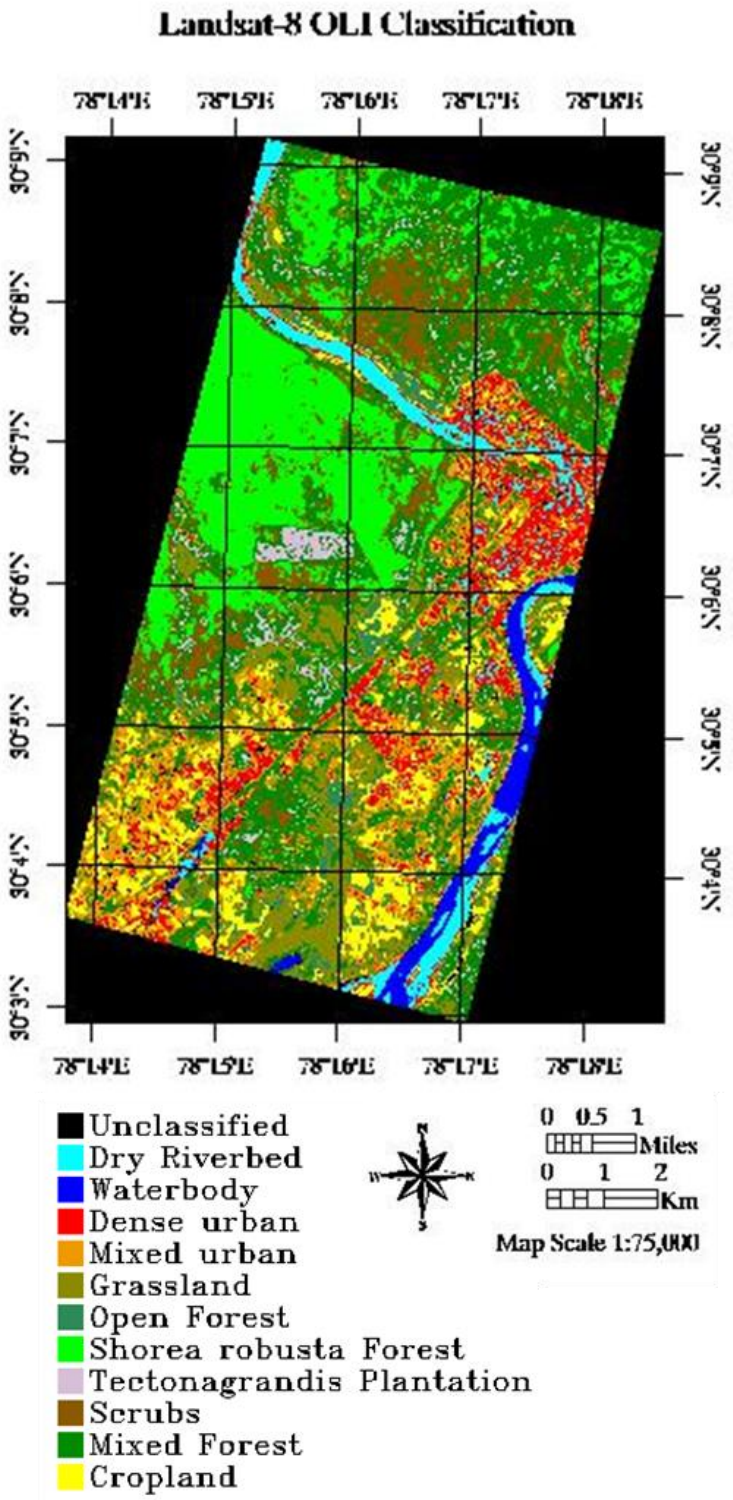

Figure 41: Classified Landsat 8 OLI

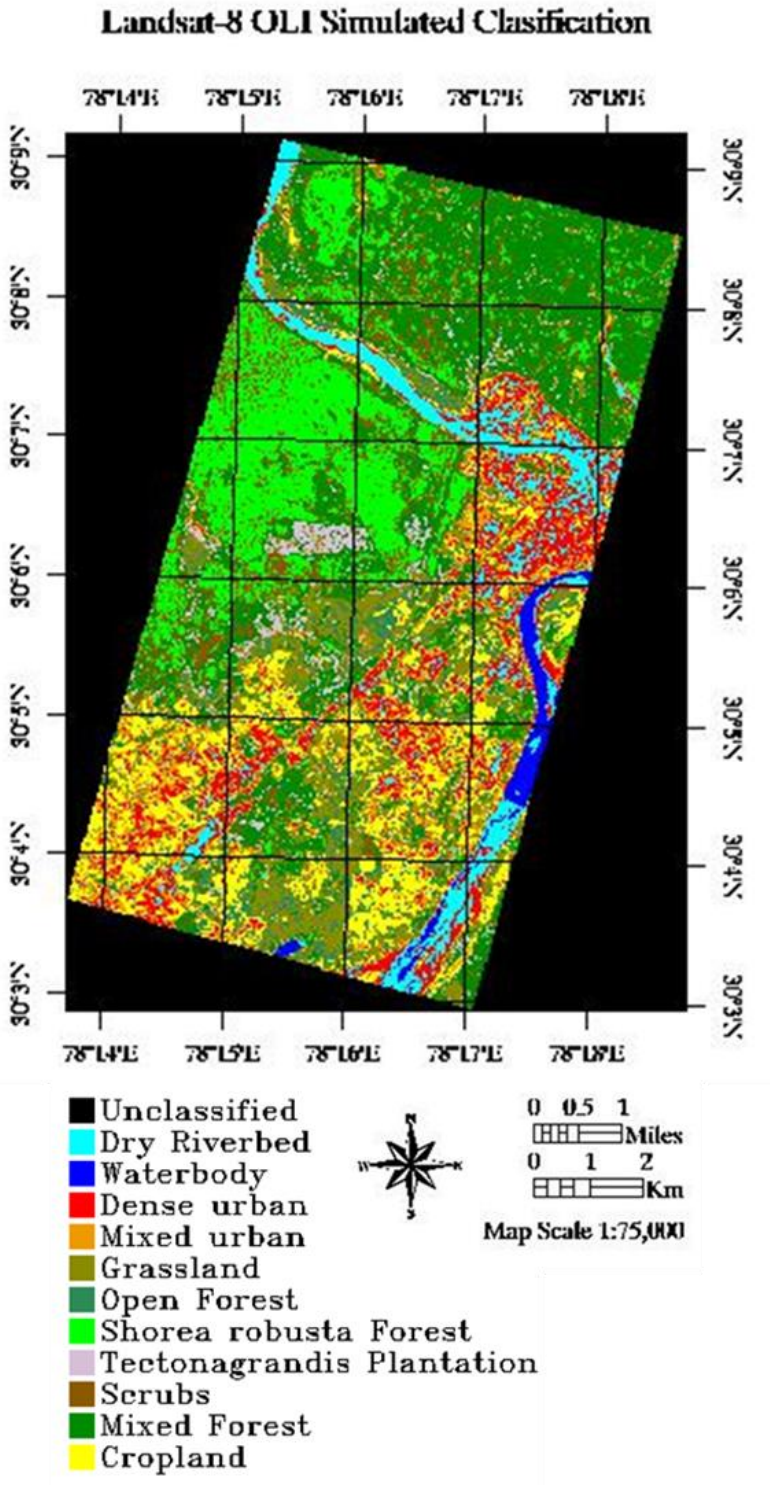

Figure 42: Classified HRS from OLI

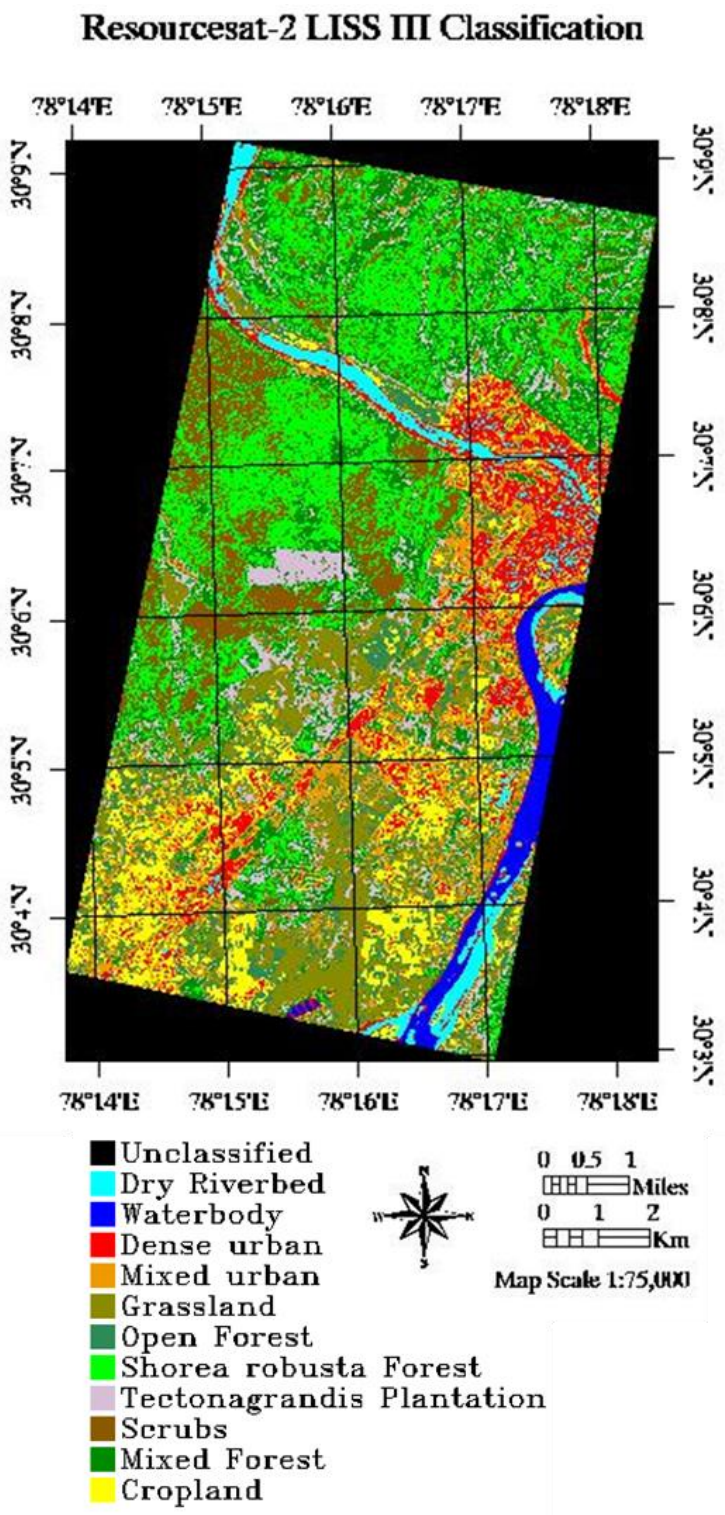

Figure 43: Classified Simulated HRS data (from Resourcesat 2 LISS III)

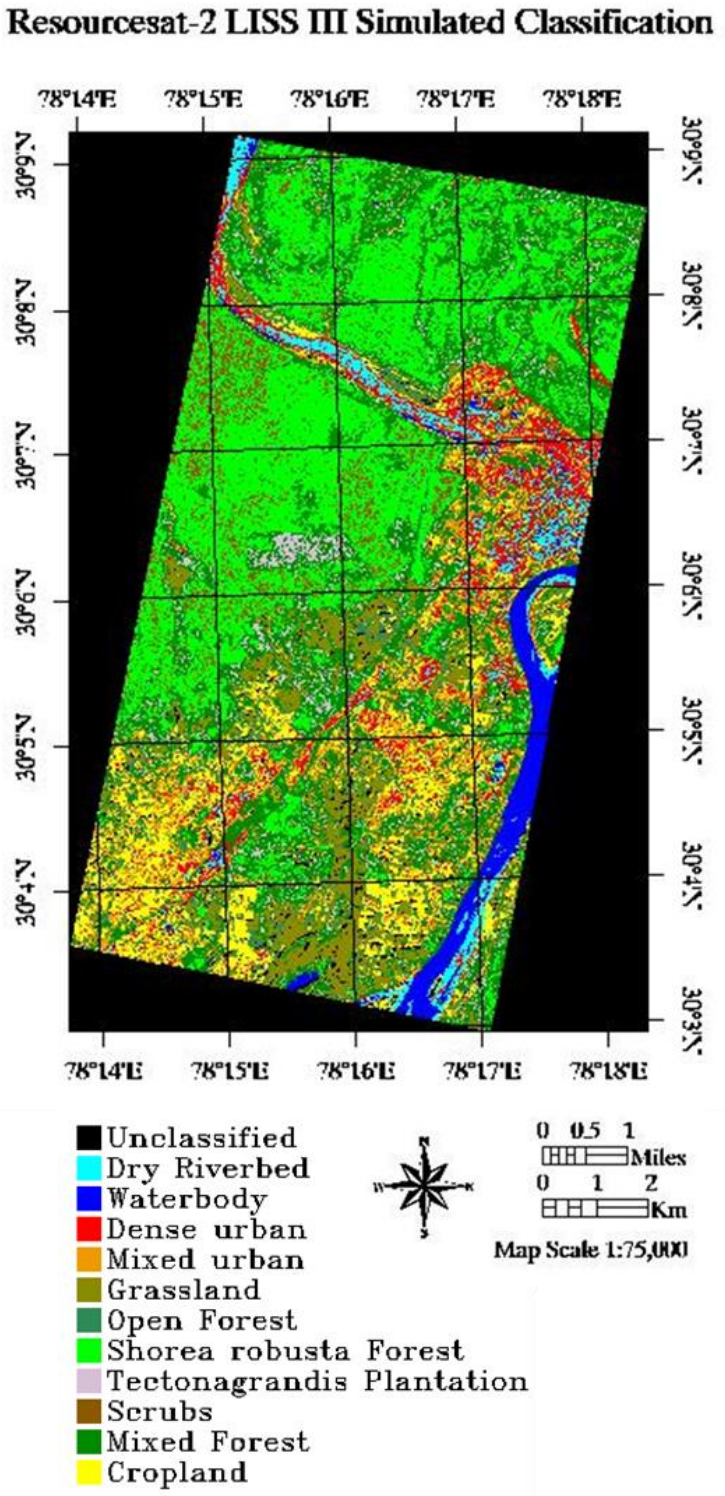

Figure 44: Classified Resourcesat-2 LISS IV data

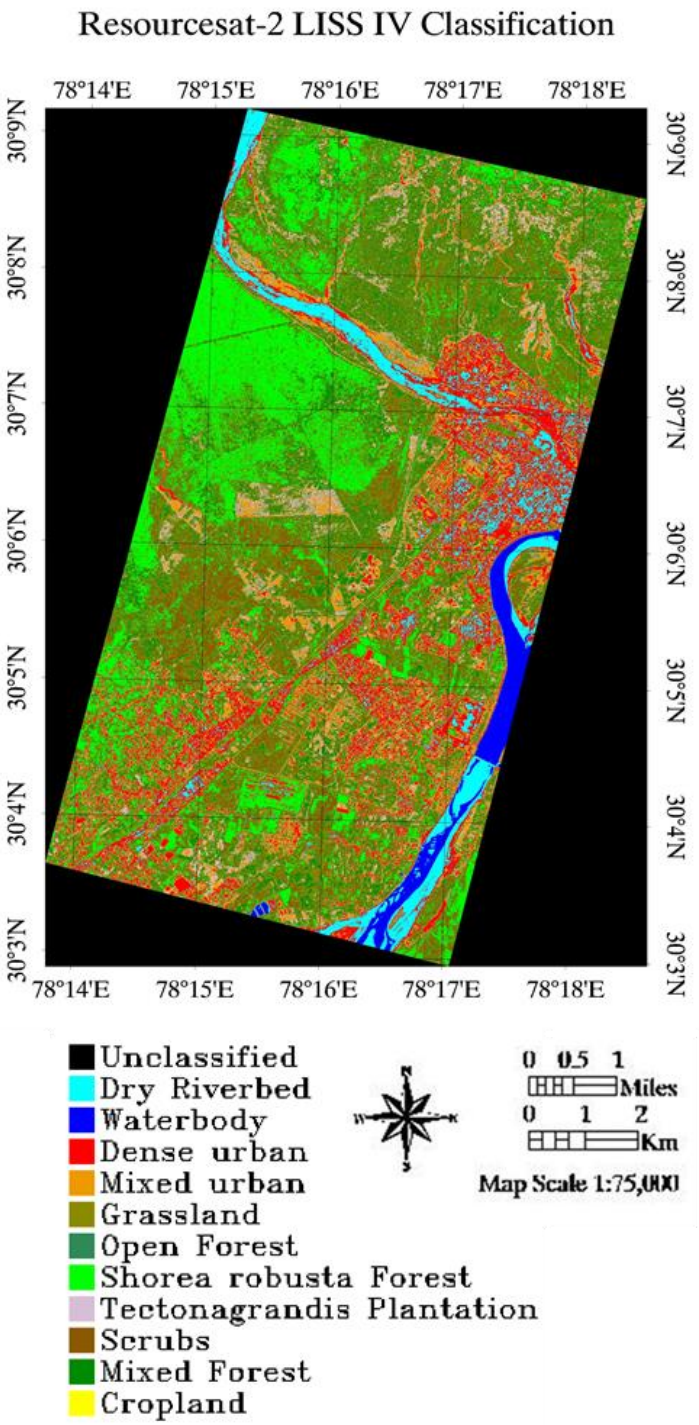

Figure 45: Classified Simulated HRS from LISS IV

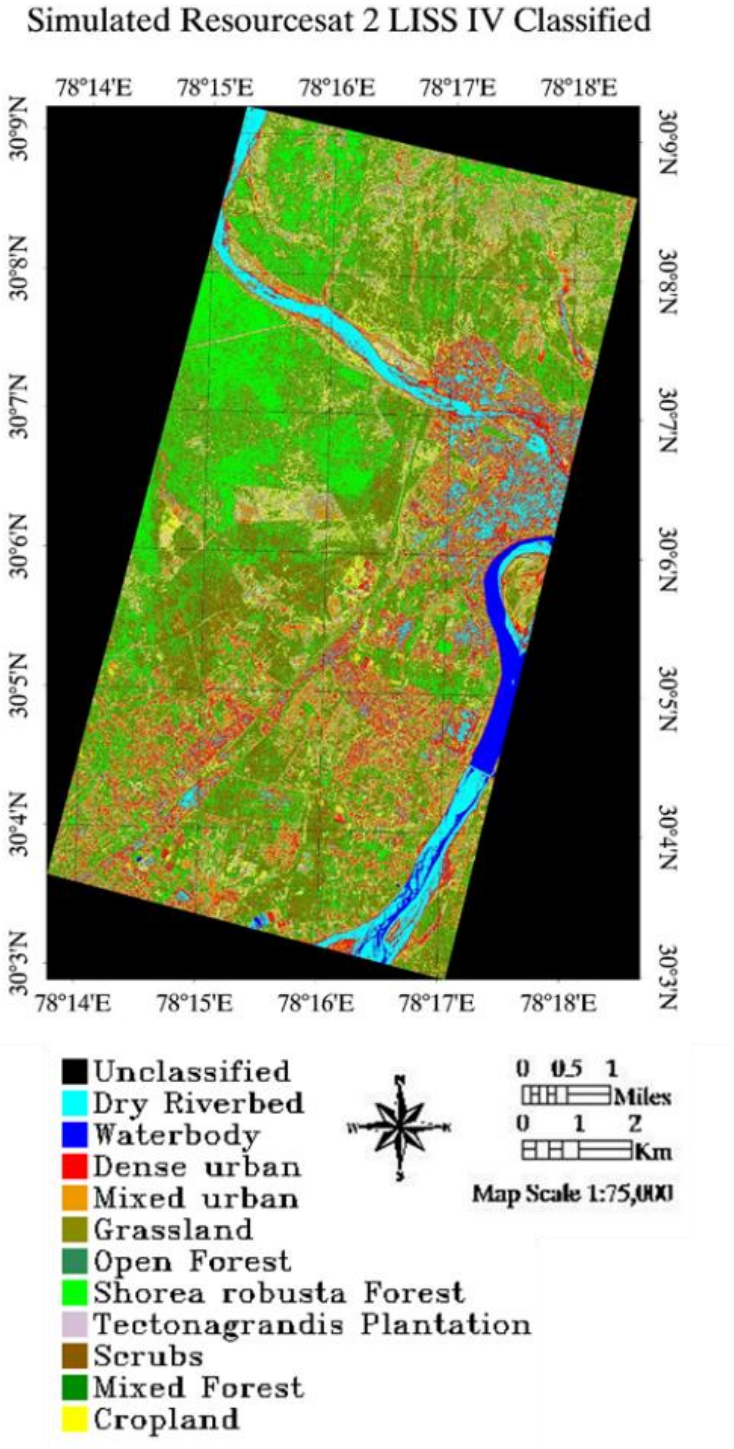

Figure 46: Classified Simulated HRS from Resourcesat 2 LISS IV

Accuracy Assessment:

- **EO-1 Hyperion**

Table 23: Accuracy Assessment EO-1 Hyperion

Class	Producer's Accuracy	User's Accuracy
Dry Riverbed	93.55	98.31
Waterbody	100	100
Dense Urban	98.59	89.74
Mixed Urban	34.92	88
Grassland	100	73.04
Open Forest	77.78	79.03
Shorea robusta	100	78.85
Tectonagrandis Plantation	55.74	100
Scrubs	89.47	100
Mixed Forest	99.34	74.75
Cropland	91.53	90
Overall Accuracy	84.82%	
Kappa	0.8296	

- **EO-1 ALI**

Table 24 : Accuracy assessment of EO-1 ALI

Class	Producer's Accuracy	User's Accuracy
Dry Riverbed	98.68	75
Waterbody	100	100
Dense Urban	59.77	45.61
Mixed Urban	5.32	7.04
Grassland	100	75.68
Open Forest	40.22	90.24
Shorea robusta	100	38.68
Tectonagrandis Plantation	19.24	65.52
Scrubs	37.56	98.67
Mixed Forest	91.91	61.27
Cropland	57.8	80.77
Overall Accuracy	58.91%	
Kappa	0.522	

- **Simulated HRS from EO-1 ALI**

Table 25: Accuracy Assessment of HRS simulated from ALI

Class	Producer's Accuracy	User's Accuracy
Dry Riverbed	86.76	86.76
Waterbody	100	100
Dense Urban	82.35	76.36
Mixed Urban	27.27	68.18
Grassland	96.43	77.14
Open Forest	85.71	76.92
Shorea robusta	92.31	70.59
Tectonagrandis Plantation	28.09	96.15
Scrubs	53.66	73.33
Mixed Forest	100	53.68
Cropland	85.11	86.96
Overall Accuracy	74.35%	
Kappa	0.717	

Table 26: Accuracy Assessment of Landsat 8 OLI

- **Landsat-8 OLI**

Class	Producer's Accuracy	User's Accuracy
Dry Riverbed	71.89	59.64
Waterbody	95.21	87.42
Dense Urban	47.21	83.2
Mixed Urban	48	54.14
Grassland	93.58	84.71
Open Forest	69.7	69.7
Shorea robusta	89.47	80.63
Tectonagrandis Plantation	75.18	88.03
Scrubs	64.29	17.53
Mixed Forest	28.9	62.5
Cropland	50.93	36.18
Overall Accuracy	62.97%	
Kappa	0.5854	

- **Simulated HRS from Landsat 8 OLI**

Table 27: Accuracy Assessment of HRS simulated from Landsat 8 OLI data

Class	Producer's Accuracy	User's Accuracy
Dry Riverbed	96.4	64.73
Waterbody	100	100
Dense Urban	55.63	76.07
Mixed Urban	19.35	69.77
Grassland	78.03	58.86
Open Forest	55.56	40.54
Shorea robusta	96.38	71.51
Tectonagrandis Plantation	72.88	90.53
Scrubs	65.59	46.92
Mixed Forest	70.04	80.5
Cropland	77.08	78.72
Overall Accuracy	69.82%	
Kappa	0.6631	

- **Resourcesat-2 LISS III**

Table 28: Accuracy Assessment of classified LISS III MRS Data

Class	Producer's Accuracy	User's Accuracy
Dry Riverbed	76.92	54.05
Waterbody	68.82	100
Dense Urban	59.62	65.46
Mixed Urban	94.12	40
Grassland	100	91.18
Open Forest	55.56	40.54
Shorea robusta	87.5	86.34
Tectonagrandis Plantation	72.88	90.53
Scrubs	63.6	85.25
Mixed Forest	67.28	59.59
Cropland	94.87	81.67
Overall Accuracy	65.70%	
Kappa	0.6034	

- **Simulated HRS from Resourcesat-2 LISS III**

Table 29 : Accuracy Assessment of HRS simulated from LISS III data

Class	Producer's Accuracy	User's Accuracy
Dry Riverbed	77.31	62.16
Waterbody	100	88.98
Dense Urban	31.96	38.75
Mixed Urban	35.85	82.61
Grassland	91.74	95.24
Open Forest	79.49	91.18
Shorea robusta	93.6	71.74
Tectonagrandis Plantation	45.41	94
Scrubs	32.89	80.43
Mixed Forest	79.43	41.48
Cropland	84.62	78.57
Overall Accuracy	69.42%	
Kappa	0.6412	

- **Resourcesat 2 LISS IV data**

Table 30: Accuracy assessment of LISS IV MRS data

Class	Producer's Accuracy	User's Accuracy
Dry Riverbed	79.34	100
Waterbody	100	54.08
Dense Urban	98.81	36.4
Mixed Urban	56.59	65.92
Grassland	86.01	86.01
Open Forest	63.16	63.16
Shorea robusta	91.22	33.5
Tectonagrandis Plantation	27.43	40.88
Scrubs	85.11	50
Mixed Forest	56.59	65.92
Cropland	0	0
Overall Accuracy	63.98%	
Kappa	0.5336	

- **Simulated HRS from Resourcesat-2 LISS IV data**

Table 31: Accuracy Assessment of HRS simulated from LISS IV MRS data

Class	Producer's Accuracy	User's Accuracy
Dry Riverbed	93.84	99.51
Waterbody	99.5	88.63
Dense Urban	87.72	47.17
Mixed Urban	88.74	75.71
Grassland	77.11	81.72
Open Forest	21.43	57.78
Shorea robusta	51.55	25.97
Tectonagrandis Plantation	36.6	45.51
Scrubs	63.64	29.91
Mixed Forest	51.43	18.75
Cropland	51.55	25.97
Overall Accuracy	79.48%	
Kappa	0.7259	

- **Comparative analysis of Accuracy Assessment**

Figure 47 shows the comparison of user's as well as producer's accuracy for each class of EO-1 ALI, Hyperion and Simulated HRS from ALI classified data. Major classes in simulated (EO-1 ALI) and hyperion have shown comparable results. The accuracy obtained from simulated HRS data from all other multispectral data (Landsat 8 OLI, Resourcesat 2 LISS III & LISS IV) have shown improved results as compared to corresponding MRS data as shown in Figure 48- 50 .

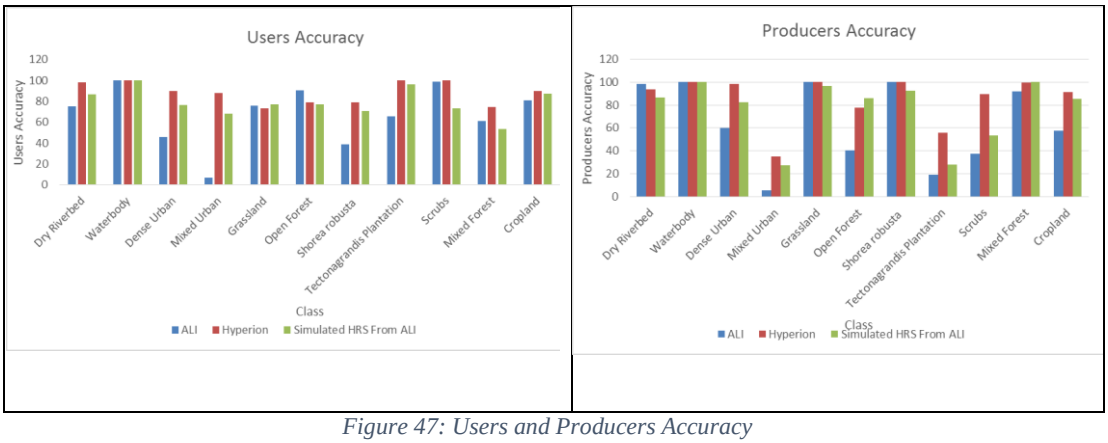

Figure 47: Users and Producers Accuracy

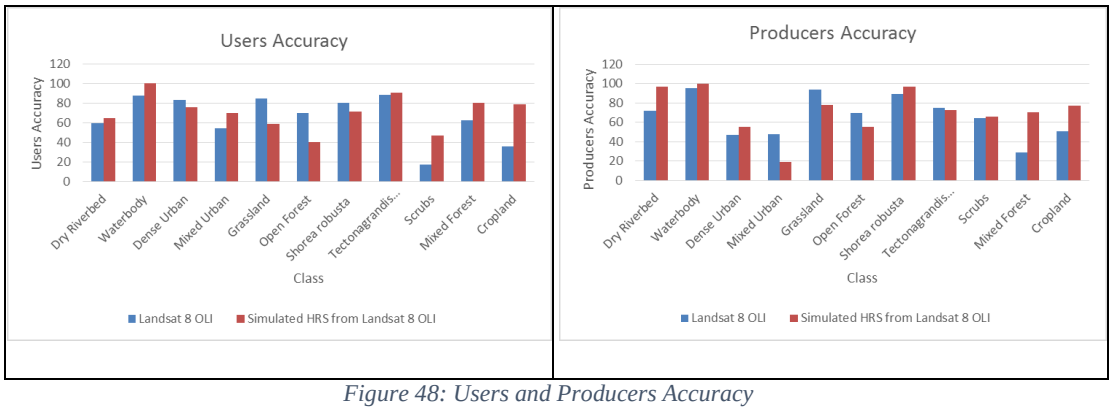

Figure 48: Users and Producers Accuracy

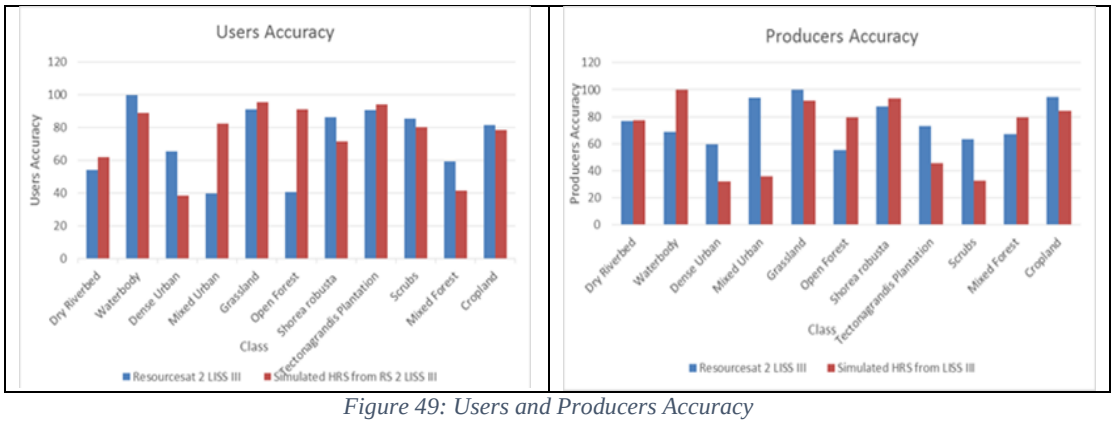

Figure 49: Users and Producers Accuracy

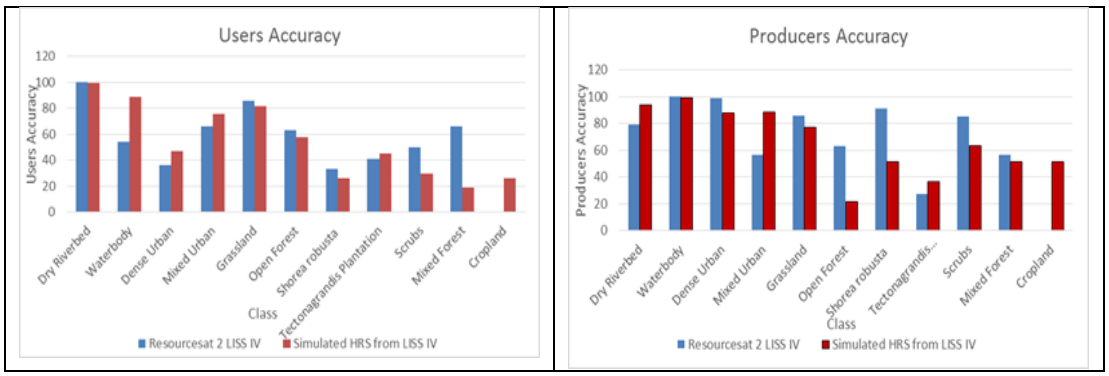

Figure 50: Users and Producers Accuracy

6 Conclusion and Future Recommendation:

6.1 Conclusion

This chapter illustrated the summary of the objectives accomplished in this project work with the scope of future advancement. The work carried out involves simulation of HRS data from available multispectral datasets using spectral reconstruction approach for detailed LULC studies. The research also demonstrated the potential of simulation of the HRS data from high resolution MRS data (RS-2 LISS IV). This will be beneficial in the cases were problem of mixed pixel exists because of the coarser resolution of the HRS datasets. The simulated high resolution HRS data can be used for target detection related studies.

Research also emphasis on use of open source programming language in the development of HRS data simulation tool box using Spy and Numpy libraries. The developed tool is a sensor independent which is capable of simulating the HRS data using any MRS Datasets.

The conclusions of the research work are presented below:

- Spectral reconstruction technique emerged out to be an effective method for HRS data simulation as it does not require any sensor dependent parameters. This technique effectively make use of inherent information of MRS data and normalized ground spectra for reconstruction of contiguous spectral narrow bands.
- HRS data simulation from EO-1 ALI, Landsat-8 OLI, LISS III and LISS-IV resulted in 70, 38, 34 and 23 spectral bands with 10 nm bandwidth.
- HRS simulated results are validated using visual interpretation, statistical, spectral separability and classification techniques. Validation of simulated HRS data contribute conclusive results which emphasises on superiority of the spectral reconstruction technique for HRS data simulation. Simulated HRS data from ALI and OLI has shown high spectral correlation with Hyperion data along with comparable SNR values. Simulated HRS results from LISS III and LISS IV have also produced high SNR values indicating satisfactory simulation.
- Spectral separability analysis for all the hyperspectral datasets (EO-1 Hyperion and simulated) with field spectra is carried out. The overall score was found to be similar for Hyperion, simulated HRS data from ALI and OLI whereas the scores are at higher end for LISS-III and LISS IV.
- One of the validation was performed using the SAM classification and it was observed that simulated hyperspectral data shows comparable results with Hyperion. The simulated results are able to separate out different LULC classes in a better way than their corresponding multispectral datasets. Apart from this the accuracy assessment results are also improved.
- Open source programming language Python emerged to be vibrant tool for implementing application specific algorithm. It provides access to libraries such as: Spectral python, Numpy & PyQt which has shown significant contribution in implementation of HRS data simulation algorithm and in development of open source tool for HRS data simulation.

6.2 Future recommendation

- Linear unmixing is the intermediate step required in simulation of HRS data. It contributes significant result only in case if the features in the mixed pixels are organised proportionally. But in case if the substances comprising the medium are not organized proportionally, then incident radiation may experience reflection with multiple feature which can destroy the conditions of linear unmixing. In such cases nonlinear unmixing technique can be used in which the features in a mixed pixels are not organized in a proportionally. This can significantly improve the HRS data simulation results.
- Very high spatial resolution data like Worldview-3 can also be tested using same algorithm for HRS data simulation.
- Customized package can be made using python for simulation of HRS data. The customized package should be developed in such a way that it can be used as add on plugin in different Satellite image processing tools available in the market.

References

- Agarwal, S., 2004. Principles of remote sensing. Satell. Remote Sens. GIS Appl. Agric. Meteorol. 23.
- Boggione, G.A., Pires, E.G., Santos, P.A., Fonseca, L.M.G., 2003. Simulation of a panchromatic band by spectral combination of multispectral ETM+ bands. Proc ISRSE.
- Börner, A., Wiest, L., Keller, P., Reulke, R., Richter, R., Schaepman, M., Schläpfer, D., 2001. SENSOR: a tool for the simulation of hyperspectral remote sensing systems. ISPRS J. Photogramm. Remote Sens. 55, 299–312.
- Daigo, M., Ono†, A., Urabe‡, R., Fujiwara, N., 2004. Pattern decomposition method for hyper-multi-spectral data analysis. Int. J. Remote Sens. 25, 1153–1166. doi:10.1080/0143116031000139872
- Harsanyi, J.C., Chang, C.-I., 1994. Hyperspectral image classification and dimensionality reduction: an orthogonal subspace projection approach. Geosci. Remote Sens. IEEE Trans. On 32, 779–785.
- Heinz, D.C., Chang, C.-I., 2001a. Fully constrained least squares linear spectral mixture analysis method for material quantification in hyperspectral imagery. Geosci. Remote Sens. IEEE Trans. On 39, 529–545.
- Heinz, D.C., Chang, C.-I., 2001b. Fully constrained least squares linear spectral mixture analysis method for material quantification in hyperspectral imagery. Geosci. Remote Sens. IEEE Trans. On 39, 529–545.
- Hossain, M., Ahadi, A.W., Kamal, G.M., 2003. Introduction to remote sensing. Afghan. Inf. Manag. Serv. AIMS Intern. Capacity Build. Initiat. U. N. Dev. Programme.
- Hyperspectral Analysis: SAM and SFF Tutorial (Using ENVI) | Exelis VIS Docs Center [WWW Document], 2015. URL http://www.exelisvis.com/docs/Whole-Pixel_Hyperspectral_Analysis_Tutorial.html (accessed 6.15.15).
- Installing PyQt4 — PyQt 4.11.4 Reference Guide [WWW Document], 2015. URL http://pyqt.sourceforge.net/Docs/PyQt4/installation.html

- Kavzoglu, T., 2004. Simulating Landsat ETM+ imagery using DAIS 7915 hyperspectral scanner data. Int. J. Remote Sens. 25, 5049–5067. doi:10.1080/01431160410001720199
- Kawishwar, P., 2007. Atmospheric Correction Models for Retrievals of Calibrated Spectral Profiles from Hyperion EO-1 Data. Int. Inst. Geo-Inf. Sci. Earth Obs. Master Thesis Enschede Neth.
- Keshava, N., 2003. A survey of spectral unmixing algorithms. Linc. Lab. J. 14, 55–78.
- Kruse, F.A., 2004. Comparison of ATREM, ACORN, and FLAASH atmospheric corrections using low-altitude AVIRIS data of Boulder, CO, in: 13th JPL Airborne Geoscience Workshop. Jet Propulsion Laboratory Pasadena, CA.
- Landsat 8 [WWW Document], 2015. URL http://landsat.usgs.gov/landsat8.php (accessed 6.15.15).
- Landsat_DN_to_Reflectance.pdf [WWW Document], 2015. URL http://www.yale.edu/ceo/Documentation/Landsat_DN_to_Reflectance.pdf (accessed 6.15.15).
- Liguo, W., Jing, Z., Luqun, D., 2009a. Spectral Unmixing Technique Based on Flexibly Selected Endmembers. IEEE, pp. 148–151. doi:10.1109/CSIE.2009.989
- Liu, B., Zhang, L., Zhang, X., Zhang, B., Tong, Q., 2009. Simulation of EO-1 Hyperion Data from ALI Multispectral Data Based on the Spectral Reconstruction Approach. Sensors 9, 3090–3108. doi:10.3390/s90403090
- Lumme, J.H., 2004. Classification of vegetation and soil using imaging spectrometer data, in: Geoscience and Remote Sensing Symposium. p. 83.
- Markelin, L., 2013. Radiometric calibration, validation and correction of multispectral photogrammetric imagery. Finnish Geodetic Institute.
- Maselli, F., 1998. Multiclass spectral decomposition of remotely sensed scenes by selective pixel unmixing. Geosci. Remote Sens. IEEE Trans. On 36, 1809–1820.
- Muramatsu, K., Furumi, S., Fujiwara, N., Hayashi, A., Daigo, M., Ochiai, F., 2000. Pattern decomposition method in the albedo space for Landsat TM and MSS data analysis. Int. J. Remote Sens. 21, 99–119. doi:10.1080/014311600211019
- Parra, L.C., Spence, C., Sajda, P., Ziehe, A., Müller, K.-R., 1999. Unmixing Hyperspectral Data., in: NIPS. Citeseer, pp. 942–948.

- Resourcesat-2_Handbook.pdf [WWW Document], 2015. URL http://bhuvan.nrsc.gov.in/bhuvan/PDF/Resourcesat-2_Handbook.pdf (accessed 6.15.15).
- Roberts, D.A., Gardner, M., Church, R., Ustin, S., Scheer, G., Green, R.O., 1998. Mapping chaparral in the Santa Monica Mountains using multiple endmember spectral mixture models. Remote Sens. Environ. 65, 267–279.
- Sahoo, R., n.d. HYPERSPECTRAL REMOTE SENSING.
- Sahoo, R.N., Pargal, S., Pradhan, S., Krishna, G., Gupta, V.K., n.d. Processing of Hyperspectral Remote Sensing Data.
- San, B.T., Suzen, M.L., 2010. EVALUATION OF DIFFERENT ATMOSPHERIC CORRECTION ALGORITHMS FOR EO-1 HYPERION IMAGER.
- Schläpfer, D., Boerner, A., Schaepman, M., 1999. The potential of spectral resampling techniques for the simulation of APEX imagery based on AVIRIS data, in: Summaries of the Eighth JPL Airborne Earth Science Workshop, JPL, Pasadena (CA). pp. 377–384.
- Schott, J., Raqueno, R.V., Raqueno, N.G., Brown, S.D., 2010. A Synthetic Sensor/Image Simulation Tool to Support the Landsat Data Continuity Mission(LDCM), in: ASPRS 2010 Annual Conference. San Diego, California.
- Settle, J.J., Drake, N.A., 1993a. Linear mixing and the estimation of ground cover proportions. Int. J. Remote Sens. 14, 1159–1177. doi:10.1080/01431169308904402
- Shaw, G.A., Burke, H.K., 2003. Spectral imaging for remote sensing. Linc. Lab. J. 14, 3–28.
- Shaw: Spectral imaging for remote sensing - Google Scholar [WWW Document], 2015. URL https://scholar.google.co.in/scholar?cluster=8610137779696503739&hl=en&as_sdt=0,5&sciodt=0,5 (accessed 6.15.15).
- Spectral Response Functions [WWW Document], 2015. URL http://www.eoc.csiro.au/hswww/oz_pi/specresp.htm (accessed 6.15.15).
- Strobl, J., Blaschke, T., Griesebner, G., AGIT-Symposium (Eds.), 2000. Angewandte geographische Informationsverarbeitung XII: Beiträge zum AGIT-Symposium Salzburg 2000 ; [vom 5. bis 7. Juli 2000]. Herbert Wichmann Verlag, Heidelberg.

- Trishchenko, A.P., Cihlar, J., Li, Z., 2002. Effects of spectral response function on surface reflectance and NDVI measured with moderate resolution satellite sensors. Remote Sens. Environ. 81, 1–18.
- Tseng, Y.-H., 2000. Spectral unmixing for the classification of hyperspectral images. Int. Arch. Photogramm. REMOTE Sens. 33, 1532–1538.
- USGS EO-1 Website - http://eo1.usgs.gov [WWW Document], 2015. URL http://eo1.usgs.gov/sensors/hyperion (accessed 6.15.15).
- Welcome to Bhuvan | ISRO's Geoportal | Gateway to Indian Earth Observation [WWW Document], 2015. URL http://bhuvan.nrsc.gov.in/bhuvan_links.php# (accessed 6.15.15).
- Welcome to Python.org [WWW Document], 2015. URL https://www.python.org/
- Welcome to Spectral Python (SPy) — Spectral Python 0.16.0 documentation [WWW Document], 2015. URL http://www.spectralpython.net/
- Yan, L., Liu, S., Liu, H., Jing, X., Cheng, C., Wang, H., 2014a. Two inverse processes: Spectral reconstruction and pixel unmixing, in: Earth Observation and Remote Sensing Applications (EORSA), 2014 3rd International Workshop on. IEEE, pp. 462–469.
- Yuan, J., Niu, Z., 2008. Evaluation of atmospheric correction using FLAASH, in: Earth Observation and Remote Sensing Applications, 2008. EORSA 2008. International Workshop on. IEEE, pp. 1–6.
- Zhang, L., Furumi, S., Muramatsu, K., Fujiwara, N., Daigo, M., Zhang, L., 2006. Sensor-independent analysis method for hyperspectral data based on the pattern decomposition method. Int. J. Remote Sens. 27, 4899–4910.